Development of a Novel Directional Backlight for Multi-User Display Applications

Zur Erlangung des akademischen Grades eines

DOKTORS DER INGENIEURWISSENSCHAFTEN (Dr.-Ing.)

von der KIT-Fakultät für
Elektrotechnik und Informationstechnik
des Karlsruher Instituts für Technologie (KIT)

genehmigte

DISSERTATION

von

M.Sc. Jundong Zhou
geb. in Hubei, China

Tag der mündlichen Prüfung: 21.02.2024

Hauptreferent: Prof. Dr. rer. nat. Wilhelm Stork
Korreferent: Prof. Dr. rer. nat. Alois Herkommer

Abstract

Display devices are used to provide visual information to the observer, which are now present in various applications, such as in consumer, automotive, medical and industrial market. In the past decades, displays are playing an increasingly important role in the daily life, hence, many efforts have been made to further develop the display technologies.

Some development activities focus on the improvement of the display visual quality, such as luminance, contrast, color space, pixel density, etc. In the meantime, users are also expecting more special functions from the display, and there is a growing demand for controlling the direction of the output light. One example is the widely applied privacy filter for computer screens, which can reduce the screen visibility at large viewing angles. The privacy filter from 3M contains a large number of micro-louvers, that can limit the viewing angle to 30° on each side [1]. Another example is the split-view function, where individual images will be sent to different directions [2–5]. This function has been commercialized by the automotive manufacturer Mercedes-Benz at the Central Information Display (CID) in several vehicle series [6, 7]. By placing a special barrier mask on the display screen, the light from one pixel can only go to the corresponding direction. This allows the driver and co-driver to view different images from the same display.

To control the light propagation direction is also critical in Three-Dimensional (3D) display applications [8, 9]. For the conventional Two-Dimensional (2D) display, the user will observe the same image at all viewing angles. But a 3D display is able to send different images into the left and the right eye of the user to evoke 3D perception. Some technologies also use an eye-tracking device to detect the user's eye positions, so that the proper image content can be directed to the corresponding eye during user movement. In the mentioned three applications (privacy screen, split-view, 3D display), the light coming out of the display is not diffusely spreading in all directions. Instead, the light will leave the display in a controlled manner.

This work wants to propose a novel display backlight concept, which is able to modulate the illumination direction. With the new proposed backlight, image contents can be sent only to the intended directions. The new concept has been initially motivated by 3D display applications. The key advantage of the proposed concept is that high-quality 3D images can be created for multiple users. However, it should be emphasized that the possible application is not limited only in 3D displays. The new backlight concept can be used in the applications, where the direction of the light needs to be modulated, for example the privacy function and the split-view function. Due to the compact design and the wide application, the new backlight concept is believed to have great potential for future display applications.

This dissertation is divided into six chapters. As this new backlight concept was originally inspired by the 3D display technologies, an overview of related 3D display technologies will be given in Chapter 1. And one drawback of the current methods, which is called side leak effect, will be pointed out. In Chapter 2, a new directional backlight concept will be introduced which allows to overcome the side leak effect. A quantitative system model will be created to demonstrate that the side leak can be eliminated by using one additional barrier layer. In Chapter 3, the proposed system model will be established in the simulation software, and the system performance can be evaluated using the simulation model. Subsequently, Chapter 4 will demonstrate the construction of a simplified prototype based on the new concept, where the component selection and the system configuration will be explained. In Chapter 5, experiments on the built-up prototype will be shown. According to the experimental results, the side leak problem can be successfully eliminated. Besides, the simulation results are highly consistent with the experiment results, which can verify the correctness and feasibility of the new backlight concept. Finally, Chapter 6 will provide a summary and give an outlook for future studies.

Zusammenfassung

Displaysysteme werden verwendet, um visuelle Informationen dem Beobachter zur Verfügung zu stellen. Heutzutage befinden sich Displaysysteme in verschiedenen Anwendungen, wie beispielsweise in Verbraucher-, Automobil-, medizinischen und industriellen Markt. In den letzten Jahrzehnten haben Displays eine immer wichtigere Bedeutung in unserem täglichen Leben erlangen. Deswegen wurde viel Zeit und Mühe investiert, um die Displaytechnologien kontinuierlich weiterzuentwickeln.

Einige Entwicklungsaktivitäten konzentrieren sich auf die Verbesserung der visuellen Qualität von Displays, wie Helligkeit, Kontrast, Farbraum, Pixeldichte usw. Gleichzeitig erwarten Benutzer auch mehr spezielle Funktionen von den Displays, und es besteht eine wachsende Nachfrage die vom Display ausgehende Lichtrichtung zu steuern. Ein Beispiel hierfür ist der weit verbreitete Blickschutzfilter für den Monitor, welcher die Sichtbarkeit des Monitors bei großen Betrachtungswinkeln reduzieren kann. Der Blickschutzfilter von 3M besteht aus einer Vielzahl von Mikroamellen, die den Betrachtungswinkel auf 30° auf jeder Seite begrenzen kann [1].

Ein weiteres Beispiel ist die Split-View-Funktion, bei der individuelle Bilder in unterschiedliche Richtungen projiziert werden [2–5]. Diese Funktion wurde vom Automobilhersteller Mercedes-Benz bei CID in mehreren Fahrzeugserien umgesetzt [6, 7]. Durch das Anlegen einer speziellen Barriereschicht auf dem Display, kann das Licht von einem Pixel nur zur bestimmten Richtung durchlaufen. Diese Funktion ermöglicht den Fahrer und Beifahrer verschiedene Bilder von demselben Display zu betrachten.

Die Steuerung der Lichtrichtung ist auch ein wesentliches Thema in 3D-Display-Anwendungen [8, 9]. Beim herkömmlichen 2D-Display sieht der Beobachter bei jedem Betrachtungswinkel immer das gleiche Bild. Aber ein 3D-Display kann zwei unterschiedliche Bilder jeweils in das linke Auge und rechte Auge schicken, um die 3D-Wahrnehmung zu erzeugen. Einige Technologien

nutzen auch ein Eye-Tracking-Gerät für die Verfolgung von Augenpositionen, damit das Bild während der Bewegungen des Nutzers in die korrekte Augenposition geschickt werden kann. Bei den genannten drei Anwendungen (Blickschutzfilter, Spit-View, 3D-Display), wird sich das von einem Display ausgehende Licht nicht diffus in alle Richtungen ausbreiten. Stattdessen verlässt das Licht das Display in einer gerichteten Weise.

In dieser Arbeit wird ein neuartiges Display-Hintergrundbeleuchtungskonzept vorgeschlagen, das die Beleuchtungsrichtung vom ausgehenden Licht modulieren kann. Die vorgeschlagene Hintergrundbeleuchtung ist in der Lage, den angezeigten Bildinhalt nur zu den gewünschten Richtungen zu schicken. Das neue Konzept wurde ursprünglich von 3D-Display-Anwendungen motiviert. Der Kernvorteil des neuen Konzepts besteht drin, dass hochwertige 3D-Bilder für mehrere Nutzer erzeugt werden können. Es sollte jedoch betont werden, dass die mögliche Anwendung nicht nur auf 3D-Displays beschränkt ist. Das neue Hintergrundbeleuchtungskonzept kann in Anwendungen eingesetzt werden, in denen die Lichtrichtung moduliert werden soll. Aufgrund der kompakten Bauform und der breiten Anwendungsmöglichkeiten wird davon ausgegangen, dass das neue Konzept ein großes Potenzial in zukünftigen Display-Anwendungen hat.

Diese Dissertation ist in sechs Kapitel gegliedert. Weil das neue Hintergrundbeleuchtungskonzept ursprünglich von 3D-Displaytechnologien inspiriert wurde, wird eine Übersicht der 3D-Displaytechnologien in Kapitel 1 gegeben. Und ein Nachteil der aktuellen Methoden, welcher als “Side-Leak-Effekt” bezeichnet wird, wird in Kapitel 1 beschrieben. In Kapitel 2 wird das neue Konzept eingeführt, welches den Side-Leak-Effekt lösen kann. Ein quantitatives Systemmodell wird erstellt, um zu zeigen dass der Side-Leak-Effekt durch den Einsatz einer zusätzlichen Barriereschicht eliminiert werden kann. In Kapitel 3 wird das vorgeschlagene Systemmodell in der Simulationssoftware aufgestellt, um die Systemleistung simulativ auswerten zu können. Anschließend wird in Kapitel 4 die Implementierung eines vereinfachten Prototyps auf Basis des neuen Konzepts dargestellt, wo die Auswahl der Komponenten und die Systemkonfiguration erläutert werden. Danach wird in Kapitel 5 das Experiment mit dem aufgebauten Prototyp vorgestellt. Laut dem Messergebnis lässt sich der Side-Leak-Effekt erfolgreich unterdrücken. Außerdem gibt es eine gute Übereinstimmung zwischen dem Messergebnis und dem Simulationsergebnis, was die Richtigkeit und die Machbarkeit des neuen Hintergrundbeleuchtungs-

konzepts bestätigt. Schließlich wird Kapitel 6 eine Zusammenfassung liefern und einen Ausblick auf zukünftige Studien geben.

Acronyms

KIT	Karlsruher Institut für Technologie
CID	Central Information Display
3D	Three-Dimensional
2D	Two-Dimensional
LCD	Liquid Crystal Display
TV	Television
CRT	Cathode Ray Tube
OLED	Organic Light-Emitting Diode
LED	Light-Emitting Diode
PID	Passenger Information Display
ICD	Instrument Cluster Display
HMD	Head-Mount-Display
DB	Directional Backlight
MVD	Multiview Display
LC	Liquid Crystal
CAD	Computer-Aided Design
PMMA	Poly Methyl Methacrylate

Contents

1 Introduction

1.1 Motivation

Nowadays display devices can be found everywhere in our daily life. To give an impression of the huge display market, some results from the Internet statistics can be listed: In 2022, over 45% of worldwide households have a computer, while over 70% of the homes own a Television (TV) [10, 11]. And around 70% of the global population have a smartphone [12].

The constantly growing display market has boosted the display development. In the past decades, we have witnessed the emergence of different display technologies [13–15]. Cathode Ray Tube (CRT) displays have been widely used in the late 20th century, until the LCD started to replace CRT displays in the mid-2000s. Then beginning from 2010, TV manufacturers have introduced the Organic Light-Emitting Diode (OLED) television into the market [16–18]. After entering the 2020s, mini-Light-Emitting Diode (LED) displays have appeared as an upgrade of the existing LCD technology [19, 20].

The above-mentioned developments have largely increased the display visual quality, in terms of luminance [21], contrast [22], color space [23], etc. However, only the improvement of image quality cannot fulfill the growing market, and the user is also expecting extra special functions of the display. One popular topic is to control the direction of the output light [24–27]. To provide some examples, several display developments in the automotive area are going to be discussed, since this work was inspired by the automotive display applications.

In 2008, two companies, Mercedes-Benz and Bosch, have developed the "Split-View" display, which has been integrated into the Mercedes S-Class at the CID [6, 7]. This display allows the driver and co-driver to view two different images simultaneously from the same screen. This function has been realized by placing a special barrier mask on the display screen, so that the light coming

from one display pixel can only go to the corresponding direction. The new feature can avoid distracting the driver when the co-driver wants to watch entertainment programs.

For the same safety reason, the automotive company Continental has announced a new "Switchable Privacy Display" in 2022, which is planned to be integrated into the Passenger Information Display (PID) [28]. Continental has developed a special backlight unit for the display, which allows vehicle information to be displayed in two different modes: private mode or public mode. In the public mode, both the driver and the co-driver can see the image on the PID. Then the PID can be switched to the private mode, where the content should only be visible for the co-driver. This can help avoid distracting the driver from the road traffic, when the co-driver is viewing multimedia content.

Then in recent years, 3D display has been a popular topic in the automotive applications, where a precise control of the light propagation direction is required. In 2021, the automotive manufacturer Hyundai has launched a new vehicle version of Genesis GV80, and the autostereoscopic 3D technology is implemented in the Instrument Cluster Display (ICD) [29]. By placing a special barrier mask in the display, two different images can be sent to the right and left eye to create 3D perception. Also in the same year 2021, the company Mercedes-Benz has launched its new S-Class with a 3D instrument cluster [30]. Similar to GV80, the new S-Class has applied the barrier mask technology to achieve 3D perception.

However, it should be noticed that the above-mentioned 3D ICD can provide 3D contents only to the driver, whereas other passengers are not able to enjoy the 3D experience from the ICD. To overcome the single user limitation, several automotive companies have investigated the multiview 3D technologies, which can enable multi-user 3D perception but will significantly degrade the image quality. Therefore, the motivation of this work is to develop a new 3D display technology, which can provide high image quality in multi-user applications.

1.2 State-of-the-art

1.2.1 Human 3D perception

Depth perception should first be explained to lay the foundation of the 3D Display. Depth perception is the visual ability to perceive the world in three dimensions, allowing us to judge the distance of an object. A large number of depth cues contribute to the depth perception, and they can be generally divided into monocular cues and binocular cues [31].

Monocular cues can provide depth information to the viewer, when the scene is observed with one eye. In contrast, binocular cues can only be obtained with two eyes. Some important monocular and binocular cues are respectively listed in Tab.1.1 and Tab.1.2.

Table 1.1: Monocular depth cues

Motion parallax	Nearby objects appear to move faster than remote objects.
Linear perspective	Parallel lines converge at a distant point.
Relative size	Objects appear to be larger when moving towards the viewer.
Occlusion	Parts of an object could be blocked by its front object.
Shading	Cast of objects gives a strong depth cue.
Texture	Details of object surface can be used to give depth cues.
Accommodation	The adjustment of the eye focal length will change the muscle tension and provide the depth cues.

A 2D display can supply the viewer with the majority of the monocular depth cues, but the binocular disparity is missing since the same image will be perceived by both eyes. Therefore, the depth perception from a 2D display could be ambiguous. The binocular disparity must be added to provide a natural and satisfactory depth perception [32].

Table 1.2: Binocular depth cues

Binocular disparity	Because there is a certain distance between the left eye and the right eye, the images perceived by two eyes would be slightly different. This disparity can be used to generate depth cues.
Convergence	When focusing on the same object, the convergence angle of the two eyes depends on the object distance.

1.2.2 Summary of autostereoscopic 3D display technologies

Various technologies have been developed to provide the missing binocular disparity to the viewer, which can be generally classified into stereoscopic- and autostereoscopic-3D displays. The stereoscopic displays require the viewer to wear special eyeglasses to obtain different images at two eyes. In the past decades, different stereoscopic technologies have emerged into the market, including the polarization method, the time-multiplexing method, the Head-Mount-Display (HMD), etc. [33].

Accommodation-Convergence conflict is a typical phenomenon for stereoscopic displays. Based on the accommodation function, the eye will focus on the display screen to see the images clearly. But the perception of different 3D images at two eyes will give the brain the information that the objects are at their “real” distance, which is further away or closer than the display screen. Therefore, the convergence of the viewer’s eye will correspond to this manipulated distance, leading to a mismatch between focal distance and convergence distance. This type of visual conflict could cause visual confusion and visual fatigue after a long-time observation [34, 35].

Besides, the need of eyeglasses strongly restricts the application area of the stereoscopic 3D displays. Therefore, a lot of efforts have been made to develop autostereoscopic technologies, where the binocular depth cues can be acquired without wearing special eyeglasses [36, 37]. Numerous technologies have been investigated to achieve the autostereoscopic viewing experience, and three

main types of autostereoscopic 3D displays will be subsequently discussed: volumetric displays, digital-holographic displays and multiview 3D displays.

A volumetric display renders and represents the object in a 3D volume, so that the viewer will have a similar perception as the direct observation of the real object [38, 39]. Fig.1.1 demonstrates two general system configurations, which can achieve the 3D volumetric representation. A rotating LED array is shown in Fig.1.1(a). Through a careful calibration of the rotating speed, the modulation and switching of the LED array, 3D images can be generated within the space swept by the rotating panel. In real applications, the high-speed rotation movement could become one critical point in the development. Another static configuration is shown in Fig.1.1(b), where multiple LCD layers are stacked in front of a projector to form a 3D display volume. When the image projection and the modulation of LCD transmission can be synchronized, 2D sections of one 3D object can be projected at the correct 3D locations to enable a true 3D perception. For the static configuration, the requirement of fast switching LCD and the low image brightness have restricted its application area.

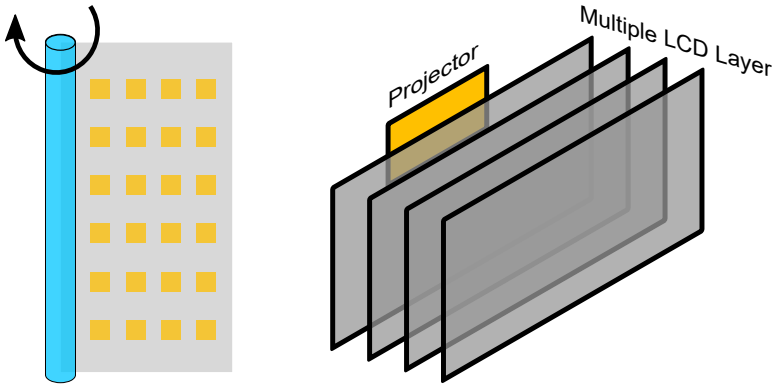

Figure 1.1: Two basic configurations of the volumetric display: (a) Dynamic configuration with a rotating LED array, (b) Static configuration with the stack of multiple LCD layers.

The second type of autostereoscopic technologies is the digital-holography, where the computer-generated hologram can be expressed on special spatial

light modulators, for example LCD. Fig.1.2 demonstrates the basic configuration of the digital-holography. Dynamic interference patterns can be displayed on the spatial light modulator, and the collimated reconstruction beam coming from a coherent light source will be used to illuminate the hologram. As a result, a virtual image with accurate 3D depth cues can be perceived by the viewer. However, the wide implementation of digital-holography still faces many technical difficulties. One main challenge is the requirement of small pixel size of the spatial light modulator, in order to achieve a high image quality. The required size is much smaller than the pixel size of conventional LCD displays. Besides, for the real-time application, the huge amount of data processing would also be a challenge for the system hardware. To alleviate the high requirements of digital-holography, SeeReal Technologies demonstrated a new approach. The essential idea of the approach is to reconstruct the wavefront only at the eye position that would be generated by the 3D object, instead of reconstructing the 3D object itself [40]. As a result, the reconstructed wave field of the 3D object can be seen within a virtual viewing window. By using an eye-tracking device, the locations of the viewer's eye can be determined, so the viewer is able to see the 3D object when moving in front of the screen. This method can enable the use of normal pixel size, and effectively reduce the amount of information to be processed [40]. Furthermore, there are numerous alternative methods to achieve holographic displays, but significant progress is still needed to realize convenient real-time applications [41–43].

The third type of autostereoscopic technology is the multiview 3D display. As illustrated in Fig.1.3(a), it's considered to use finite number of perspectives to approximate the continuously distributed light field of 3D objects [31]. The recording of perspectives at different positions can be easily achieved with the help of 3D modeling software. By adding some special structures into the traditional 2D display, which will be later explained, the multiview 3D display is able to send multiple 2D images to different directions. At the observation plane with distance L to the display, different zones with width W are created, as illustrated in Fig.1.3(b). Within each zone, a certain 2D image can be perceived, which is also called a "view". Then different perspectives of the 3D object should be assigned to the corresponding views. By a proper design of the multiview display, the left eye and the right eye of the viewer can be located at different zones. As a result, two eyes will receive two different perspectives of the 3D object. The brain is able to analyze this disparity and generate the corresponding depth perception. Due to the compatibility with

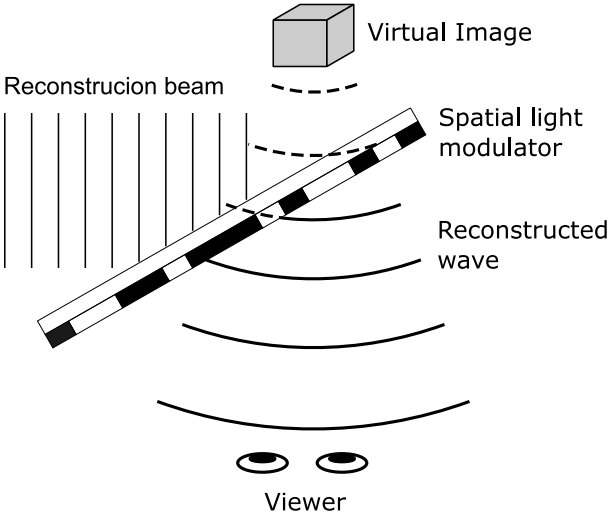

Figure 1.2: Image reconstruction at the digital-holography.

the conventional 2D display and the simple implementation, the multiview technology has been widely used in the commercialized products.

1.2.3 Overview of the multiview 3D technologies

Various concepts have been developed to build up multiview 3D displays. Two technologies, lenticular lens and parallax barrier, have been widely spread considering the image quality and the implementation complexity [31, 44]. Fig.1.4(a) shows the operation principle of a 2-view 3D display based on the parallax barrier technology. A special barrier layer is placed on a conventional 2D display panel. Light emitting from the display pixel will be blocked by the barrier, so that it can only propagate through the gap between barriers. With a proper barrier design, the light from all green pixels can only enter the left eye, whereas the light from all blue pixels can only enter the right eye. Therefore, two eyes will see different groups of pixels on the display panel. Depth perception can be evoked, when two correct perspectives of the 3D object are assigned to the blue and green pixel group respectively.

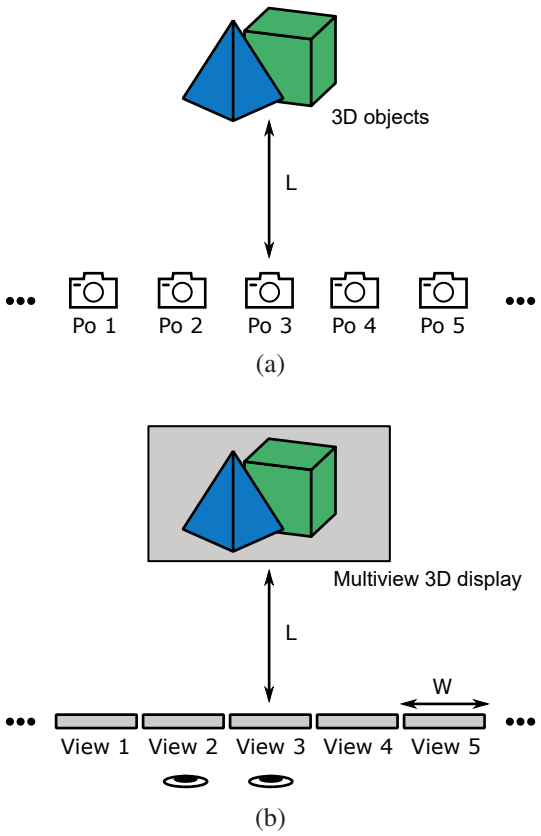

Figure 1.3: Principle of the multiview 3D display: (a) Only finite number of perspectives will be recorded from 3D objects, by placing the camera at different positions in the 3D modeling software. "Po" in the figure stands for position. (b) The Multiview 3D display can send the recorded camera images to the corresponding viewing angles.

The 2-view barrier display can be extended to a multiview display, as illustrated in Fig.1.4(b). Instead of two independent pixel groups shown in Fig.1.4(a), the display pixels are now divided into four different groups. After selecting the correct barrier parameters, four viewing zones can be created at the designed location. Then four perspectives of the 3D object should be allocated to the four

pixel groups, so the eye at each viewing zone can perceive the corresponding 3D image, which enables the depth perception.

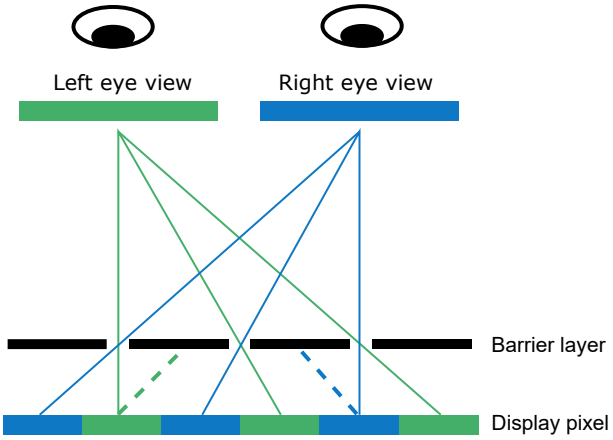

(a)

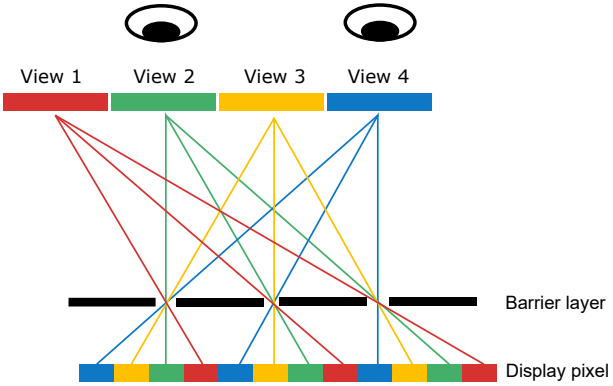

(b)

Figure 1.4: Principle of the parallax barrier technology: (a) 2-view 3D display, (b) 4-view 3D display. Light will be blocked by the black barrier, thus can only propagate through the gap between barriers. By using the correct parameters, light from one specific pixel group can only be seen at special viewing positions.

A lenticular lens sheet consists of a linear array of plano-convex cylindrical lenses, which can be combined with traditional 2D displays to realize multiview 3D displays. Fig.1.5 demonstrates the basic configuration of the lenticular multiview display, where the display pixels are also divided into four groups. By a proper design of the lenticular lenses, the light from one pixel group can be refracted towards the same viewing zone, as shown in Fig.1.5. Similar to the barrier technology, depth perception will be created when two eyes are seeing different perspectives of the 3D object.

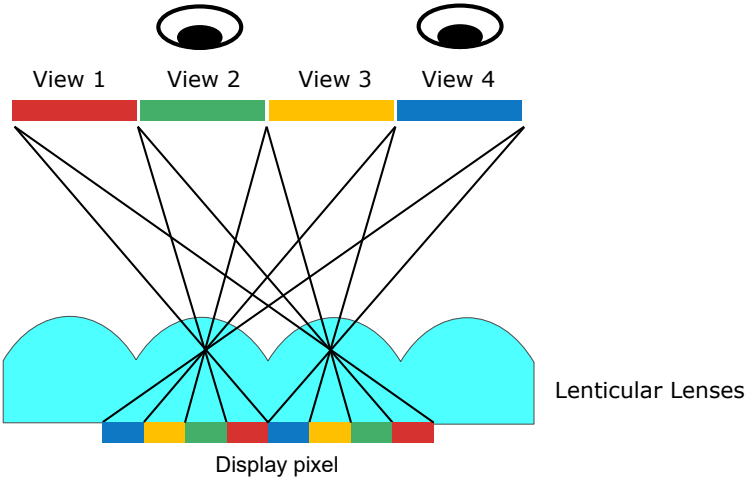

Figure 1.5: Principle of the lenticular lens technology. Light from one pixel group will be refracted into the same direction, forming one view.

Apart from the two mentioned methods, multiview 3D display can also be produced by combining a LCD with a special pattern of diffraction gratings [45, 46]. Fatta *et al.* introduced a multi-directional diffractive backlight to generate full-parallax 3D images for a wide viewing angle [47]. Fig.1.6 illustrates this design concept. Special grating patterns are etched or deposited on the surface of the light guide plate, and will be illuminated by collimated light. As a result of first-order diffraction, light is scattered in a well-defined direction characterized by the diffractive gratings, which can be carefully designed to implement the multiview configurations. By placing a LCD on top of the diffractive backlight,

a 64-view 3D display has been established in the experiments, which can produce 3D images with full motion parallax within 90° viewing angle [47].

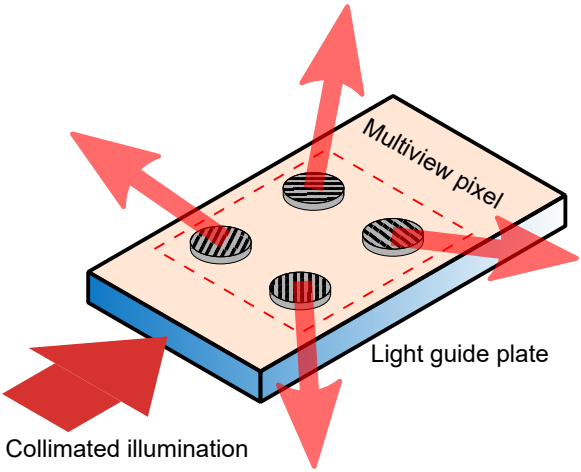

Figure 1.6: Diffractive directional backlight for multiview 3D displays. Special grating patterns are produced on the light guide plate. The incoming collimated light will be scattered towards the designed directions by the diffraction gratings. [47]

Other configurations to build up multiview 3D displays, for example reflection-based and projection-based technologies, will not be further analyzed considering the restricted applications [48, 49]. As for the diffraction-based method, compared with the barrier and lenticular technology, the need of collimated backlight and the fabrication of diffraction gratings have added the implementation difficulty. Furthermore, the diffractive system suffers from the efficiency issue, which is lower than 10% for the diffractive backlight proposed in [47]. These drawbacks have prevented the large commercialization of the diffraction-based multiview display.

Due to the simple implementation, parallax barrier and lenticular lens have been widely used in various 3D display products. For example, the barrier technology can be found in the Sharp mobile phone and the Nintendo 3DS gaming console [50, 51]. The lenticular lenses have been used in the Sony spatial reality display and the 3D TV from Dimenco, Alioscopy, etc. [52–54].

Despite of the large application area, it should be noticed that all multiview technologies share some common disadvantages, and two major issues are:

- **Resolution**: For a display with N views, the resolution of the 3D image is 1/N of the original 2D display. As demonstrated in Fig.1.4(b) and Fig.1.5, the left eye is only able to see the green pixels of the display, so the perceived resolution is 1/4 of the 2D display.
- **Image Flip**: When moving across the viewing zones, the eye perceives a change of the 3D image. The viewer's left eye may see the 3D image intended for the right eye and vice versa. This causes a wrong depth perception and a "flip" artifact, which could confuse the viewer [55].

There are also many other disadvantages, such as the restricted viewing positions, limited number of views, the accommodation-convergence conflict, etc. Both the lenticular and the barrier technology suffer from the listed drawbacks. But the light transmission of the lenticular lenses is much higher than the barrier layer. The transmission of the lens array could easily pass 90%, while at least 50% of the incident light will be blocked by the barrier layer. This property gives the lenticular technology a large advantage in display applications, where the power consumption and the brightness are critical parameters. For example in automotive applications, considering the sunlight illumination, the required display luminance is normally much higher than for indoor displays. And the power consumption should also be carefully controlled since the display will be mounted into the cockpit system, which means the heat dissipation is more challenging than for free-standing displays such as TV and computer monitors. Hence, this work intends to further develop the lenticular technology to improve the 3D display performance.

1.2.4 Introduction of the slanted lens design

Improvements through the slanted lens design

Lots of methods have been suggested to overcome the disadvantages of lenticular 3D displays. In 1997, Berkel *et al.* proposed to use slanted lenses to compensate the image flip at view transitions as well as the resolution reduction [56], which becomes a standard method for almost all lenticular multiview

3D displays. At first Berkel *et al.* built up a 4-view 3D display, where the lenticular lenses are placed parallel to the display panel [57]. As explained before, the image flip can be observed at the transition between two views. This effect is illustrated in Fig.1.7(a), where horizontally seven subpixels are covered under one lens to generate seven views. The LCD Panel is located at the focal plane of the lenticular lenses, so the horizontal distance from the subpixel to the lens side surface corresponds to the viewing angle. Therefore, all points on the dashed line A, which represents view 3, can be seen simultaneously by the eye at one specific viewing angle. Similarly, all points on the dashed line B, representing view 4, will be directed to a different viewing angle. Between line A and B, there would be some positions where only the black mask on the display panel is magnified, and one specific position is represented by the solid line in Fig.1.7(a). Then if the eye is located at the viewing angle corresponding to this solid line, it will see a projection of the black mask, which is a low-intensity image. This can be described as picket fence effect [56]. As a result, when moving across the view transitions, the eye will experience not only a steep change of the 3D image, but also a dark image of the black mask.

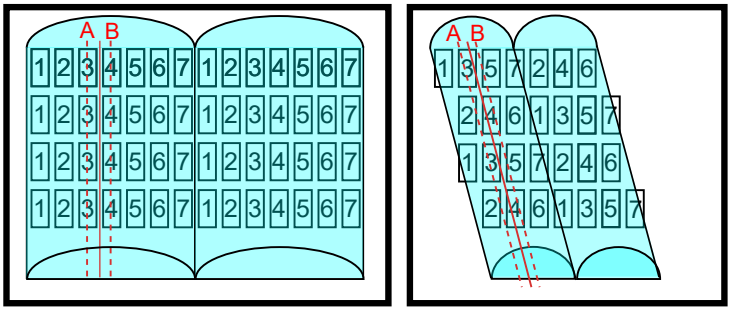

Figure 1.7: Two types of lens array placement: (a) Lens array parallel to the display panel, (b) Lens array slanted to the display panel. The small rectangles represent the display subpixels and the numbers in the rectangle indicate the view number which the individual subpixel belongs to.

Another disadvantage of the parallel placement is the imbalanced resolution reduction. In the horizontal direction, only one out of the seven subpixels under one lens unit can be projected to the eye, as shown in Fig.1.7(a), whereas all pixels in the vertical direction can be simultaneously observed by one eye.

Therefore, in the perceived 3D image, the horizontal resolution is 1/7 of the original horizontal resolution, but the vertical resolution remains the same. Hence, the 3D image has a very asymmetric distribution of resolution.

These two drawbacks can be largely improved using the slanted lens design, which is illustrated in Fig.1.7(b). Same as the parallel placement, seven views will be generated from the system. But the lens array is now slanted to the display panel at an angle of atan(1/6), when the aspect ratio of the subpixel is three to one [56]. Considering that the distance from the subpixel to the lens side surface will determine the viewing angle, all points on the slanted dashed line A will be seen at a specific viewing angle, representing view 3. Then view 4 could be generated by the dashed line B. By taking a close look at line A, it can be observed that although view 3 predominates at the corresponding viewing angle, a small portion of view 2 will still be simultaneously projected. Also at line B, view 4 will predominate with some contribution from view 5. Hence, the eye perception at any viewing angle would be the combination of at least two adjacent views. If the eye is now moving from the viewing angle of line A to the viewing angle of line B, it will perceive a transition in which view 3 gradually fades out and view 4 fades in. The intermediate state is illustrated by the solid line, where view 3 and view 4 contribute roughly the same to eye perception. In this way, a smooth transition between adjacent views can be created. It should also be noticed that the viewing angle, where only the black mask is projected to, disappears with the slanted design. Therefore, the picket fence effect can also be eliminated [56].

Furthermore, the slanted design can also improve the imbalanced resolution reduction. As shown in Fig.1.7(b), the subpixels belonging to one specific view are now more evenly distributed in the horizontal and vertical directions. Therefore, the resolution loss is assigned to both directions, which can provide a better image quality. Berkel has further investigated how the number of views can influence the 3D image resolution, indicating 4-view and 9-view configurations could provide a better visual appearance [58]. Due to the above mentioned improvements, slanted lens design has been widely used in the lenticular multiview displays. Many 3D TV products based on slanted lenticular lenses have already been commercialized, including manufacturer such as Vizio, Alioscopy, RealD, Philips, Sharp, Toshiba and TLC [31].

Crosstalk caused by the slanted lens design

The slanted lens design can significantly increase the performance of lenticular multiview displays. However, the price to be paid for the improvement is that there is now crosstalk between the views [56, 59]. The term "crosstalk" can be explained with Fig.1.8. The green curve represents the intensity distribution of view 3 at different viewing angles, which is obtained by moving the camera on the observation plane. During the camera recording, only subpixels of view 3 are turned on in the display panel, whereas subpixels of all other views are turned off. The dashed line A marks the viewing angle where view 3 shows the highest intensity. In the same way, intensity distribution of view 4 can also be registered, which is plotted as the yellow curve in Fig.1.8, and the peak position is demonstrated by the dashed line B. Then it's assumed that the left eye is located at line A, and the right eye is at line B. As a result, the left eye sees predominantly view 3, but view 4 can still be perceived with a lower intensity. Then crosstalk at line A can be defined as the ratio of view 4 intensity to view 3 intensity, which is considered as a critical parameter in 3D image quality.

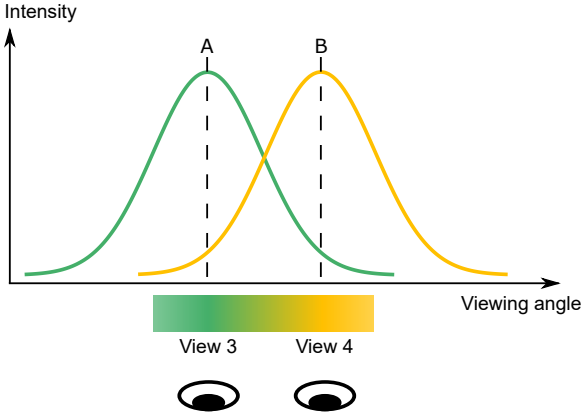

Figure 1.8: Demonstration of the crosstalk caused by the slanted lens design. The horizontal axis stands for the viewing angle, and the vertical axis represents the measured view image intensity. View 3 is depicted by the green curve and view 4 is described by the yellow curve. At the viewing angle with the highest view 3 intensity, which is marked by the dashed line A, a certain intensity of view 4 can still be observed. This leads to the crosstalk in the perceived 3D image, which can affect the depth perception.

As illustrated in Fig.1.8, the left eye sees mainly view 3 and the right eye sees primarily view 4. To create the desired depth perception, there should be a disparity between the two views. However, due to crosstalk, the left eye is now also able to see view 4, which should only be observed by the right eye. This effect could significantly reduce the image quality and visual comfort [60]. Moreover, the influence of crosstalk will rise with the increase of disparity between the left eye view and the right eye view, when a large object depth should be created [61]. A small amount of crosstalk can lead to headaches under a big view disparity. Therefore, the crosstalk will limit the degree of depth that is allowed to be implemented in the 3D display. The experiments carried out by Kooi *et al.* show that 5% would be the threshold value for an acceptable crosstalk, while a crosstalk higher than 25% can extremely reduce the viewing comfort [62].

The typical crosstalk of current lenticular multiview 3D displays is higher than 20% [63], which indicates a huge degradation of image quality and depth perception. Hence, a lot of studies have been carried out to reduce the crosstalk caused by the slanted lens design. Li *et al.* proposed a weighting method to adjust the intensities of the corresponding subpixels from the two neighboring view images, which can effectively reduce the crosstalk [64]. Moreover, active crosstalk reduction based on the eye-tracking camera has been investigated by many studies. Nam *et al.* proposed to find out the luminance profile of the 3D display in advance, and then calculate the most appropriate color value according to user's eye position. This method could reduce the crosstalk from 19.1% to 2.6% [63]. Furthermore, some studies suggested to use eye-tracking to detect eye position and dynamically adjust the view mapping, where the image assigned to all viewing zones will be decided in real time [65–67]. And the crosstalk can be reduced below 5% through the dynamic view mapping [66].

Remaining issues of the slanted lens design

The reduction of crosstalk has been discussed in the previous subsection, but there are still several issues that require improvement in the context of lenticular multiview displays. The use of slanted lens design can largely improve the 3D image quality, especially in terms of the imbalanced resolution and the image flip. However, it should be noticed that the slanted lens design can only alleviate the two problems, and these two issues will continue to degrade the system

performance. Although the resolution reduction can be distributed into the horizontal and vertical directions, the overall resolution of the final view image is still reduced by a factor equal to the number of views N, since only one out of N subpixels will be used to create one specific view image. Dodgson analyzed how the number of views could influence the image perception, and pointed out that at least six views are necessary to create a comfortable viewing experience [68]. This indicates that the resolution of the 3D image is normally less than 1/6 of the original resolution, which is a large degradation. Some studies proposed to use liquid crystal lens to achieve 2D/3D switchable display, where the focal length of the lens can be dynamically adjusted [69–71]. Similar 2D/3D switching concepts have also been realized by using electrowetting lenticular lens [72, 73]. Although in 2D mode the eye can obtain the original resolution of the display, the view image resolution in 3D mode will still be reduced to 1/N of the original display.

Regarding the image flip issue, slanted lens design can create a smooth transition between adjacent views. But another flip effect would still exist between the central viewing zone and the side viewing zones. The formation of different viewing zones is illustrated in Fig.1.9. The display pixel array is positioned at the focal plane of the lenticular sheet, and one red subpixel is turned on to represent one view. As shown in the figure, the light coming from the red subpixel is initially diffuse, so it can meet multiple lenses. Then the light will be collimated towards different directions at different lenses, depending on the distance between the subpixel and the optical axis of the corresponding lens. Therefore, the lens array will project one view image from the display panel into different angles, which can be described as side leak or side lobe [74].

In Fig.1.9, one view is used to illustrate the side leak, which makes the view image appear periodically on the observation plane. Based on this knowledge, the view distribution of a 5-view 3D display can be demonstrated in Fig.1.10, where all five views will repeat themselves. View 1 to view 5 near the centerline of the display form the central viewing zone, and the other repeating views towards two sides will create side viewing zones. As previously explained in Fig.1.3, five perspectives of the 3D object will be assigned to the five views, so the eye at each view can observe a different 3D image. When the two eyes are located within one viewing zone, as indicated by the two blue eyes in the central viewing zone, two proper perspectives can be projected into the eyes and the designed 3D depth perception is achieved. However, the user could also move to

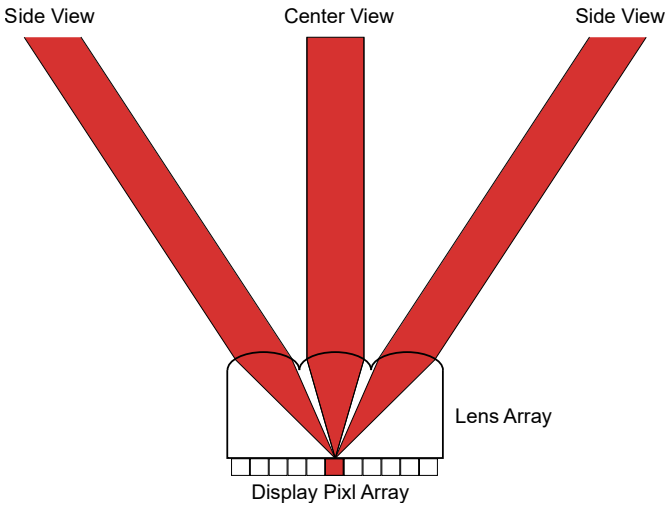

Figure 1.9: Demonstration of the side leak effect of a lens array: The display pixel array is located at the focal plane of the lenticular sheet, so the diffuse light coming from one red subpixel will meet multiple lenses, and get collimated into different directions.

the boundary between two viewing zones, as represented by the two green eyes in Fig.1.10. In this situation, the left eye is seeing the rightmost perspective of the 3D object, whereas the right eye is seeing the leftmost perspective, which could lead to a reverse depth perception. Although this drawback can be improved by increasing the number of views and optimizing the configuration of view images, it's not able to eliminate the image flip between two viewing zones.

When the 3D display is limited to single user applications, some studies have proposed to track the eye position in real time, and conduct the dynamic assignment of the view image to overcome the image flip [75,76]. However, extending the suggested methods to multi-user applications still faces significant challenges.

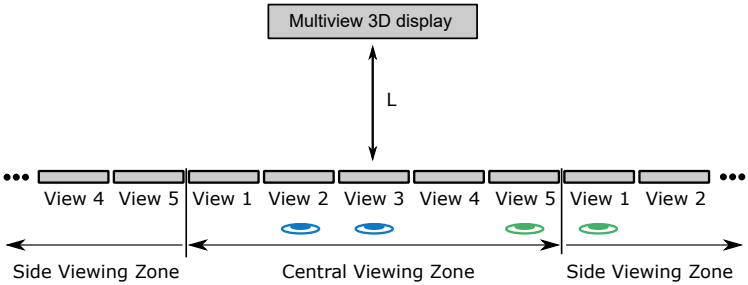

Figure 1.10: Image flip effect between different viewing zones, indicated by the two green eyes. The left eye will see the rightmost perspective and the right eye will see the leftmost perspective, leading to a wrong 3D perception. When moving across the transition zone, the eye will experience a significant change of the view image.

1.2.5 Introduction of the directional backlight based on time-multiplexing

To further improve the resolution loss and the image flip of lenticular multiview displays, time-multiplexing methods have been recently investigated in some studies [77–79]. Time multiplexing is based on the persistence of vision, which refers to the phenomenon that the visual perception of an object will remain for a certain time after the light rays from that object have stopped to enter the eye [31, 80]. Therefore, even if the light from the object is entering the eye discontinuously with dark intervals in between, the eye is still able to fuse the bright and dark impressions together into a continuous perception of that object, when the frequency of the light incidence is higher than the threshold of the visual system. Generally 60 Hz is considered as the threshold to provide a comfortable and steady observation.

Time-multiplexing method has already been widely applied in various 3D display technologies. For stereoscopic technology, active Liquid Crystal (LC) shutter glass can be used to enable time multiplexing by regularly modulating the LC transmission, so that the left eye and the right eye can get the corresponding view image from the display at different frames. The active LC shutter glass has been commercialized in the cinema [81], in TV [82] and many other products, since this method can reach the full spatial resolution of the monitor or projector. As for the multiview technology, Lee *et al.* proposed to use an

extra LCD as the active barrier layer [83]. At one specific display frame, one eye is still only able to see 50% of the entire pixels. In the next frame, by adjusting the pattern demonstrated on the active LCD barrier, the eye can then see another 50% pixels, which are invisible in the previous frame. Under a high display switching frequency, the eye is able to fuse these two frames into one full resolution image.

In 2011, Liou *et al.* has proposed a time-multiplexing multiview 3D display based on lenticular lens array combined with an active dynamic LED array [80]. The basic structure is shown in Fig.1.11. Unlike the traditional design, the LCD panel without backlight unit is now located on top of the lens sheet, while an extra LED array is placed on the focal plane of the lens array. So the light coming from one LED pixel will be collimated by the lens above, as demonstrated in Fig.1.11. As a result, the LCD pixels on top of this lens will be illuminated into a certain direction, which is determined by the relative horizontal position of the LED pixel regarding the corresponding lens. Then the LED pixels can be classified into one group, when they have the same relative horizontal position to their upper lenses. By activating one group of LED pixels, the whole LCD panel will be illuminated towards one direction, as shown in Fig.1.11. Therefore, the LCD can be projected into multiple directions, by switching different groups of LED pixels. The lens sheet coupled with the LED array would create a new Directional Backlight (DB), which can provide a directional illumination for the subsequent system.

Based on the proposed DB, Liou *et al.* has demonstrated a 4-view autostereoscopic display with time multiplexing [80]. The frame configuration is illustrated in Fig.1.12, where a whole display frame with 1/60 second (around 16.67 milliseconds) is divided into four subframes with 1/240 second (around 4.17 milliseconds) duration respectively. In each subframe, a different view image will be shown on the LCD panel. The LCD is hence described as image LCD. The lens array together with the LED array are simplified into one DB unit in Fig.1.12. Different groups of LED pixels will be activated in each subframe, so the view image can be illuminated into different directions. As a result, a 4-view 3D display can be realized, which has the same functions as the lenticular multiview display demonstrated in Fig.1.5. Through a proper optical design, the left eye and the right eye of the user will enter different viewing zones, and observe two different view images to acquire the depth perception. Although the eye at one viewing zone will see the corresponding

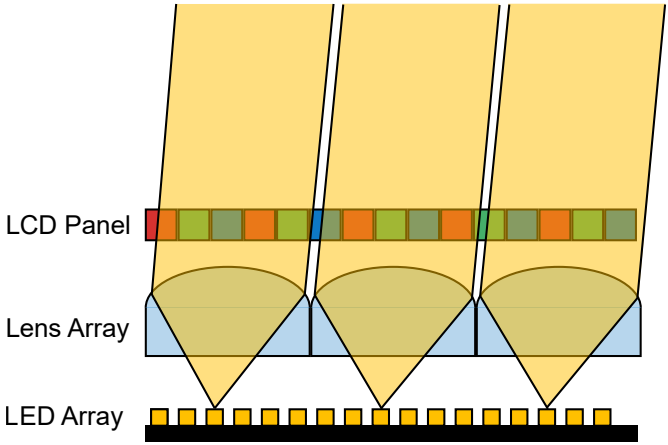

Figure 1.11: Structure of the time-multiplexing 3D display based on the directional backlight, which consists of a lens array and a newly introduced LED array. By turning on one specific group of LED pixels, the whole LCD panel will be illuminated into the same direction. [80]

view image only for 1/240 second during one display frame with 1/60 second, the eye is still able to fuse the perceived images into a continuous observation due to persistence of vision. To realize this function, the refresh rate of the image LCD should achieve 240 Hz.

With the suggested DB and time-multiplexing concept, the 4-view 3D display can provide a full-resolution view image to the eye [80]. In each subframe, the whole image LCD will be projected into one viewing zone. So the eye at one viewing zone is able to perceive all pixels of the image LCD, which enables the perception of a 3D view image with full resolution of the original LCD panel. This is a huge improvement compared with the conventional multiview technologies. But the new multiview 3D display with DB still suffers from image flip between the central and side viewing zones, because the side leak also exists between the lens sheet and the LED array. Similar to the side leak shown in Fig.1.9, the diffuse light from one LED pixel in DB will meet multiple lenses and get collimated into multiple directions. As a result, one view image on LCD will be illuminated into different angles in one subframe, which leads to the side leak and the image flip.

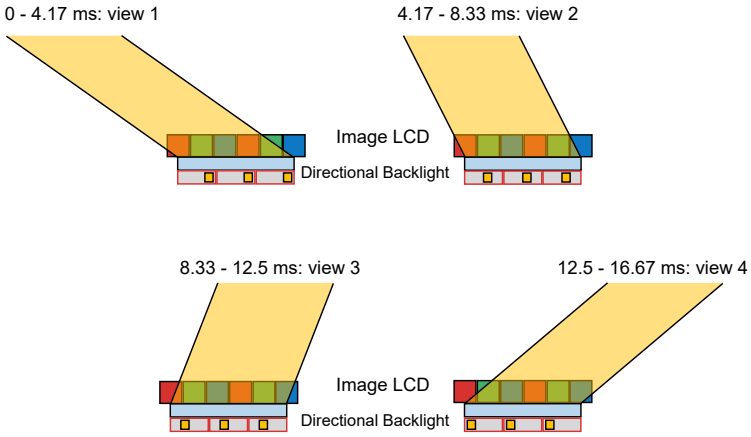

Figure 1.12: Frame configuration of the time-multiplexing 3D display with the directional backlight. A whole display frame takes 1/60 second, which is divided into four subframes with respectively 1/240 second duration. Four different view images will be shown on the LCD panel in each subframe. By activating different groups of LED pixels, the directional backlight can project the view image into different directions [80].

Various methods have been developed in the past decade to improve the DB technology [84–86]. Yang *et al.* demonstrated a time-multiplexing autostereoscopic display based on a similar DB concept, where an eye-tracking device was proposed to improve the 3D performance [87]. A 120 Hz LCD is required to create two subframes for the time multiplexing. In the first subframe, the left eye position of the user will be detected, then the desired image for the left eye will be shown on the image LCD, and the DB will be configured to illuminate the image LCD towards the left eye. Similarly, in the second subframe, the DB will illuminate the intended image to the user's right eye. In this case, the left eye or the right eye can always perceive the desired view image, independent on the eye position. There is no more predefined spatial distribution of view images. This can solve the image flip for single user application. However, the side leak will still lead to conflicts in the multi-user observation, which is further illustrated in Fig.1.13. As explained before, when one group of LED pixels is activated in the DB, the view image on LCD will be illuminated into multiple directions. The right eye of user 1, indicated by the color blue, is located in direction 1. Assuming that the left eye of user 2, indicated by the

color green, is also located in direction 1. This means when one image should be sent to the right eye of user 1, this image will be simultaneously perceived by the left eye of user 2, and vice versa. This conflict would degrade the 3D perception quality in multi user applications.

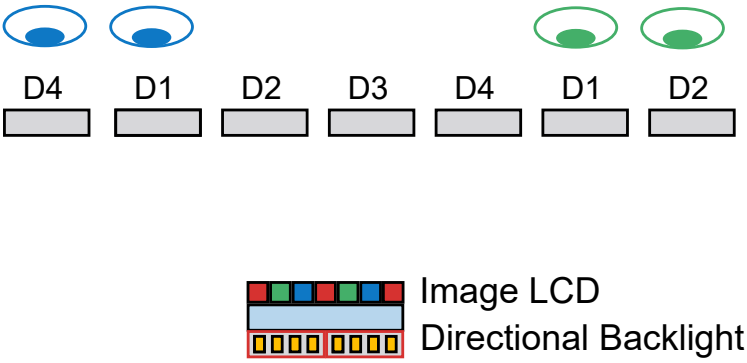

Figure 1.13: Demonstration of the view conflict in multi-user applications due to the side leak. "D" in the figure stands for illumination direction, when one specific group of LED pixels is turned on in the DB. User 1 is indicated by the two blue eyes, and the right eye is located in direction 1. User 2 is described by the two green eyes, and the left eye is also located in direction 1. This leads to the right eye of user 1 seeing the intended content for the left eye of user 2, and vice versa.

To get rid of the side leak and enable a high quality multi-user application, Miyazaki proposed an adapted DB concept in 2014, which consists of a parallel light source and a steering optical system [88]. The parallel light source can provide parallel light emission in a spatially-controlled pattern, realized by a DLP projector combined with a Fresnel lens. The light from the light source will then enter the steering optical system, consisting of a slanted cylindrical lens array and vertical diffusers. Because the light will propagate into the cylindrical lens in a collimated form, it can be achieved that only one lens will be illuminated by an individual light pattern. Therefore, the side leak can be completely eliminated, and it's able to create a better multi-user observation without view conflict. Nevertheless, this new DB concept requires a large construction space, which is over one meter for the demonstrated prototype [88]. Considering the construction space and the low light efficiency, this DB concept still has a long way to go before commercialization.

Furthermore, several studies proposed to use stacks (multiple layers) of thin cylindrical lenses to build up DB for multi-user applications [89,90]. However, the large construction space and the illumination non-uniformity should be further improved before it can be widely applied. In this section, the DB concepts based on the lens array have been analyzed. It is important to note that various alternative methods have also been developed to modulate the backlight illumination direction, such as employing a special light-guide plate [91–93]. However, these methods still encounter the challenge of the image flip during the user movement.

1.2.6 Summary of existing 3D display technologies and their limitations

The drawbacks of the discussed 3D display technologies are listed in Tab.1.3. It should be pointed out that there is still a large number of other different technologies to build a 3D display, and this section intends to analyze some typical methods to give an overview of each field. As explained before, the multiview technology has been widely applied due to its simple implementation and the compatibility with conventional 2D displays. This work aims to further develop the lenticular multiview technology due to its high transmission, which is beneficial in many applications.

The use of a slanted lens array can improve the imbalanced resolution reduction and the image flip between adjacent views. However, as already discussed, these two drawbacks cannot be completely eliminated by the slanted design. The overall resolution of a view image is only 1/N of the original display panel. The image flip will still appear between the central viewing zone and the side viewing zones.

DB has been recently proposed to create a full resolution view image through time multiplexing [80]. The lens array and an extra LED array make up the DB, whereas the image LCD is placed on top of the lens array. By activating different groups of LED pixels, the DB can illuminate the whole upper LCD into different directions. Therefore, the eye at one direction can see all pixels of the LCD in one subframe, hence receiving the full resolution of the LCD.

Table 1.3: Limitations of some existing 3D display technologies

Technology	Limitations
Stereoscopic display	Requirement of wearing special eyeglasses.
Volumetric display (rotating LEDs)	High speed movement, low resolution.
Volumetric display (multiple LCD)	Low System efficiency
Digital-holography	Large amount of data processing.
Multiview Display (MVD) (common drawbacks)	Resolution Reduction, image flip, limited viewing positions.
Barrier based MVD	At least 50% brightness loss.
Diffraction based MVD	Low efficiency, expensive components.
Slanted lenticular MVD	Crosstalk between viewing zones.

The DB concept can be combined with eye-tracking, so that each eye of the user can always get the intended view image [87]. For single user observation, the image flip during head movement can be completely eliminated. But the new DB concept still suffers from the side leak between the LED pixels and the lens array, that the light rays coming from one LED pixel will meet multiple lenses and get collimated into different directions. As demonstrated in Fig.1.13, the side leak will lead to the projection of the image LCD into multiple directions in one subframe, which could cause view conflict between multiple users.

To enable high quality multi-user applications, some new optical designs have been suggested [88, 89]. However, the proposed concepts generally require a large construction space, and suffer from illumination non-uniformity, which are still far away from the commercialization. After going through the recent development progress of the lenticular DB, it can be seen that there is high demand of a new compact DB design, which can eliminate the side leak and provide excellent multi-user viewing experience. Development of such a new DB is also the motivation of this work. In the subsequent sections, conception, modeling, simulation and construction of the new DB will be explained respectively.

2 Concept

This chapter will describe the modeling and configuration of the new proposed system concept. At first a quantitative model of the original directional backlight will be established to observe the side leak effect. Then one additional LC layer will be introduced into the system to eliminate the side leak. The position of the added LC layer and its modulation will be subsequently discussed.

2.1 System modeling of the original directional backlight concept

2.1.1 Model of the lenticular lens

In the directional backlight concept, the LED array is located on the focal plane of the lens array. According to the position of the LED pixel on the focal plane, the lens can collimate the incident light from one LED pixel into the intended direction. Because the lens array lays the foundation of the directional backlight, the lens design will be first analyzed in the system modeling.

As mentioned before, the lenticular lens is a plano-convex cylindrical lens. The thin lens model is not applicable to the lenticular lens, because normally the lens thickness cannot be ignored compared to the lens radius. Therefore, the thick lens model should be used to describe the lens array, with one general model demonstrated in Fig.2.1.

The deduction process of the lens parameters will be skipped in this section, since this topic has been extensively covered in various publications. Based on the calculation demonstrated in one book [94], Eq.2.1 to Eq.2.4 can be obtained:

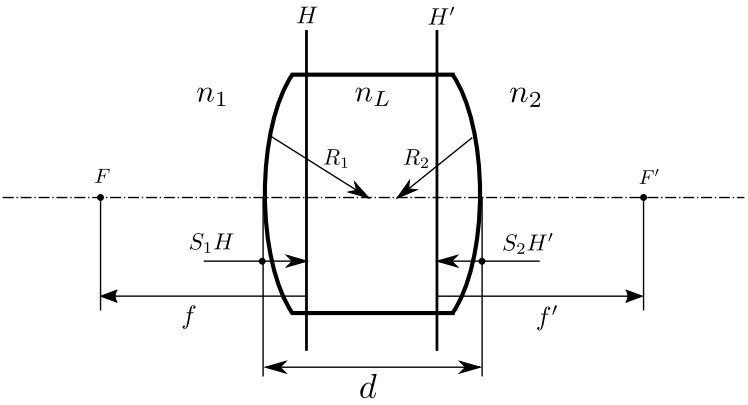

Figure 2.1: Thick lens model. F, F': front and rear focal points. f, f': front and rear focal lengths. H, H': front and rear principal planes. S_1H, S_2H': Distance from the front/rear lens vertex to the front/rear principle plane. R_1, R_2: front and rear radii. n_1, n_L, n_2: refractive index of the front medium, lens, and rear medium. d: thickness of the lens.

$$f' = \frac{n_L \cdot n_2 \cdot R_1 \cdot R_2}{(n_2 - n_L) \cdot (n_L \cdot R_1 - d \cdot n_L + d \cdot n_1) + R_2 \cdot n_L \cdot (n_L - n_1)} \tag{2.1}$$

$$f = \frac{n_L \cdot n_1 \cdot R_1 \cdot R_2}{(n_1 - n_L) \cdot (n_L \cdot R_2 - d \cdot n_L + d \cdot n_2) + R_1 \cdot n_L \cdot (n_L - n_2)} \tag{2.2}$$

$$S_2H' = \frac{R_2 \cdot n_2 \cdot (n_L - n_1) \cdot d}{(n_2 - n_L) \cdot (n_L \cdot R_1 - d \cdot n_L + d \cdot n_1) + R_2 \cdot n_L \cdot (n_L - n_1)} \tag{2.3}$$

$$S_1H = \frac{R_1 \cdot n_1 \cdot (n_L - n_2) \cdot d}{(n_1 - n_L) \cdot (n_L \cdot R_2 - d \cdot n_L + d \cdot n_2) + R_1 \cdot n_L \cdot (n_L - n_2)} \tag{2.4}$$

In the real application, $R_1 \rightarrow \infty$ will be assumed because the lens front surface is a plane. And air will be supposed to exist at the right side, leading to $n_2 = 1$. By introducing the two substitutions, $R_1 \rightarrow \infty$ and $n_2 = 1$, into Eq.2.1 to 2.4, the expressions can be further simplified:

$$f' = \frac{R_2}{1 - n_L} \tag{2.5}$$

$$f = \frac{n_1 \cdot R_2}{n_L - 1} \tag{2.6}$$

$$S_2H^{'} = 0 \tag{2.7}$$

$$S_1H = \frac{n_1}{n_L} \cdot d \tag{2.8}$$

Based on Eq.2.7, the model of a lenticular lens can be adapted, as demonstrated in Fig.2.2.

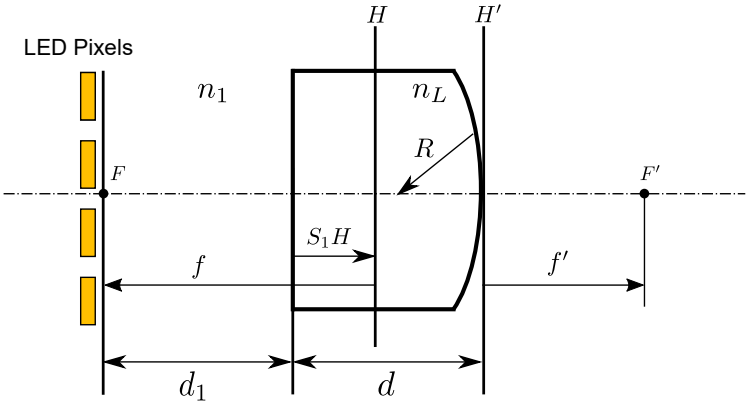

Figure 2.2: Model of the lenticular lens. LED pixels are located on the front focal plane, and d_1 stands for the distance between the LED pixels and the lens front surface.

2.1.2 Determination of the lens parameters

With the established lens model, parameters of the lenticular lens can be determined by analyzing the view distribution. It should be pointed out that several studies have already described the deduction process, from which valuable insights will be incorporated into this subsection [95]. For the lens design, some system parameters need to be defined in advance, which can be called "Given Parameters". The four given parameters are listed in Tab.2.1. Then the lens parameters, that should be decided through the system modeling, are summarized in Tab.2.2.

Table 2.1: Given Parameters for the lens array modeling

L	Optimum viewing distance, from the eye to the lens array.
a	Distance between two adjacent viewing directions
m	Number of viewing directions
t	LED pixel pitch

Table 2.2: Parameters of the lens array to be decided

d_1	Distance from the LED pixel to the lens front surface
n_1	Refractive index of the front medium
d	Lens thickness
n_L	Refractive index of the lens
R	Radius of the lens curvature
p	Lens pitch

The radius R will be first determined with the help of Fig.2.3. Two LED pixels are located on the front focal plane of the lens to generate the first and the second illumination direction, D_1 and D_2. One green ray and one blue ray, originating from the center of the two LED pixels, are drawn in the figure to represent the light propagation. Both rays are parallel to the optical axis. Because the green LED pixel is assumed to be located on the optical axis, the green ray will leave the lens without direction change. The blue ray will

be refracted towards the rear focal point F' and then proceeds in the second illumination direction.

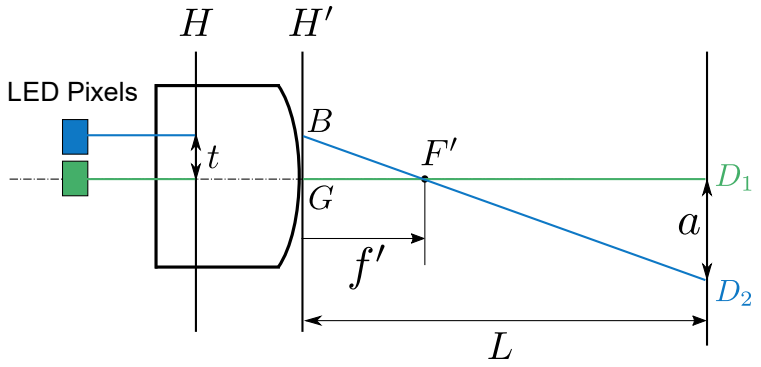

Figure 2.3: Illustration of the system parameters to determine the lens radius. The image LCD is not drawn in the figure because it will mainly affect the light transmission, whereas its influence on the light propagation direction can be neglected.

In Fig.2.3, the two triangles $\triangle F'GB$ and $\triangle F'D_1D_2$ are similar. The length of legs in the two right triangles can be expressed as:

$$F'G = f', BG = t, F'D_1 = L - f', D_1D_2 = a. \tag{2.9}$$

According to the similarity theory, Eq.2.10 can be obtained:

$$\frac{BG}{D_1D_2} = \frac{F'G}{F'D_1}. \tag{2.10}$$

Combining Eq.2.5, Eq.2.9 and Eq.2.10, the radius R can be deduced:

$$R = \frac{L \cdot t \cdot (n_L - 1)}{a + t}. \tag{2.11}$$

In the next step, the lens pitch p should be calculated. The geometrical relationship between the LED pixel pitch and the lens pitch is demonstrated in Fig.2.4. It is assumed that the light from the center of every red pixel will be refracted into the illumination direction D_1. For simplification only one ray parallel to

the optical axis will be drawn in the figure to represent the light propagation. For lens 0 at the bottom of the figure, the red pixel is supposed to be located on the optical axis, so the emitted ray will propagate to D_1 without direction change. For lens n on the top of the figure, the light of the corresponding red pixel should also be sent to D_1. A proper relative position P_nV_n, which is the distance between the n^{th} red pixel and the optical axis of lens n, is required to refract the light towards D_1.

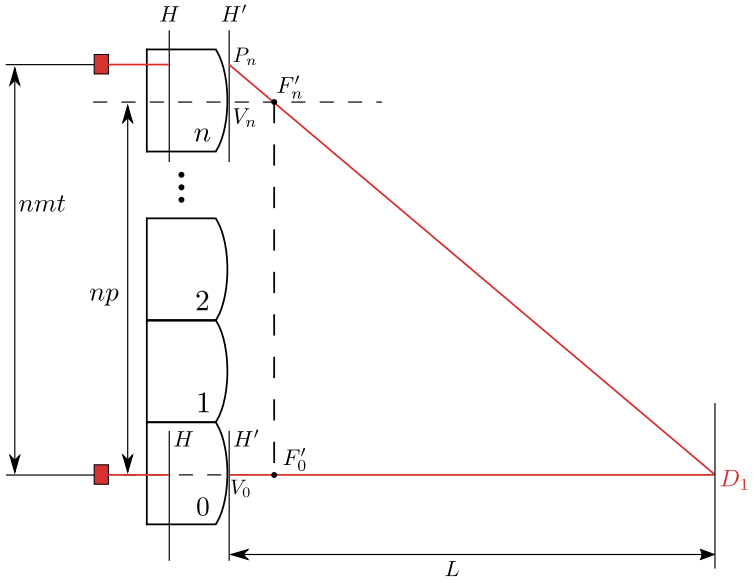

Figure 2.4: Geometrical analysis of the lens pitch. It is assumed that the light generated from the center of every red pixel will be sent to the illumination direction D_1.

The length of P_nV_n can be expressed as:

$$P_nV_n = n \cdot m \cdot t - n \cdot p, \tag{2.12}$$

where m represents the number of illumination directions, and t represents the LED pixel pitch. So the term $m \cdot t$ stands for the length of one LED pixel unit, which is the sum of every individual LED pixel pitch.

In Fig.2.4, the two triangles $\triangle P_n V_n F_n'$ and $\triangle F_n' F_0' D_1$ are similar. The length of other three legs in the two right triangles can be expressed as:

$$F_n' V_n = f', F_n' F_0' = n \cdot p, F_0' D_1 = L - f'. \tag{2.13}$$

According to the similarity theory, Eq.2.14 can be derived:

$$\frac{P_n V_n}{F_n' F_0'} = \frac{F_n' V_n}{F_0' D_1}. \tag{2.14}$$

Combining Eq.2.12, Eq.2.13 and Eq.2.14, the lens pitch p can be determined:

$$p = \frac{a}{a+t} \cdot m \cdot t. \tag{2.15}$$

The last step is to determine the thickness of each layer. Because the LED pixels should be located on the focal plane of the lens, following condition has to be fulfilled:

$$f = d_1 + S_1 H. \tag{2.16}$$

Based on Eq.2.8, Eq.2.11 and Eq.2.16, Eq.2.17 can be obtained to deduce the layer thickness:

$$\frac{d_1}{n_1} + \frac{d}{n_L} = \frac{L \cdot t}{a+t}. \tag{2.17}$$

d_1 and n_1 are the thickness and refractive index of the front medium, while d and n_L describe the lens thickness and refractive index. In the system design, n_1 and n_L would be first determined by specifying the material. Then different combinations of d_1 and d are feasible when Eq.2.17 can be satisfied.

2.2 Description of the side leak effect

This section will describe the side leak effect based on one assumed directional backlight system. To provide a quantitative demonstration, real values should be assigned to the system parameters. The first step is to determine the given system parameters, which are demonstrated in Tab.2.3. It should be noticed

that the parameters in Tab.2.3 are created only to demonstrate the side leak, and they do not correspond to the real application. According to the established system modeling, the lens parameters can be calculated, and then listed in Tab.2.4. As explained before, various combinations of d_1 and d are possible to build up the system, and two example values are shown in Tab.2.4.

Table 2.3: Given parameters of the example directional backlight system

L	a	m	t	n_1	n_L
600 mm	30 mm	6	1 mm	1.5	1.5

Table 2.4: Deduced parameters based on system modeling (unit in mm)

R	p	$d_1 + d$	d_1 (example)	d (example)
9.68	5.81	29.03	15	14.03

Based on the calculated parameters, a scalable diagram of the example direction backlight can be demonstrated in Fig.2.5. There are now six individual LED pixels under one lens, which can be referred as one LED pixel unit. The leftmost LED pixel is aligned with the edge of the leftmost lens. The period of one LED pixel unit is 6 mm, which is larger than the lens period. Therefore, after six units, there would be a noticeable shift between the rightmost LED pixel and the edge of the rightmost lens.

As previously mentioned, the emitting light from one LED pixel is diffuse and it will propagate in all directions. The LED emission characteristic can be described by the relative illuminance over radiation angle. By going through the product specification of LEDs used in different applications [96], the 50% relative illuminance will appear approximately between 50° and 60° radiation angle. And the relative illuminance will drop rapidly at larger angles. If 60° is taken to analyze the light emission, the number of illuminated lenses within ±60°can be calculated:

$$\frac{2 \cdot (d_1 + d) \cdot \tan 60°}{p} \approx 17. \tag{2.18}$$

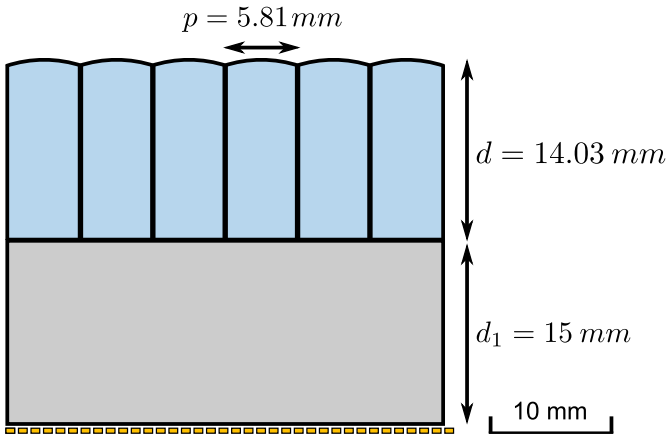

Figure 2.5: Scalable diagram of the example directional backlight. Six lens units and six LED pixel units are drawn in the figure.

So at least 17 lenses will be illuminated when one LED pixel is turned on, which leads to 17 illuminated zones. The distance between two adjacent zones is 180 mm, which can be obtained through $m \cdot a$. To further analyze the side leak effect, two special zones are illustrated in Fig.2.6, where every second LED pixel (seen from the left side) within one LED pixel unit is turned on. For simplification only four lenses and three LED pixel units are drawn in the figure. The green light rays from the LED pixels will hit the left neighboring lenses, generating the green illuminated zone at the designed viewing distance. The blue light rays will meet the right neighboring lenses and get collimated towards the blue zone. Then the distance between two zone centers would be 360 mm. This means if every second LED pixel is activated, both the green zone and the blue zone will be lighted up. As a result, the eyes at these two zones can always simultaneously see the content on the image LCD. View conflict would appear between two users, when one eye of the first user is located within the green zone, and one eye of the second user is located within the blue zone.

Fig.2.6 only demonstrates one possible situation of view conflict, where the light rays towards the left neighboring lens and the right neighboring lens will create two illuminated zones. According to Eq.2.18, the light from one LED

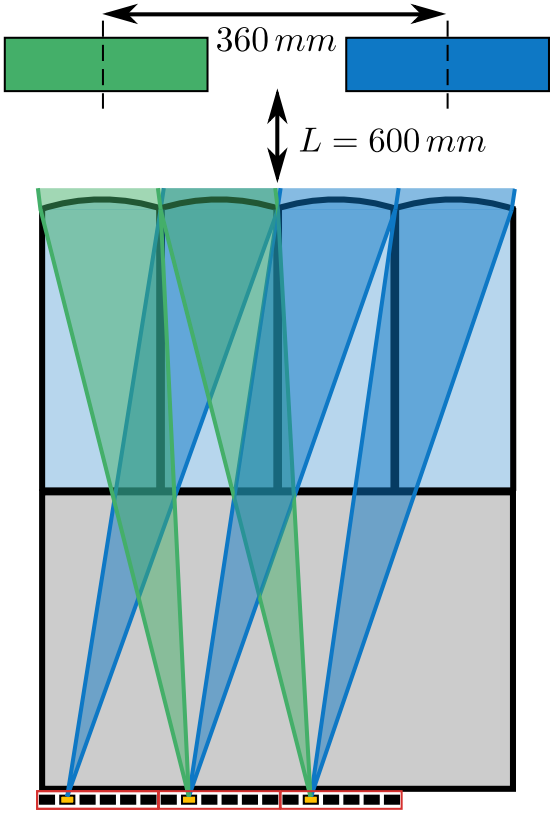

Figure 2.6: Demonstration of two simultaneously illuminated zones caused by the side leak. Every second LED pixel (seen from the left side) within one LED pixel unit is activated. Light rays towards the left neighboring lenses will create the green zone, while the rays to the right neighboring lenses will form the blue zone.

pixel is able to hit more than 17 lenses, thus creating over 17 illuminated zones. If the eyes of different users are located within these illuminated zones, view conflict will also appear. In the next section, the view conflict illustrated in Fig.2.6 will be first studied to show the design principle, and other conflict situations will be subsequently taken into consideration.

2.3 Elimination of the side leak by using one additional liquid crystal layer

The DB model established in the last section will still be used in this and the following sections to demonstrate the new concept. In Fig.2.6, two conflict zones are created from the green light rays and the blue light rays, which propagate respectively towards the left and the right neighboring lens. As a result, it is impossible to send two different image contents to these two areas. The view conflict can only be solved through an independent control of the green rays and the blue rays. This means in one display subframe, the LED pixel will only emit the green rays whereas the blue rays should not exist. In this way, the image LCD will only be illuminated into the green zone. Then in the next display subframe, the LED pixel will only emit the blue rays while the green rays should disappear. However, because the light emission of the LED pixel is diffuse, the independent control of different light rays cannot be reached in the original concept.

This work proposes to use an additional LC layer to achieve the independent control of light rays. As demonstrated in Fig.2.7, an extra LC layer (without backlight) is inserted between the lens array and the LED matrix backlight. Since the key function of this LC layer is to selectively block the emitted light rays from LED pixels, it can be described as “Barrier LCD”. A special white-black image pattern is shown on the barrier LCD, and it is assumed that the refractive index of the major components in the barrier LCD is also 1.5. Referring to Fig.2.7 (a), the green light rays can propagate through the white pattern without direction change, and they will continue to hit the left neighboring lenses. On the contrary, the blue light rays will be blocked by the black pattern on the barrier LCD. Hence the light from one LED pixel will not hit its right neighboring lens. In this way, the green illuminated zone at the optimal viewing distance will still be created, with the blue zone being eliminated through the barrier LCD. Another configuration of barrier LCD is shown in Fig.2.7(b), while the blue rays can propagate through the barrier LCD whereas the green rays will be blocked by the black pattern.

This new system concept with barrier LCD is able to solve the view conflict caused by the side leak. For the white-black image pattern demonstrated in Fig.2.7(a), the directional backlight can provide the illumination only to the green zone, while the light rays for generating the blue zone will be blocked. If

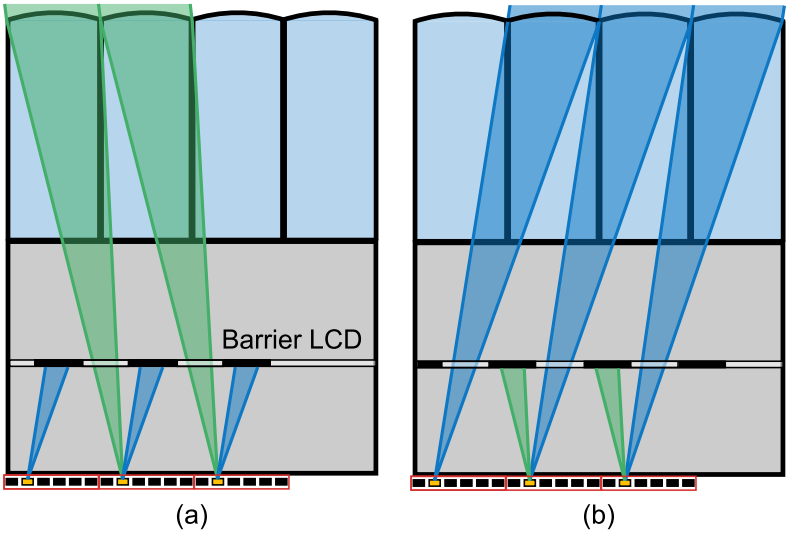

Figure 2.7: Use of one additional LC layer to selectively block the emitted light rays from LED pixels. By showing the proper black-white image pattern on the extra LC layer: (a) The green light rays can maintain their original propagation directions, and the blue light rays will be blocked. (b) The blue light rays can maintain their original propagation directions, and the green rays will be blocked.

one eye is currently located in the green zone, the intended image content for this eye can be shown on the image LCD. During this subframe, only the eye in the green zone can see the desired image. Then in the next subframe, a reverse white-black pattern can be shown on the barrier LCD, which should block the green rays while allow the blue rays to maintain the original propagation, as shown in Fig.2.7(b). The image LCD will only be projected to the blue zone during this subframe. Hence, the system is able to send one certain image only to the eye in the blue zone.

Fig.2.7 has demonstrated that the new proposed barrier LCD is able to selectively block the unwanted light rays from the LED pixel. As a result, the view conflict between two view zones, which are 360 mm away from each other, can be eliminated in the assumed DB system. This improvement makes it possible to generate a better multi-user viewing experience.

Suppose that two viewers are observing the display, and the eye positions can be obtained through eye-tracking device. Then four subframes are necessary to send four different images to the corresponding eyes. The system configuration of each subframe is illustrated in Fig.2.8. To indicate the function of the barrier LCD, it is assumed that the right eye of the green user and the left eye of the blue user are both located within the same illumination direction "D1", where the distance between these two eyes would be around 360 mm. Considering that the average pupillary distance is 65 mm and the space between two adjacent viewing directions is 30 mm, the position of other eyes can be determined and drawn in Fig.2.8.

Regarding the configuration of the image LCD, the intended image content for the four eyes should be successively shown on the image LCD in four subframes. Then the barrier LCD and the LED array need to be properly adjusted to provide the required illumination. In the first subframe, every fifth LED pixel will be turned on. For simplification, only one LED pixel unit is drawn in the LED array in Fig.2.8. Since view conflict doesn't exist for D5, the barrier LCD can be set to a white image. But in the second and third subframe, different white-black patterns should be shown on the barrier LCD to block the unwanted light rays, while every first LED pixel remains to be activated. Finally in the last subframe, every third LED pixel will be turned on, with a white image on the barrier LCD.

The new system concept combines the barrier LCD, the eye-tracking device and the time-multiplexing method. The advantages of the initial directional backlight design, such as the full resolution image and the elimination of image flip [80, 87], can still be maintained with the new concept. In addition, in the multi-user application, as demonstrated in Fig.2.7 and Fig.2.8, the potential view conflict between two users can be solved. Furthermore, a compact structure is secured since only an extra LC layer is inserted into the original system, which is beneficial for the commercialization. Hence, there is a large potential to develop this improved DB design to provide high quality multi-user applications.

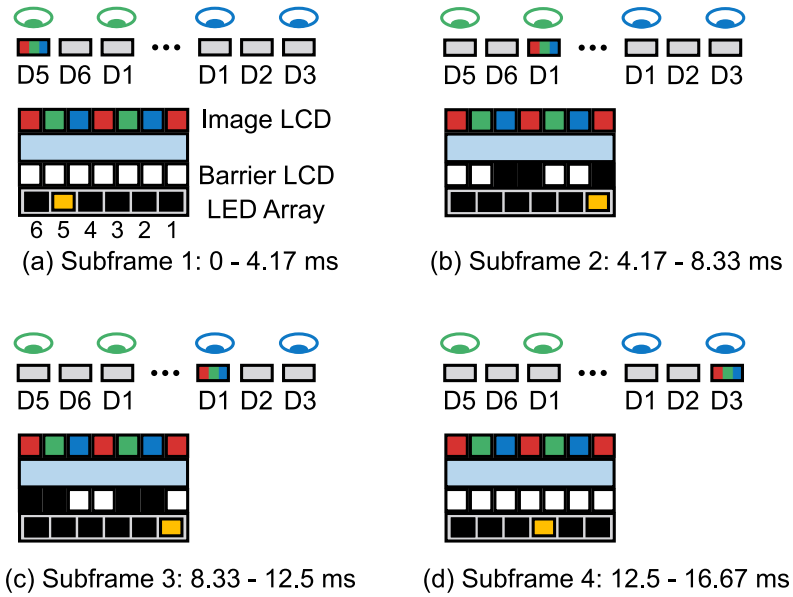

Figure 2.8: Simplified system configuration of four subframes with the new DB concept, where only one LED pixel unit is illustrated. Two viewers are observing the display, where the right eye of the green viewer and the left eye of the blue viewer are corresponding to the same illumination direction D1. The designed image contents for the four eyes will be shown on the image LCD in four successive subframes, then the barrier LCD and the LED array will be adapted in each subframe:(a) Every fifth LED pixel is turned on, and a white image is shown on barrier LCD. (b) Every first LED pixel is turned on, and a special white-black pattern is shown on barrier LCD. (c) Every first LED pixel is turned on, and a special white-black is shown on barrier LCD. (d) Every third LED pixel is turned on, and a white image is shown on barrier LCD.

2.4 System modeling considering the new barrier LCD

2.4.1 Position of the barrier LCD

A DB model with six illumination directions has been built up in Sec.2.3. With the new introduced barrier LCD, the system model should be further

developed to achieve the designed function. At first, the position of the barrier LCD should be determined. A simplified system model from Sec.2.3, which is not in scale with the real system parameters, is demonstrated in Fig.2.9.

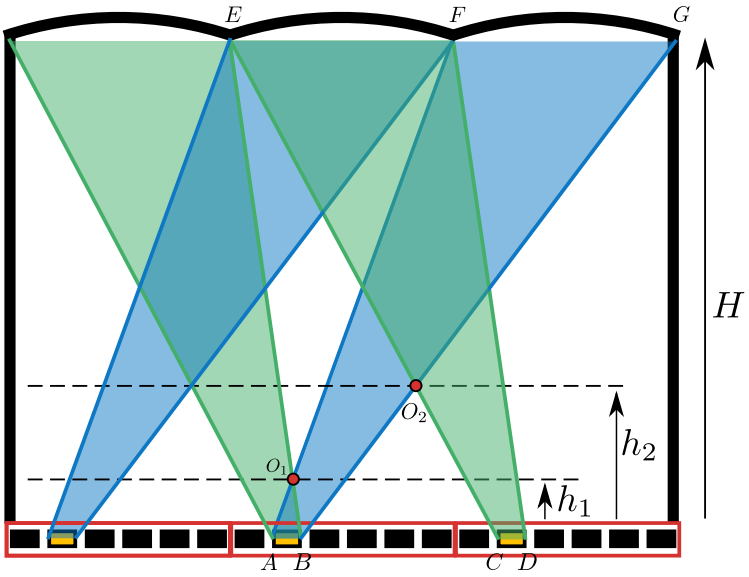

Figure 2.9: Determination of the barrier LCD position. In order to selectively block the blue rays and the green rays, barrier LCD has to be placed between h_1 and h_2. Sizes drawn in the figure are not scalable with the real system parameters.

In Fig.2.9, H is the vertical distance from the matrix backlight to the transition point of two lenses. For the assumed DB, H can be calculated:

$$H = |f| - (R - \sqrt{R^2 - (p/2)^2}),\ H \approx 28.58\,\text{mm}. \tag{2.19}$$

The function of the barrier LCD is to selectively block the blue and the green light rays. According to Fig.2.9, the barrier LCD must be located between h_1 and h_2 to reach the independent modulation. h_1 can be solved through the triangle similarity between $\triangle O_1AB$ and $\triangle O_1EF$:

$$\frac{h_1}{H-h_1}=\frac{t}{p},\ h_1=\frac{t\cdot H}{p+t}\approx 4.2\,\text{mm}, \tag{2.20}$$

where the width of the LED pixel AB is assumed to be equal to the LED pixel pitch t for simplification. And h_2 can be calculated based on the similarity between $\triangle O_2BC$ and $\triangle O_2EG$:

$$\frac{h_2}{H-h_2}=\frac{(m-1)\cdot t}{2p},\ h_2=\frac{t\cdot H}{p\cdot\frac{2}{m-1}+t}\approx 8.6\,\text{mm}. \tag{2.21}$$

h_1 and h_2 have specified two extreme positions of the barrier LCD, where the blue rays can just be separated from the green rays. To reach a clear separation, the gaps between the blue rays and the green rays should be evenly distributed. Fig.2.10 illustrates the gaps between the light rays when the barrier LCD is set to be at height h to the matrix backlight. x_1 stands for the distance from the right edge of the green ray to the left edge of the blue ray. And x_2 shows the distance from the right edge of the blue ray to the left edge of the green ray.

According to Fig.2.10, x_1 can be deduced through similarities between $\triangle O_1KJ$ and $\triangle O_1AB$:

$$\frac{x_1}{t}=\frac{h-h_1}{h_1}. \tag{2.22}$$

Then x_2 can be determined based on the similarities between $\triangle O_2IG$ and $\triangle O_2EF$:

$$\frac{x_2}{2p}=\frac{h_2-h}{H-h_2}. \tag{2.23}$$

By applying the condition $x_1=x_2$ into Eq.2.22 and Eq.2.23, h can be determined:

$$h=\frac{t\cdot h_1\cdot(H-h2)+h_1\cdot h_2\cdot 2\cdot p}{t\cdot(H-h_2)+h_1\cdot 2\cdot p},\ h\approx 7.32\,\text{mm} \tag{2.24}$$

In this case, x_1 and x_2 can be calculated:

$$x_1=x_2\approx 0.74\,\text{mm}. \tag{2.25}$$

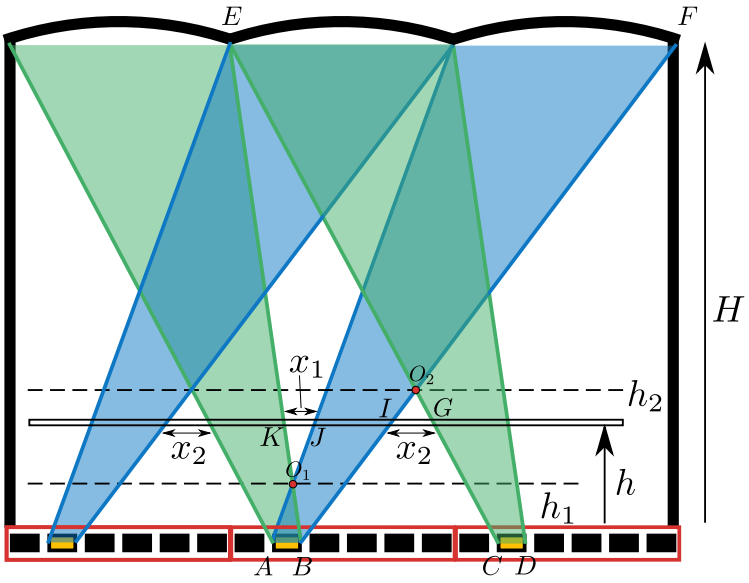

Figure 2.10: Further determination of the optimum barrier LCD position h, where the gaps between the green rays and the blue rays should be evenly distributed. This indicates an equal value of x_1 and x_2.

To achieve an independent control of the blue and the green rays, the pixel size p_b of the barrier LCD should be at least two times smaller than the gap between two rays. Hence, the pixel size p_b should fulfill:

$$p_b < \min\left(\frac{x_1}{2}, \frac{x_2}{2}\right), \; p_b < 0.37\,\text{mm}. \tag{2.26}$$

2.4.2 Influence of the barrier LCD position

When moving away from the optimum position h, a smaller pixel size of the barrier LCD will be required, as can be inferred from Fig.2.10. This will lead to a higher manufacturing cost and a lower transmission of the barrier LCD. However, it should also be noticed that h is not in the middle of h_1 and h_2. The distance from the optimum position to the upper boundary h_2 is about 1.3 mm,

whereas the distance to the lower boundary h_1 is around 3.1 mm. Suppose that the tolerance of the barrier LCD position is ±1 mm. This means if the barrier LCD is eventually located 1 mm higher than the designed value, the required pixel size of the barrier LCD can be deduced:

$$x_1 \approx 0.98\,\text{mm},\ x_2 \approx 0.17\,\text{mm}.\ p_b < 0.085\,\text{mm}. \tag{2.27}$$

Then the required pixel size can also be determined if the barrier LCD is located 1 mm lower than the optimum position:

$$x_1 \approx 0.5\,\text{mm},\ x_2 \approx 1.33\,\text{mm}.\ p_b < 0.25\,\text{mm}. \tag{2.28}$$

Considering the assembly tolerance, the require pixel size would vary within $[0.085\,\text{mm}, 0.37\,\text{mm}]$, where the minimum is almost four times smaller than the value calculated in Eq.2.26. Especially the position error upwards will lead to a large reduction of the pixel size, due to fact that the optimum position h is much closer to the upper boundary.

By simply moving the barrier LCD to the middle position 6.4 mm between h_1 and h_2, the asymmetry issue can be alleviated. Under the same position tolerance ±1 mm, the range of the required pixel size can be deduced based on Eq.2.22 and Eq.2.23, which is $[0.14\,\text{mm}, 0.26\,\text{mm}]$. The minimum value has been improved compared with the previous position, whereas the maximum value is decreased. It can be seen that all parameters are strongly coupled with each other. Therefore, during the determination of the barrier LCD position, the assembly tolerance and the LCD pixel size should be simultaneously taken into account.

For the given DB system, h_1 and h_2 have been determined in Eq.2.20 and Eq.2.21. These two equations can also be used to evaluate the system parameters. The number of viewing directions m can be taken as example. To achieve the desired function of the barrier LCD, m has to fulfill the following requirement:

$$h_2 > h_1 \implies m \geq 4. \tag{2.29}$$

Hence, at least four view directions are needed to guarantee an independent modulation of the light rays. It can also be concluded that a larger m can lead to a bigger space $(h_2 - h_1)$ for the barrier LCD, and the gap between light rays x_1, x_2 will also rise with an increasing m. However, m cannot be arbitrarily

increased, since the lens pitch will rise proportionally to m, as expressed in Eq.2.15. If the lens pitch continues to grow, the paraxial approximation cannot be fulfilled, and there will be an increasing mismatch between the intended and the real ray propagation.

2.4.3 Analysis of more side leak situations

Till now it has been demonstrated how to eliminate the side leak between the green rays and the blue rays, where the green rays will hit the left neighboring lens and the blue rays will hit the right neighboring lens. The distance between the two conflict viewing directions, which can be referred as "Conflict Distance" would be 360 mm. In the real application, two viewers can stand with various distances to each other. If the distance between two eyes is an integral multiple of 180 mm, view conflict would appear due to the side leak.

Among the conflict distances, the distance of 180 mm will not be considered since it is seldom for two viewers to come so close to each other. The distance of 360 mm has been discussed in the previous sections. Then the side leak, which leads to a conflict distance of 540 mm, is illustrated in Fig.2.11. The green rays will continue to hit the left neighboring lens, and the blue rays are now changed to hit the second lens on the right side.

To achieve an independent control of the light rays, the barrier LCD can only be placed within a limited range (h_1, h_2). The determination of h_1 and h_2 is similar to Eq.2.20 and Eq.2.21 based on triangle similarity, hence the process will not be explained in detail. The results can be expressed as:

$$h_1 = \frac{t \cdot H}{2 \cdot p + t} \approx 2.26\,\text{mm}. \tag{2.30}$$

$$h_2 = \frac{t \cdot H}{p \cdot \frac{3}{m-1} + t} \approx 6.37\,\text{mm}. \tag{2.31}$$

Compared with the required range (4.2 mm, 8.6 mm) of the 360 mm conflict distance, there is still a common area between the two situations. If the barrier

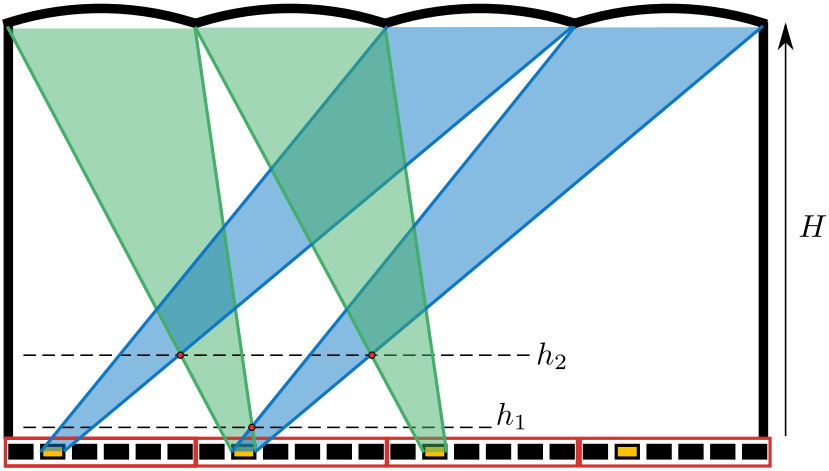

Figure 2.11: Demonstration of one side leak situation in the assumed DB system, where the conflict distance is 540 mm. The green rays still hit the left neighboring lenses, while the blue rays will hit the second lens on the right side. Sizes drawn in the figure are not scalable with the real system parameters.

LCD is located within (4.2 mm, 6.37 mm), it is able to eliminate the side leak of both conflict distances.

After analyzing more side leak situations, a general law can be concluded. Suppose that the conflict distance is n times 180 mm, h_1 and h_2 can be expressed as:

$$h_1 = \frac{t \cdot H}{(n-1) \cdot p + t}, \; h_2 = \frac{t \cdot H}{p \cdot \frac{n}{m-1} + t}. \tag{2.32}$$

According to Eq.2.32, h_1 and h_2 at conflict distances from 360 mm to 1440 mm can be calculated and listed in Tab.2.5. It can be seen that the conflict distance 360 mm and 900 mm can not be simultaneously eliminated, since the maximum allowed height h_2 at 900 mm is equal to the minimum allowed height h_1 at 360 mm. By placing the barrier LCD within (4.2 mm, 5.06 mm), it is only able to suppress the conflict distance at 360 mm, 540 mm and 720 mm.

However, if it could be assumed that the conflict distance of 360 mm is not relevant for the application, the elimination of the side leak can be extended

Table 2.5: h_1 and h_2 at several conflict distances (unit in mm)

Conflict Distance	360	540	720	900	1080	1260	1440
h_1	4.20	2.26	1.55	1.18	0.95	0.80	0.69
h_2	8.60	6.37	5.06	4.20	3.58	3.13	2.77

to a larger area. Because the maximum allowed height $h_2 = 2.77$ mm at 1440 mm is still larger than the minimum allowed height $h_1 = 2.26$ mm at 540 mm, the height range [2.26 mm, 2.77 mm] would be theoretically suitable for all conflict distances from 540 mm to 1440 mm. So the area, where the side leak elimination is applicable, has been significantly enlarged when the 360 mm conflict distance could be neglected. Therefore, based on the real application, the system parameters can be carefully designed to provide a better performance.

2.5 Modulation of the barrier LCD

After the position of the barrier LCD has been discussed, the modulation of the barrier LCD will be studied in this section. One schematic model of DB is demonstrated in Fig.2.12 to help analyze the geometrical relationships. The left edge of the lens array is aligned with the left edge of the LED array, and the barrier LCD is located with distance h to the LED array.

Suppose that the N^{th} LED counted from the left side within the first LED pixel unit is turned on, which is represented by the yellow LED pixel $N_L N_R$ in Fig.2.12. The distance from the origin of coordinates to the left edge of the N^{th} LED can be expressed as:

$$ON_L = (N-1) \cdot t. \tag{2.33}$$

Again the width of LED pixel is assumed to be the same with LED pitch for simplification. And the distance ON_R can be expressed as:

$$ON_R = N \cdot t. \tag{2.34}$$

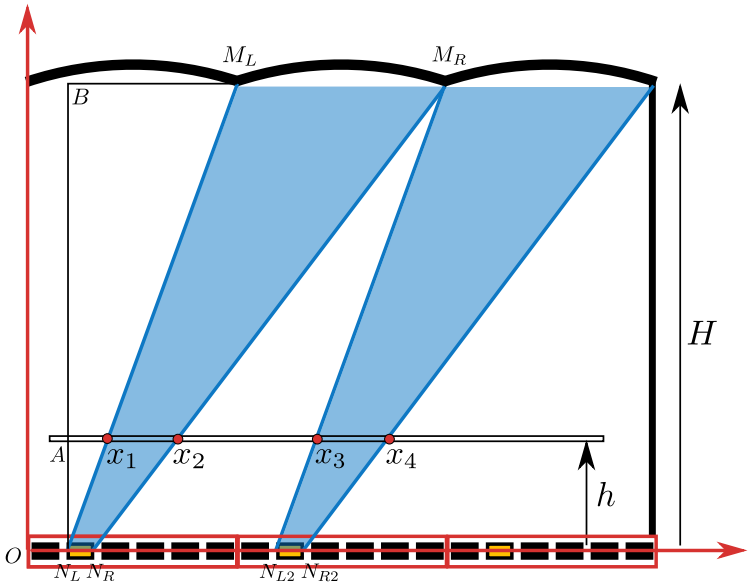

Figure 2.12: Schematic model of the DB to determine the modulation of the barrier LCD. The left edge of the lens array is aligned with the left edge of the LED array. Every second LED pixel from the left side within one LED pixel unit is turned on to represent the N^{th} pixel group. And the light rays towards the right neighboring lens are drawn to represent the side leak at the M^{th} lens on the right side.

Then the light rays, which propagate towards the M^{th} lens on the right side, are illustrated in Fig.2.12. M_L and M_R are the left and right edge of the M^{th} lens. The distance BM_L and BM_R can be deduced:

$$BM_L = M \cdot p - ON_L = M \cdot p - (N-1) \cdot t. \tag{2.35}$$

$$BM_R = (M+1) \cdot p - ON_L = (M+1) \cdot p - (N-1) \cdot t. \tag{2.36}$$

Based on the similarity of $\triangle N_L A x_1$ and $\triangle N_L B M_L$, the distance Ax_1 can be determined:

$$\frac{Ax_1}{BM_L} = \frac{N_L A}{N_L B},\ Ax_1 = (M \cdot p - (N-1) \cdot t) \cdot \frac{h}{H} \tag{2.37}$$

In the trapezoid $N_L N_R M_R M_L$, the distance $x_1 x_2$ can be deduced:

$$x_1 x_2 = N_L N_R + (M_L M_R - N_L N_R) \cdot \frac{h}{H},\ x_1 x_2 = t + (p - t) \cdot \frac{h}{H} \tag{2.38}$$

Then the horizontal coordinate of x_1 and x_2 can be expressed as:

$$x_1 : (M \cdot p - (N-1) \cdot t) \cdot \frac{h}{H} + (N-1) \cdot t. \tag{2.39}$$

$$x_2 : ((M+1) \cdot p - N \cdot t) \cdot \frac{h}{H} + N \cdot t. \tag{2.40}$$

For the light rays originating from the corresponding LED pixel in the second LED pixel unit, the two marginal rays will intersect with the barrier LCD at x_3 and x_4, as demonstrated in Fig.2.12. Within the trapezoid $N_L N_{L2} M_R M_L$, the distance $x_1 x_3$ can be expressed as:

$$x_1 x_3 = N_L N_{L2} + (M_L M_R - N_L N_{L2}) \cdot \frac{h}{H},\ x_1 x_3 = m \cdot t + (p - m \cdot t) \cdot \frac{h}{H}. \tag{2.41}$$

Then the calculation of $x_3 x_4$ is similar to $x_1 x_2$, as previously shown in Eq.2.38. In this way, the horizontal coordinate of x_3 and x_4 can also be deduced, and the results will not be demonstrated.

This geometrical analysis can be iterated for each LED pixel unit to determine the intersection points of the marginal rays and the barrier LCD. Furthermore, with the knowledge of the barrier LCD pixel size, the position of the corresponding pixels on the barrier LCD can also be calculated. As a result, when a specific side leak situation is defined, the modulation of the barrier LCD, namely the white-black image pattern, can be determined based on Eq.2.39, Eq.2.40 and Eq.2.41.

2.6 Applications with the new directional backlight concept

In the previous sections, the concept, the configuration and the modulation of the barrier LCD have been explained. With a proper system design, the new DB concept with the barrier LCD is able to eliminate the view conflict between two users. This improvement can allow many new applications, some of which will be demonstrated in this section.

Fig.2.13 shows the key function of the new display system, which consists of the proposed DB and one image LCD. The display is able to send four different images towards four different directions at four subframes. If two users are observing this display, four eyes of user 1 and user 2 can receive four different images, which are respectively represented by the blue, green, red and yellow rectangle in Fig.2.13. In one subframe, one certain image will be shown on the image LCD and get projected to the designed direction. Each subframe will last 1/4 of a normal display frame with 16.67 ms. Hence, an entire frame can still be repeated with 60 Hz to avoid flickering. The system configuration in each subframe has already been explained in Fig.2.8, so it will not be further discussed in this section.

The key function of the new display system is to send four different images to the four eyes of two users. Based on this feature, various new applications can be created by adjusting the image contents in four subframes. Fig.2.14 demonstrates one sequence of image contents, which can enable high quality 3D images for two users. Two perspectives of the 3D objects will be generated, and the left perspective will be perceived by the two left eyes of user 1 and user 2, while the right perspective will be sent to the two right eyes. In this way, the eye is constantly receiving the correct 3D image. This is a significant progress compared to the DB proposed in [80,87], where the view conflict caused by the side leak will largely reduce the system performance in two-user applications. Therefore, with the new display system, high quality 3D perception for two users can be created, which enables a full resolution 3D image without flipping effect.

Another sequence of image contents, which can be used to create split-view function, is illustrated in Fig.2.15. Two different images, represented by the blue tetrahedron and the green cube, are prepared for the split-view function.

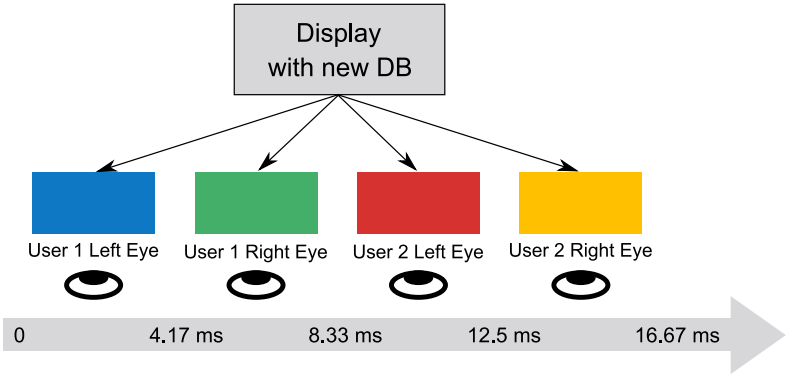

Figure 2.13: Key function of the display with the proposed DB concept. By putting an image LCD on the new DB, the display system is able to send four different images towards the four eyes of user 1 and user 2. The four images are represented by the blue, green, red and yellow rectangle in the figure. Each image will be shown for 1/4 of a normal display frame with 16.67 ms.

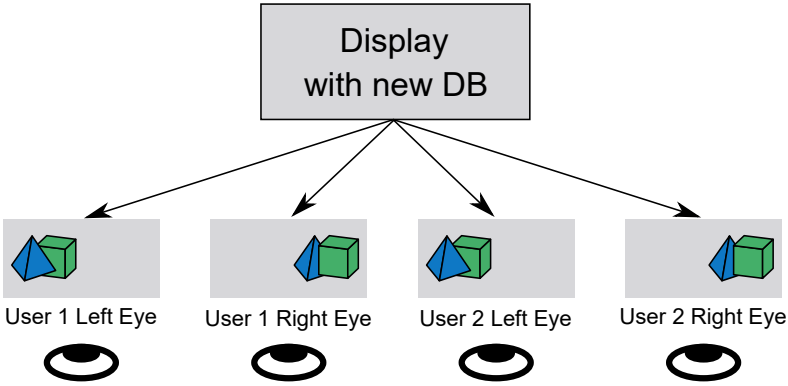

Figure 2.14: Application of the new DB: high quality 3D images for two users. Two perspectives of the 3D objects will be created and respectively sent to the left eyes and right eyes of the two users.

The tetrahedron image will be sent to the two eyes of user 1 in the first two subframes, while the cube image will be sent to user 2 in the last two subframes. As a result, user 1 and user 2 can get two different image contents

from the display. This split-view feature would be a huge advantage of the new display system. Neither the original DB concept nor the traditional 3D display technologies can achieve the split-view function.

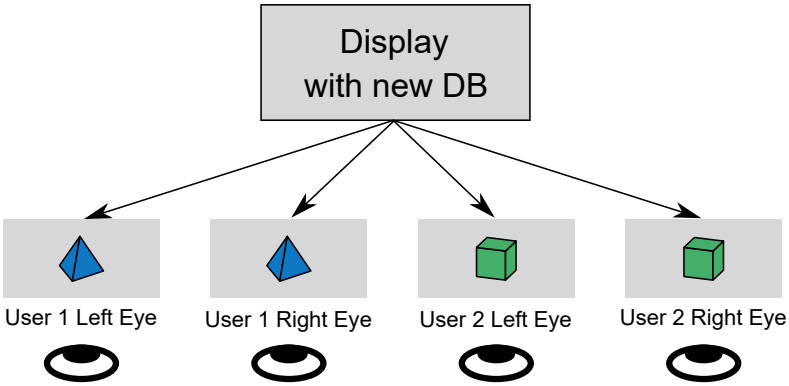

Figure 2.15: Application of the new DB: Split-view function for two users. The two eyes of user 1 will see the tetrahedron, while the two eyes of user 2 will see the cube.

There are still many other new applications, which will not be expanded in this section. It should be emphasized that the key function of the new DB concept is to send different images into different directions. Therefore, the application area should not be limited within 3D display. This concept could be used in the applications where the direction of the light needs to be modulated, such as the split-view function shown in Fig.2.15. It is strongly believed that this new DB concept has a huge potential in the future multi-user display applications.

2.7 Summary of the proposed directional backlight concept with the barrier LCD

In this chapter, a new DB concept has been demonstrated to suppress the side leak, and provide high quality multi-user applications. The side leak effect has been first studied with a quantitative model of the original DB system. An extra barrier LCD has been suggested to eliminate the side leak and the resulted view conflict between two viewers. Then the position of the barrier

LCD has been investigated, where the assembly tolerance and the pixel size of the barrier LCD are found to play an important role. After the determination of system parameters, the modulation of the barrier LCD has been studied by analyzing the required pixel arrangement, when a certain side leak case has to be eliminated. Finally, based on the proposed DB concept, several prominent use cases have been discussed, which extend beyond the 3D display application. The key function of this concept, that different images can be sent to the intended directions, is supposed to have a wide application area.

3 Simulation

This chapter will focus on the simulation of the new DB concept. At first, the application area of the display will be discussed, which will help to determine all system and component parameters. Then the system model will be established in the simulation software in order to evaluate the concept. At last the simulation results will be discussed.

3.1 Determination of the system parameters

The proposed DB concept can create a high-quality image for two-user applications. This chapter will investigate one typical two-user situation: the driver and co-driver in the vehicle. Nowadays there are various displays in the cockpit, such as ICD, CID and PID, as previously mentioned. Among them, CID is designed to simultaneously serve the driver and co-driver. Therefore, the proposed DB concept will be applied to the CID, and the simulation model should be established based on the CID scenario. According to the vehicle configuration, an assumed observation situation is demonstrated in Fig.3.1. The observation plane is 600 mm away from the display. Two users are located on the left and right side of the plane, both with 300 mm distance to the center of the observation plane. The user can also move in the vehicle, and the movement range is supposed to be [−100 mm, 100 mm]. It should be pointed out that these parameters are only selected as example to build the simulation model, and they may not match the actual vehicle application.

The next step is to determine other system parameters based on the configuration in Fig.3.1. In terms of the viewing zone width, Dodgson pointed out that by setting the width value under 40 mm, the interpupillary interference could be well eliminated [68]. Hence, the distance between two adjacent viewing directions a is set to be 30 mm.

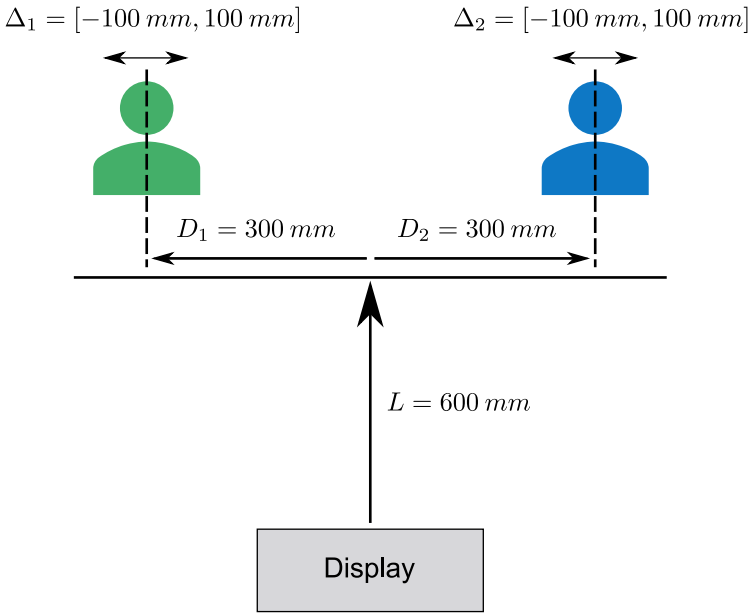

Figure 3.1: Illustration of the assumed CID scenario. The users are located 600 mm away from the display. The green user and the blue user are both 300 away from the center of the observation plane. Two users can also move within [−100 mm, 100 mm] of the nominal position.

Regarding the number of viewing directions, its influence on the configuration of the barrier LCD has been discussed in Sec.2.4. To reach a balance between the assembly tolerance and the image quality, the number of viewing directions is set to be 10. As illustrated in Fig.3.2, the width of a whole viewing zone is 300 mm, which consists of 10 viewing directions. Based on the assumed CID scenario, the green user will be constantly located in the "Left viewing zone 1", and the blue user will always be located in the "Right viewing zone 1". In the subsequent analysis, "Left viewing zone 1" will be referred as left viewing zone and "Right viewing zone 1" will be called right viewing zone for simplification.

Then the LED pixel pitch and the refractive index of components can be assigned with some assumed values, which are demonstrated in Tab.3.1. Ac-

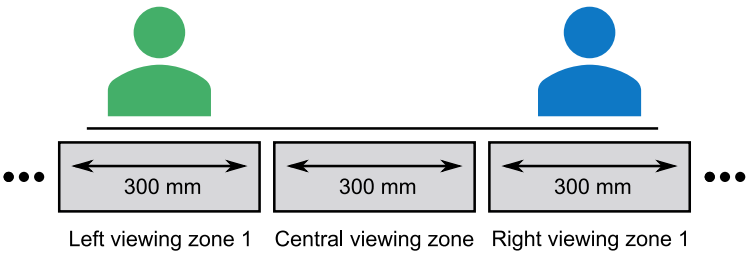

Figure 3.2: Distribution of the viewing zones. Each viewing zone contains 10 viewing directions, leading to a 300 mm width. The green user will be within "Left viewing zone 1", whereas the blue user will be located in "Right viewing zone 1".

Table 3.1: Given parameters of the directional backlight system

L	a	m	t	n_1	n_L
600 mm	30 mm	10	0.6 mm	1.51	1.51

cording to the explained system modeling in Sec.2.1, the lens parameters can be calculated, which can be seen in Tab3.2. It should be noticed that various combinations of d_1 and d are possible to meet the requirement. The accurate value of d_1 and d will be determined depending on the location of the barrier LCD.

Table 3.2: Calculated system parameters (unit in mm)

R	p	$d_1 + d$
6	5.88	17.76

In the last step of system modeling, the configuration of the barrier LCD should be determined. For the given DB system, the conflict distance caused by side leak will appear at 300 mm, 600 mm, 900 mm, etc. According to the assumed scenario shown in Fig.3.1, the distance between two users will be within [400 mm, 800 mm]. Therefore, only the conflict distance at 600 mm needs to be considered. One side leak situation, that is able to create conflict distance at 600 mm, is demonstrated in Fig.3.3. The green rays from the LED pixel will hit the left neighboring lens and get collimated to the green user,

Table 3.3: Calculated parameters of the barrier LCD (unit in mm)

h_1	h_2	h	p_b (pixel size)	x_1x_3
1.57	5.35	4.31	$p_b < 0.52$	5.97

while the blue rays will be directed to the blue user. To selectively block the green rays and the blue rays, the barrier LCD should be placed within the distance (h_1, h_2) to the LED array.

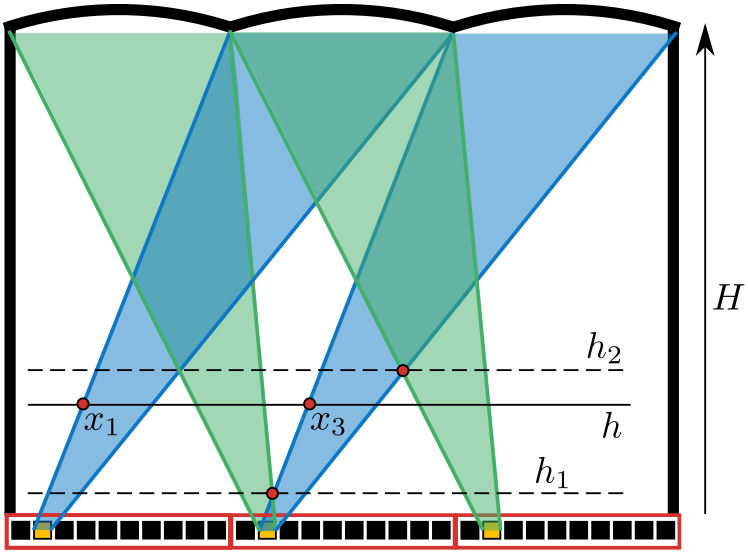

Figure 3.3: Demonstration of one side leak situation in the new established DB. Every second LED pixel from the left side is turned on to emit light. The green rays will eventually reach one eye of the green user, while the blue rays will propagate to one eye of the blue user.

According to the system modeling described in Sec.2.4, the parameters of the barrier LCD can be determined and shown in Tab3.3. In the parameter deduction, the height of the barrier LCD is set to be at the optimum distance h, that can lead to an equal gap between the light cones and thus a minimum required LCD pixel size.

A LCD contains two polarizers, two glass layers, one LC layer, etc. In the first stage, in order to verify the concept, there is no need to conduct a complete modeling of the LCD including all components. In the simulation, only the key function of the barrier LCD will be considered, which is the modulation of the incident light. Therefore, for simplification, the barrier LCD will be modeled as a thin layer with 0.1 mm thickness, where every point on the layer can be set as transparent or absorbing to simulate the white-black image pattern. Subsequently, the thickness of the lens array and the front medium can also be determined and shown in eq.3.1, since they are separated by the barrier LCD.

$$d_1 = 4.21\,\text{mm}, d = 13.45\,\text{mm}. \tag{3.1}$$

Till now all system parameters have been determined based on the assumed CID application shown in Fig.3.1. In the following sections, the system model should be built up in the simulation software to verify the functionality of the new concept.

3.2 Introduction of the simulation model in the software

The software program OpticStudio from the company Zemax is used in this work to carry out the simulations. OpticStudio is an optical design program that can be used to analyze imaging optics, illumination systems and laser optic design. OpticStudio can perform standard sequential ray tracing through optical elements, as well as non-sequential ray tracing for analysis of stray light [97]. For the DB concept, there is no pre-defined path for the light rays. A ray hitting an object can be reflected, refracted, absorbed or split into child rays. So the simulation model will be set up in the non-sequential mode.

There are four major components to be established in the simulation: the LED array, the front medium, the barrier LCD and the lens array. LED pixel can be represented by the object “Source Two Angle” in OpticStudio. The LED pitch is same to the assumed value in Tab.3.1, which is 0.6 mm. Based on the assumed user location in Fig.3.2, the horizontal half radiation angle of “Source Two Angle” is determined as 60° to include all possible user locations. Considering

the limited positions of the user's eye height, the vertical half radiation angle is set to be 20° to reach a more concentrated radiation in the vertical direction.

The front medium can be considered as a connection plate between the LED array and the barrier LCD. Therefore, it will be represented by the object "Rectangular Volume" in OpticStudio. The glass type "BK7" is chosen as the material of this plate based on the assumed refractive index value. Regarding the barrier LCD, it is the combination of two arrays: one array of transparent "Rectangular Volume" and another array of absorbing "Rectangular Volume".

The lens array has a relatively complicated geometry, so the 3D model of the lens array will be first established in an extra Computer-Aided Design (CAD) software SolidWorks, as demonstrated in Fig.3.4(a). The length and width of the lens array is set to be 294 mm and 112 mm respectively. Then the 3D model can be imported into OpticStudio, as shown in Fig.3.4(b). The material "BK7" will be assigned to the imported lens array to approach the assumed refractive index.

The DB system can be established with the four major components. A screenshot of the DB model in OpticStudio is demonstrated in Fig.3.5(a), with only one LED pixel turned on. The barrier LCD is not visible in the screenshot since it is still set to be transparent in the model. Side leak can also be observed in Fig.3.5(a), that the emitted blue rays will be directed into different directions at different lenses. To record the luminance distribution of the DB, a detector plane is placed at the designed viewing distance 600 mm, as shown in Fig.3.5(b).

3.3 Simulation results of the directional backlight without barrier LCD

Based on the created DB model, simulations will be conducted to first analyze the DB output without using the barrier LCD. Because the component configurations and the ray propagation have been already explained in detail, this section will directly demonstrate the simulation results.

In the first simulation, every fifth LED pixel is turned on in the LED array to provide the illumination. Fig.3.6 gives a qualitative description of the system

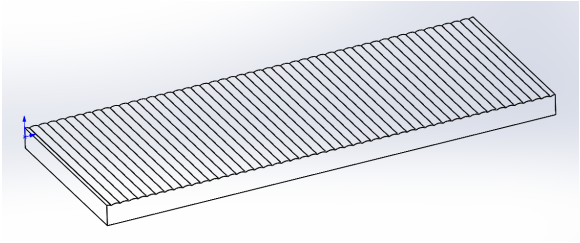

(a)

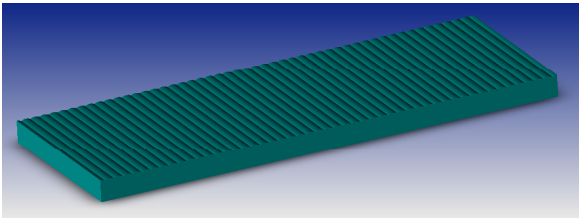

(b)

Figure 3.4: Modeling of the lens array with 294 mm length and 112 mm width. (a) Creation of the 3D model in SolidWorks. (b) 3D Model imported in OpticStudio.

output. The ray propagation after the lens array is shown in Fig.3.6(a), and the illuminated area on the detector plane is shown in Fig.3.6(b). Based on the assumed user positions, only the simulation results within the horizontal area (−400 mm, 400 mm) of the detector plane will be discussed in this chapter. As expected, three viewing zones will be illuminated by the DB when one viewing direction is activated.

Then the luminance of the DB should be quantitatively evaluated. The luminance assessment in the simulation should also be practical for the experiment, because the simulation result will be subsequently compared with the experiment results. Fig.3.7(a) illustrates the assessment method used in this work. The white dashed line represents the horizontal centerline on the detector. A large number of virtual pixels will be set on the centerline to record the incident rays, with one pixel highlighted as the small white circle in Fig.3.7(a). The pixel pitch is set as 1 mm in the simulation. For each pixel, the average

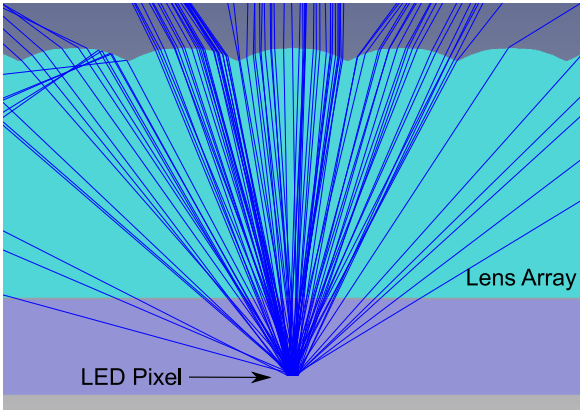

(a)

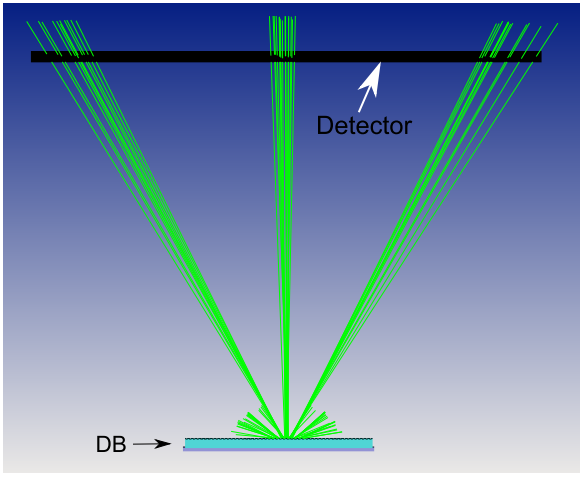

(b)

Figure 3.5: Screenshot of the system modeling in OpticStudio. (a) Modeling of the DB system with one LED turned on. (b) The detector plane is placed 600 mm away from the DB to record the luminance distribution. To provide better readability in each figure, rays are drawn in different colors in (a) and (b).

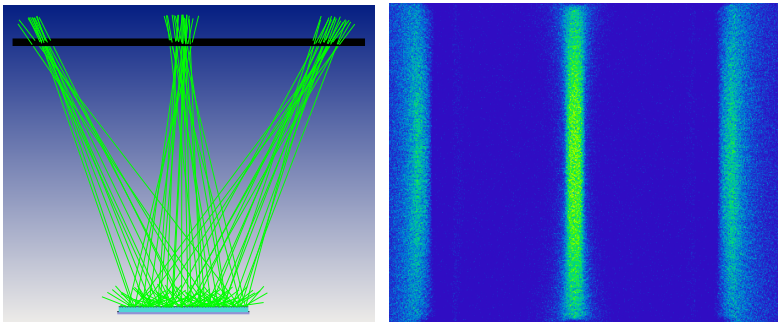

(a) (b)

Figure 3.6: Qualitative description of the system output, when every fifth LED pixel is turned on. (a) Demonstration of the ray propagation after the lens array. (b) Distribution of the illuminated area on the detector plane.

luminance of the yellow square, which is located on the center of the lens array top surface, will be calculated in the simulation. The yellow square has the size 23.52 mm × 23.52 mm, where 23.52 mm is equivalent to the width of four lenses. In the subsequent simulations, the luminance will also be calculated from the same square on the lens array. Hence, this assessment method will not be further repeated.

After the designed luminance at every pixel along the horizontal centerline is calculated in the simulation, the luminance distribution of viewing direction 5 can be plotted in Fig.3.7(b). It should be mentioned that the obtained luminance value is proportional to the assumed LED power in the simulation. In the real application, it has to be adapted according to the LED specification.

As previously explained, only the luminance distribution from −400 mm to 400 mm in the horizontal direction will be considered in the simulation. Within this range, the fifth LED pixel group can lead to three illuminated zones on the detector plane. As can be seen in Fig.3.7(b), the illuminated area is more concentrated in the center than the peripheral positions. In the formation of the side viewing zones, the rays will have a large angle with the optical axis of the corresponding lens. So the paraxial approximation can not be fulfilled, leading to a more disperse distribution towards two sides. Moreover, peak positions of the luminance distribution are given in Tab.3.4. The peak distance between

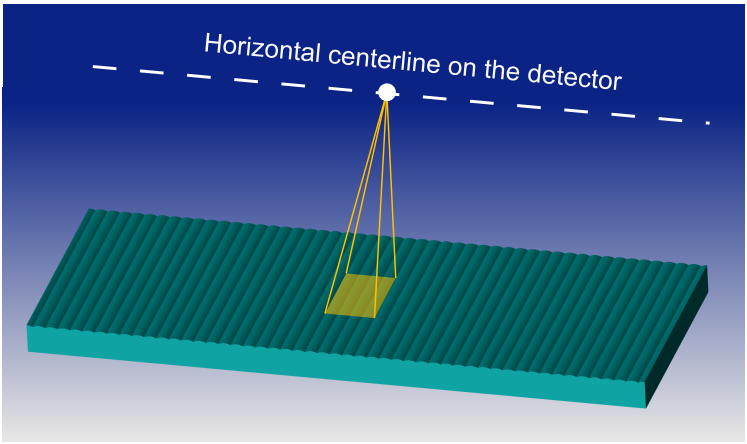

(a)

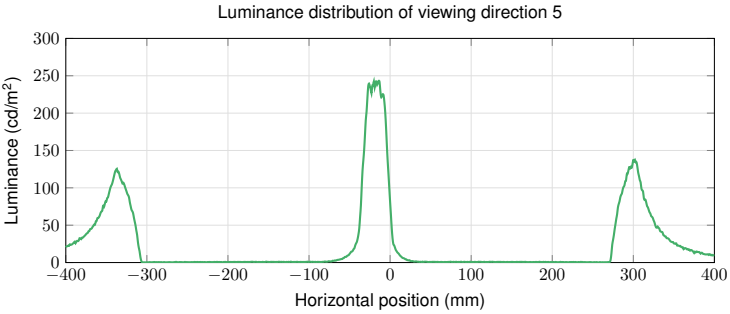

(b)

Figure 3.7: Luminance distribution of viewing direction 5. (a) Definition of the luminance assessment in the simulation. A certain number of pixels will be added to the horizontal centerline of the detector, with 1 mm pixel pitch. For each pixel, the average luminance of the yellow square will be calculated. The yellow square is located on the center of the lens array top surface, with the side length 23.52 mm, which corresponds to the total width of four lenses. (b) Simulated luminance distribution of viewing direction 5 along the white horizontal centerline shown in (a).

Table 3.4: Peak positions of direction 5, 6 and 7 in three viewing zones

Viewing zone	Left	Central	Right
Direction 5 peak position (mm)	−337	−14	302
Direction 6 peak position (mm)	−307	17	333
Direction 7 peak position (mm)	−276	49	364

the central viewing zone and left viewing zone of direction 5 is 323 mm, and the peak distance between the central viewing zone and the right viewing zone is 316 mm. The deviation from the designed viewing zone width 300 mm can also by explained by lens aberrations.

Then in the second simulation, only the sixth LED pixel group will be activated. Because the simulation results of the ray propagations and the illuminated areas are very similar to the results of viewing direction 5, these two diagrams will not be demonstrated. The luminance distribution along the centerline is plotted in Fig.3.8 together with the result of the fifth LED pixel group. The illuminated area is also more concentrated in the center than the peripheral positions. As can be seen from Tab.3.4, the peak distance between viewing direction 5 and 6 in the central viewing zone is 31 mm, which can accord with the design value 30 mm. Similarly, the peak distance between viewing direction 5 and 6 in the left viewing zone can be calculated as 30 mm, while the peak distance in the right viewing zone is obtained as 31 mm. This indicates that the system parameters have been correctly designed.

Subsequently in the third simulation, only the seventh LED pixel group will be turned on to provide the illumination. The obtained luminance distribution is demonstrated in Fig.3.9 together with the result of the fifth and the sixth LED pixel group. According to the peak positions given in Tab.3.4, the peak distance of direction 5 and 7 in the central viewing zone is 63 mm, which can match the designed value. A peak distance near 60 mm can also be observed in the left and right viewing zone, which are 61 mm and 62 mm respectively.

Based on the luminance distribution of direction 5 and 7, the interocular crosstalk can be estimated. The peak distance of the two directions is close to the average interpupillary distance, therefore, the crosstalk value can be calculated at the corresponding peak positions. For direction 5, the crosstalk caused by

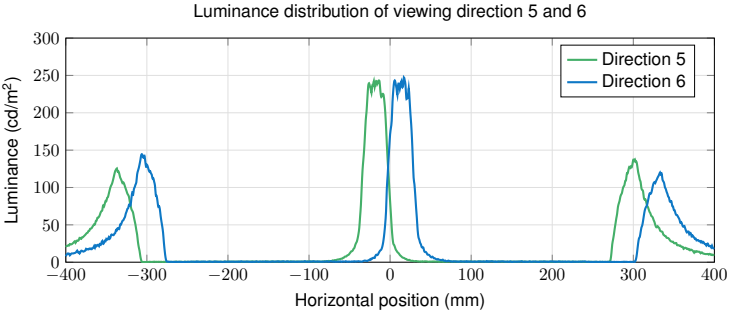

Figure 3.8: Demonstration of the luminance distribution of viewing direction 5 and 6 along the horizontal centerline.

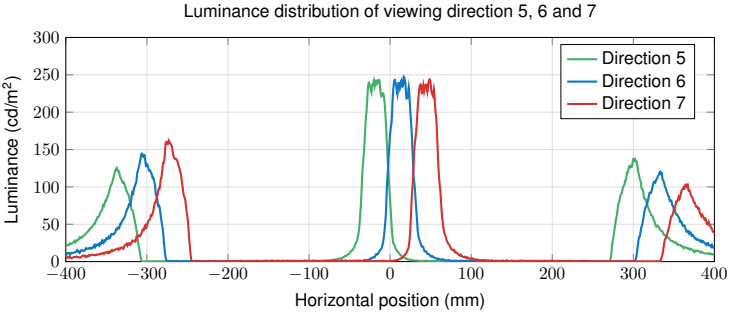

Figure 3.9: Demonstration of the luminance distribution of viewing direction 5, 6 and 7 along the horizontal centerline.

direction 7 can be calculated and shown in Tab.3.5, with the maximum crosstalk 13.28% at −337 mm. Then for direction 7, the crosstalk caused by direction 5 is given in Tab.3.6, with the maximum crosstalk 18.76% at 364 mm. The crosstalk value at other horizontal positions will be covered in the subsequent analysis.

After the simulation of all 10 viewing directions, the luminance distribution of all directions can be shown in Fig.3.10. It is clear that all distribution profiles are concentrated in the central viewing zone, and will become dispersed towards two sides. If the luminance values of all peak positions are compared, it can

Table 3.5: Crosstalk at three peaks of direction 5 luminance distribution

Direction 5 peak position	−337 mm	−14 mm	302 mm
Direction 5 Luminance (cd/m^2)	125	243	137
Direction 7 Luminance (cd/m^2)	16.6	0.76	0.48
Crosstalk	13.28%	0.31%	0.35%

Table 3.6: Crosstalk at three peaks of direction 7 luminance distribution

Direction 7 peak position	−276 mm	49 mm	364 mm
Direction 5 Luminance (cd/m^2)	0.28	0.88	19.32
Direction 7 Luminance (cd/m^2)	160	244	103
Crosstalk	0.18%	0.36%	18.76%

be found that the peak luminance will decrease with a larger distance to the horizontal center, which corresponds to the radiation characteristic of the LED pixel.

To provide a quantitative crosstalk description, the crosstalk value within (−400 mm, 400 mm) will be plotted in Fig.3.11. Every red dot represents the calculated crosstalk at one peak position of the corresponding luminance distribution. Then all dots are connected with the green lines to form the diagram. It should be noticed that at each peak position, the crosstalk caused

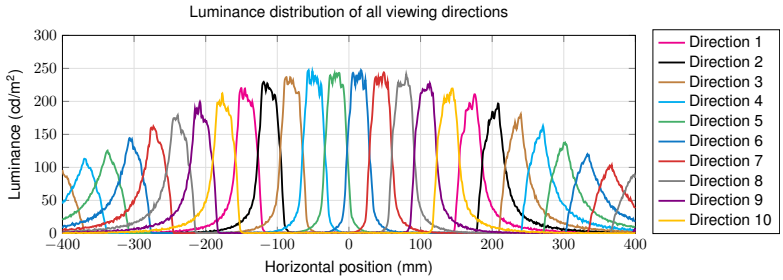

Figure 3.10: Demonstration of the luminance distribution of all 10 viewing directions.

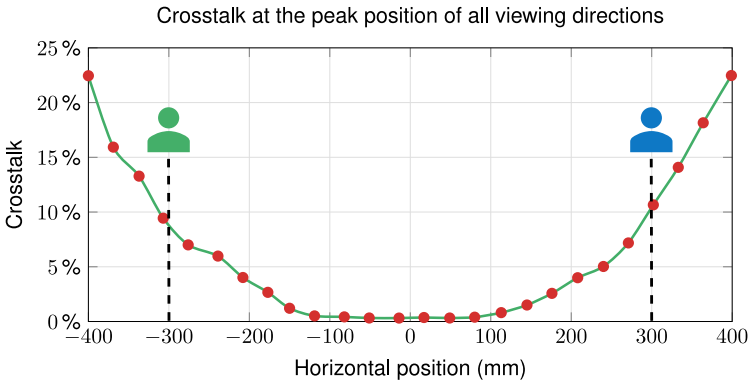

Figure 3.11: Illustration of the crosstalk value within (−400 mm, 400 mm). The crosstalk value at the peak positions of the luminance profile is calculated. Every red dot in the figure represents the calculated crosstalk at one peak position. Crosstalk will increase with a larger distance to the horizontal center, and all crosstalk values are under 25%.

by the two viewing directions, whose direction number is ±2 of the currently analyzed direction, have been compared. For example, when evaluating the crosstalk at the peak position of direction 5, the luminance of direction 3 and 7 at this position should be both considered. Then the larger crosstalk value will be used in Fig.3.11. It can be seen that the crosstalk will grow with an increasing distance to the horizontal center.

As mentioned in Sec.1.2, experiments have shown that the crosstalk higher than 25% will largely reduce the 3D viewing comfort [62] . However, the typical crosstalk value of the lenticular multiview 3D displays is higher than 20% [63], which could lead to a noticeable viewing discomfort. For the proposed DB concept, all crosstalk values within (−400 mm, 400 mm) are under 25%, as illustrated in Fig.3.11. Two users have also been drawn in Fig.3.11 based on the assumed CID application. It can be seen that the crosstalk at the nominal user position is around 10%. Considering the horizontal user movement of ± 100 mm, the crosstalk will vary within (4%, 22.5%), which can ensure an acceptable 3D visual quality. Moreover, there are many proposed methods to further reduce the crosstalk value, for example through dynamically adjusting the view intensity [63], or by applying the fusion of viewing zones [65]. Since

the dynamic crosstalk reduction is not the focus of this work, it will not be further discussed.

To summarize, the simulation results without using the barrier LCD have been discussed in this section. The result analysis has been focused on two aspects: the luminance distribution of the viewing directions and the crosstalk value. Based on the crosstalk evaluation, the application in CID can provide a better 3D visual comfort compared to the lenticular multiview 3D displays.

3.4 Simulation results with the barrier LCD

Till now, the barrier LCD has been set as a transparent layer in the simulation. This section will demonstrate the effect of the proposed barrier LCD through simulation results. One view conflict case in CID application can be illustrated using the luminance distribution of viewing direction 5, as shown in Fig.3.12 where three illuminated areas are created within (−400 mm, 400 mm). It is assumed that the left eye of the green user belongs to the left viewing zone of viewing direction 5, whereas the right eye of the blue user corresponds to the right viewing zone. Due to this view conflict, it is impossible to send two different contents to these two eyes.

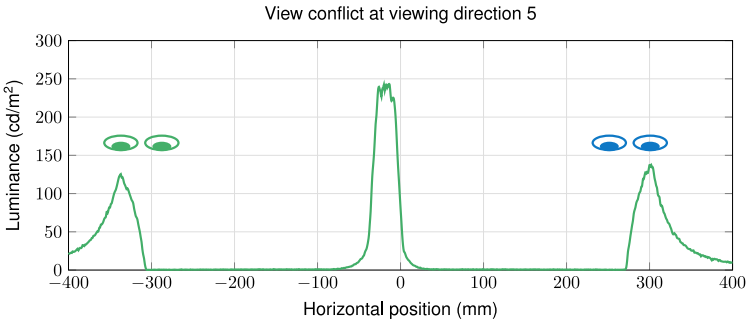

Figure 3.12: Demonstration of one view conflict situation. The left eye of the green user and the right eye of the blue user both belong to viewing direction 5, but are located respectively in the left and the right viewing zone.

The function of the barrier LCD is to selectively block the light rays towards the unwanted viewing zone. In OpticStudio, the barrier LCD is modeled as an array of “Rectangle Volume”, then the simulation can be carried out by setting the corresponding elements to be “Absorbing” in OpticStudio. Because the configuration of the barrier LCD has already been explained in detail, this section will directly demonstrate the simulation results after using the barrier LCD.

At first, the barrier LCD has been set to block the illumination towards the left viewing zone, when every fifth LED pixel is activated to form viewing direction 5. The simulation results can be seen in Fig.3.13, consisting of three sub-images: the ray propagation after the lens array, the illuminated area on the detector plane and the luminance distribution along the centerline. According to Fig.3.13, it is obvious that the illumination in the left viewing zone has been significantly suppressed.

The luminance distribution from Fig.3.6 and Fig.3.13(c) can be compared in one diagram to further study the barrier LCD function. Two distributions are drawn simultaneously in Fig.3.14, where the green curve represents the original simulation result without using the barrier LCD, and the red curve describes the luminance distribution after setting up the barrier LCD. In the left viewing zone, the luminance at the peak position -337 mm is reduced from 125 cd/m^2 to a value lower than 0.1 cd/m^2. The values at other horizontal positions in the left viewing zone are also close to zero. Regarding the right viewing zone, the peak luminance at 302 mm has varied from 137 cd/m^2 to 134 cd/m^2, which can be considered as unchanged after the use of the barrier LCD. At other positions within the right viewing zone, two distribution profiles can almost coincide with each other.

Apart from the left and the right viewing zone, it should be pointed out that the luminance distribution in other viewing zones could also be influenced by the barrier LCD. As demonstrated in Fig.3.14, the luminance value in the central viewing zone has been largely decreased, since the light rays towards these directions will be partly blocked by the opaque areas on the barrier LCD. However, the luminance reduction in other viewing zones will not affect the CID application, because only the illuminated area in the left and right viewing zone can be perceived by the users, according to the assumed user positions. As a result, with the proposed barrier LCD, the illumination for the left eye of

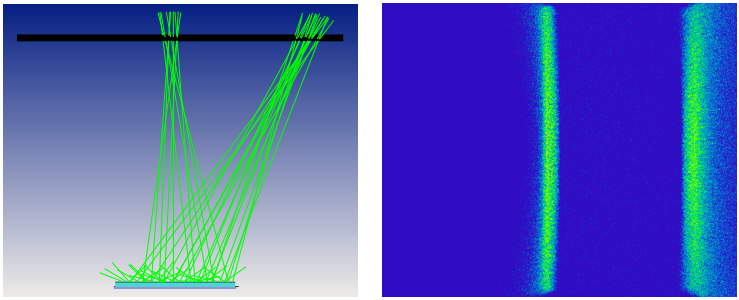

(a) (b)

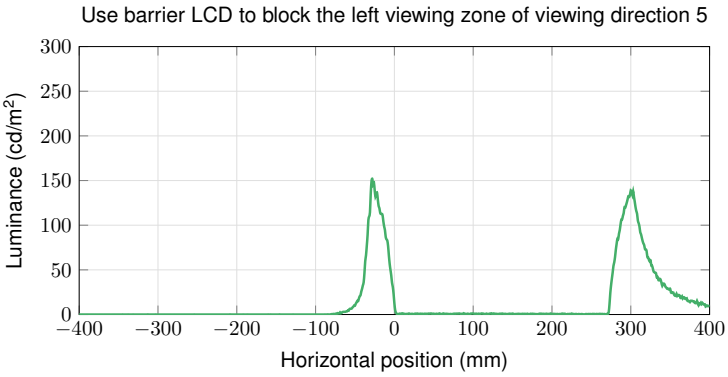

(c)

Figure 3.13: Simulation results when the barrier LCD is set to block the left viewing zone of viewing direction 5. (a) Demonstration of the ray propagation after the lens array. (b) Distribution of the illuminated area on the detector plane. (c) Luminance distribution along the horizontal centerline. It is clear that the illumination in left viewing zone is successfully eliminated.

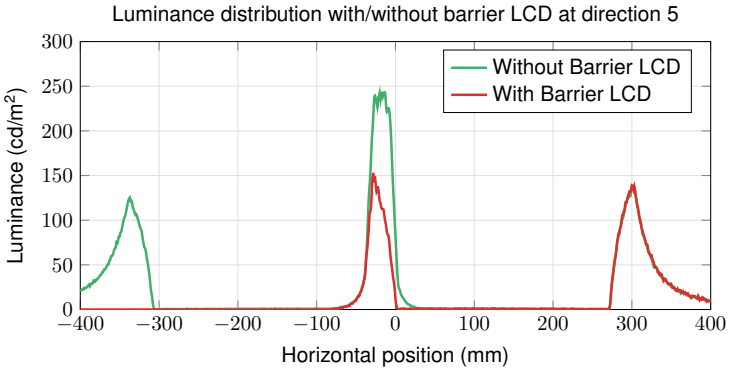

Figure 3.14: Comparison of the luminance distribution of viewing direction 5 with/without barrier LCD. The green curve represents the simulation result without using barrier LCD, and the red curve stands for the luminance distribution with a properly configured barrier LCD. After the use of barrier LCD, the illumination in the left viewing zone can be eliminated, while the distribution profile in the right viewing zone remains roughly unchanged.

the green user can be eliminated, while the perception of the blue user's right eye will not be influenced.

In the second simulation, the barrier LCD will be set to block the light rays towards the right viewing zone. The ray propagation and the illuminated areas on the detector plane will not be shown to avoid redundancy. The luminance distribution along the centerline of the detector plane is demonstrated in Fig.3.15, where the red curve represents the simulation result with the new barrier LCD. The original luminance distribution without using barrier LCD is still represented by the green curve. It can be seen that the illumination in the right viewing zone has been successfully eliminated, where the luminance at the peak position 302 mm is reduced from 137 cd/m^2 to a value lower than 0.3 cd/m^2. In the left viewing zone, the peak luminance at -337 mm is slightly changed from 125 cd/m^2 to 127 cd/m^2, which can be considered as constant after using the barrier LCD. At other positions within the left viewing zone, the green curve and the red curve can also coincide with each other.

The simulation results shown in Fig.3.14 and Fig.3.15 proved that the view conflict of viewing direction 5 can be solved by the barrier LCD. Although the

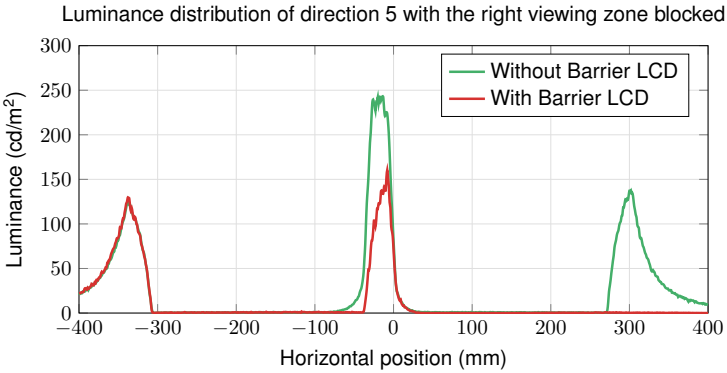

Figure 3.15: Simulation results when the barrier LCD is set to block the right viewing zone of viewing direction 5. The green curve represents the previous simulation result without using barrier LCD, and the red curve stands for the new luminance distribution with the barrier LCD activated. After the use of barrier LCD, the illumination in the right viewing zone can be eliminated, while the distribution profile in the left viewing zone also remains roughly unchanged.

block of the central viewing zone is irrelevant in the CID application, corresponding simulations can also be conducted to verify the functionality of the barrier LCD. With a proper system configuration, the simulation results are demonstrated in Fig.3.16. Based on the ray propagation and the luminance distribution, it can be concluded that the central viewing zone has been effectively suppressed.

The simulation results of viewing direction 5 with the barrier LCD have been analyzed in detail. In addition, the barrier LCD can also be configured to block the unwanted viewing zones of other viewing directions. Simulation results of viewing direction 6 and 7 with the barrier LCD are illustrated in Fig.3.17. Fig.3.17(a) shows the original luminance distribution without activating the barrier LCD, which will be used as reference to evaluate the distributions after activating the barrier LCD. Then in the simulation, the barrier LCD has been set to block the left viewing zone of these two viewing directions, and the simulation results are plotted in Fig.3.17(b) together with the original luminance distributions. The yellow and the black curves represent the simulation results after using the barrier LCD. The illumination in the left viewing zone can be

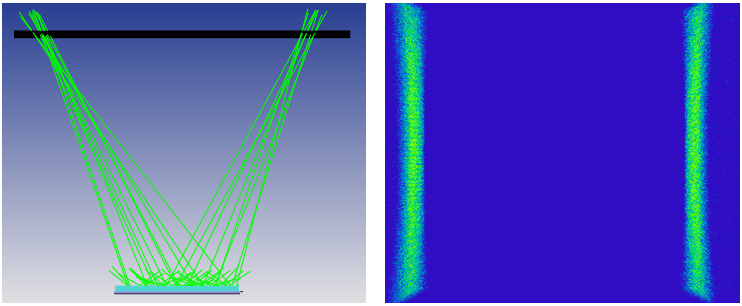

(a) (b)

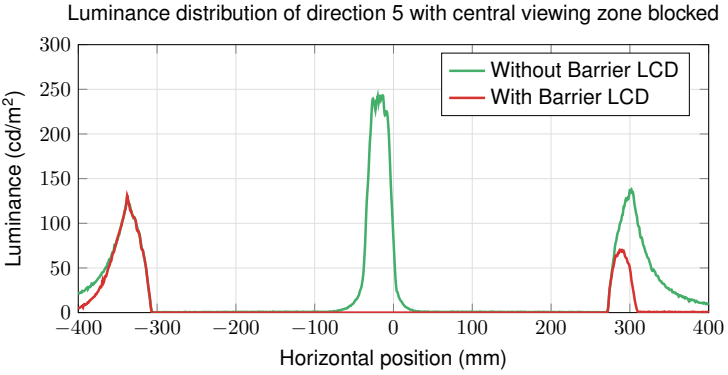

(c)

Figure 3.16: Simulation results when the barrier LCD is set to block the central viewing zone of viewing direction 5. (a) Demonstration of the ray propagation after the lens array. (b) Distribution of the illuminated area on the detector plane. (c) Luminance distribution along the horizontal centerline. It is clear that the illumination towards the central viewing zone is successfully eliminated.

eliminated, whereas the curve in the right viewing zone can highly match the original distribution profile.

Subsequently, the barrier LCD can be adjusted to block the right viewing zone of direction 6 and 7, with the simulation results shown in Fig.3.17(c). The yellow and the black curves also represent the luminance distributions after using the barrier LCD. It is obvious that the illumination in the right viewing zone has been effectively blocked, while the left viewing zone remains roughly the same compared to the original distributions. The analysis of Fig.3.17 has proved that the proposed new concept can successfully solve the side leak and thus the view conflict of viewing direction 6 and 7.

As for the other seven viewing directions, similar effects can also be observed with a proper barrier LCD configuration. The simulation results of other viewing directions will not be shown because of the high similarity to the results of viewing direction 5, 6 and 7.

According to the demonstrated simulation results, the intended function of the barrier LCD has been verified through the simulation. The proposed DB system with the barrier LCD is now able to selectively block the light rays towards the unwanted viewing zone. For the assumed CID application, the rays into the left and the right viewing zone can be separately modulated. Furthermore, the block of the central viewing zone has also been observed in the simulation of viewing direction 5. Therefore, the potential view conflict in the CID application can be solved.

3.5 Simulation of lens array tolerance

The designed function of the barrier LCD has been investigated in the last section. During the simulation of the DB system, all parameters have been assigned with the calculated value. However, in the real production, the final size cannot be precisely manufactured equal to the nominal value, and there must be a tolerance range. Among the three main components (matrix backlight, barrier LCD and lens array), the parameter variation of the lens array will significantly influence the ray propagation and the system output. In practice, a precise manufacturing process of the lens array demands high cost and is often too difficult to achieve [98]. Hence, this section will focus on the output

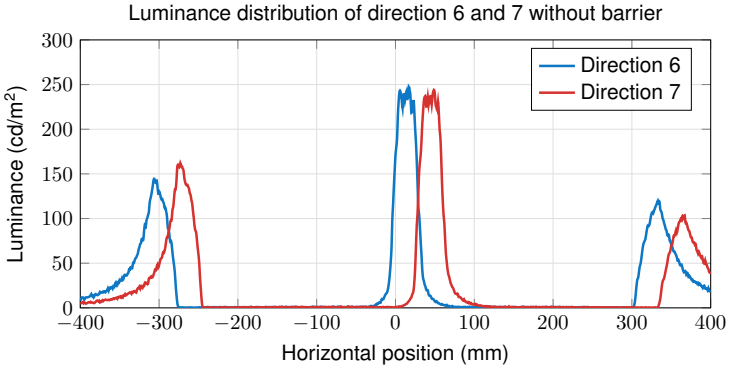

(a)

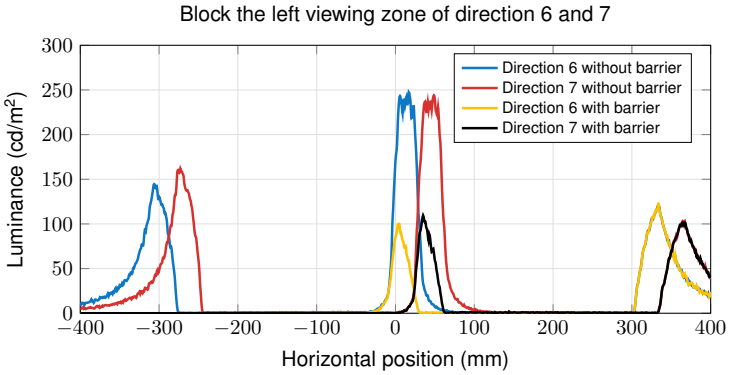

(b)

Figure 3.17: Simulation results of viewing direction 6 and 7 with the barrier LCD. (a) Original luminance distribution without the barrier layer. (b) Comparison of the distributions after the barrier LCD has been set to block the left viewing zone. It is obvious that the illumination in the left viewing zone has been eliminated and the right viewing zone is not affected. (c) Continued on the next page.

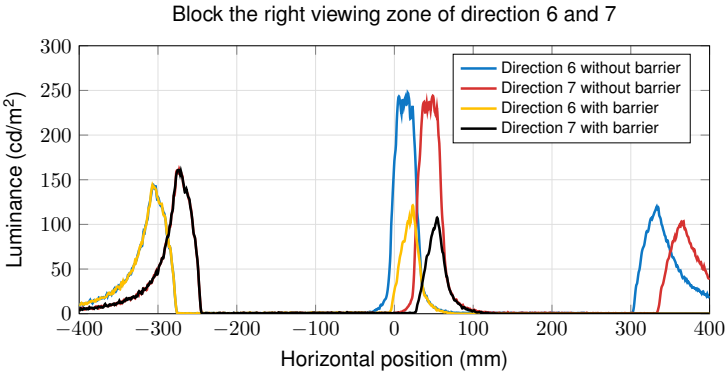

(c)

Figure 3.17: continued-(c) Comparison of the distributions after the barrier LCD has been set to block the right viewing zone. It can be seen that the right viewing zone has been effectively suppressed, whereas the left viewing zone remains roughly unchanged.

variation under different lens array parameters. In the subsequent sections, viewing direction 5 will be used to study the influence of four lens parameters: lens radius, lens pitch, fillet radius between lenses and lens thickness.

Furthermore, it is important to note that the tolerance of the lens parameters is strongly dependent on the manufacturing process. Since the milling technology was employed to produce the lens array in this work, the tolerance of the milling technology will be used as a reference in the following sections. Other manufacturing technologies, such as the combination of photo-lithography and etching techniques, or the utilization of nanoimprint lithography, can also be used to produce micro lens array, which can generally provide a higher precision but will not be discussed in this work [99].

3.5.1 Lens radius

At first the lens radius will be analyzed, whose nominal value is 6 mm. Through the investigation into several milling manufacturing companies [100], it has been found that the tolerance can be well controlled within ± 0.05 mm. Then simulations can be carried out to study the luminance distribution with two

boundary values, 6.05 mm and 5.95 mm, when viewing direction 5 is activated. The results are demonstrated in Fig.3.18(a), where the red curve represents the distribution with 5.95 mm lens radius, and the blue curve stands for the distribution with 6.05 mm lens radius. The original distribution with the nominal value 6 mm is drawn as the green curve. From Fig.3.18(a), it can be observed that the three distribution profiles can almost coincide with each other.

To have a further understanding on the variation of lens radius, two extreme radius values, 5.5 mm and 6.5 mm, will be studied. The luminance distribution with the two extreme radii can be seen in Fig.3.18(b), where the red curve represents the distribution with 5.5 mm lens radius and the blue curve represents the distribution with 6.5 mm lens radius. Compared with the green curve, which stands for the distribution with the nominal lens radius, the distance between two viewing zones has evidently varied for the red and the blue curve. Moreover, the luminance distribution of the red curve is more dispersed in each viewing zone, leading to a smaller peak value.

Based on the simulation results shown in Fig.3.18(a), it can be concluded that the system performance will be guaranteed with the radius tolerance ± 0.05 mm. For a larger radius variation, the distribution profile will show more obvious disparities, as demonstrated in Fig.3.18(b). However, as explained before, a radius tolerance of ± 0.05 mm can be reached by the current milling manufacturing technology. Therefore, the lens radius should not become a critical parameter in the manufacturing process.

3.5.2 Lens pitch

The lens pitch is the second parameter to be analyzed, whose nominal value is 5.88 mm. To investigate the influence of the lens pitch variation, the luminance distributions with different lens pitches have been simulated, when the viewing direction 5 is activated. The result is demonstrated in Fig.3.19(a), where the green curve represents the original distribution with the nominal pitch value. By observing the red curve and the blue curve, it can be concluded that a variation within 5 µm is still acceptable, since these two curves can still roughly match the green curve. Compared with the lens radius, the DB system is very sensitive to the change of the lens pitch. Once the variation is higher than 20 µm, there would be a large disparity between the distribution profiles, as can be seen at

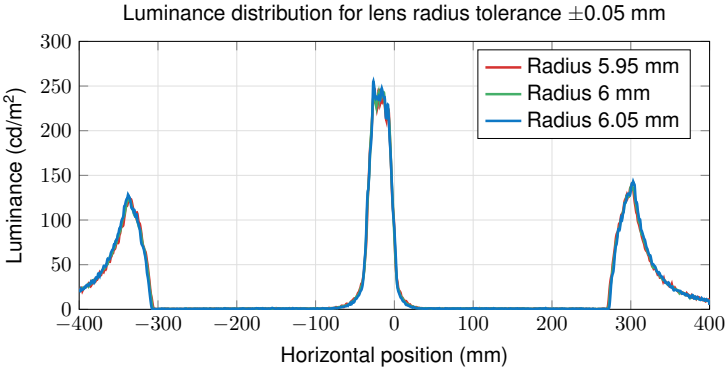

(a)

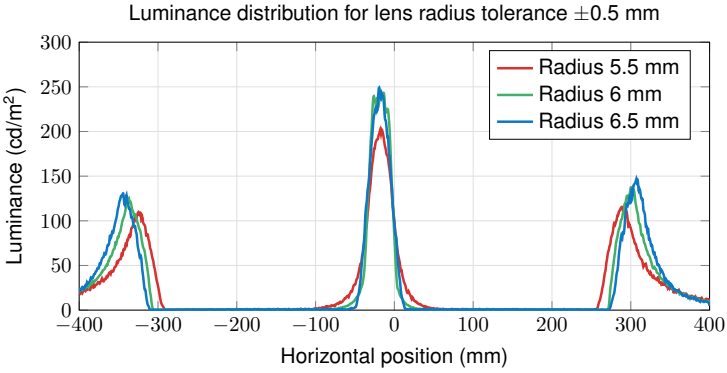

(b)

Figure 3.18: Luminance distribution with different lens radius values, when viewing direction 5 is activated. The green curve in each figure describes the distribution with the nominal radius value 6 mm. (a) Lens radius of 5.95 mm and 6.05 mm. The red curve represents the distribution with 5.95 mm radius, and the blue curve stands for the distribution with 6.05 mm radius. (b) Lens radius of 5.5 mm and 6.5 mm. The red curve represents the distribution with 5.5 mm radius, and the blue curve stands for the distribution with 6.5 mm radius.

the yellow curve with 5.86 mm pitch value. As a result, ± 5 µm is assumed to be the threshold tolerance of the lens pitch.

Then the function of the barrier LCD can be tested with this assumed tolerance. Under the pitch value 5.875 mm, the barrier LCD has been set to block the left viewing zone, and the simulation result is shown in Fig.3.19(b). The green curve and the red curve represent the luminance distribution before and after using the barrier LCD. The illumination area in the left viewing zone can be well eliminated with the barrier LCD. However, it should be pointed out that there exists a slight disparity between the two curves in the right viewing zone, which is caused by the change of the lens pitch. Since the barrier LCD configuration has been decided based on the nominal lens pitch value, some rays towards the right neighboring lens will be blocked under a different lens pitch.

Similar results can also be observed in Fig.3.19(c), where the barrier LCD is configured to block the right viewing zone. Therefore, the system performance can still be ensured with the tolerance ± 5 µm of the lens pitch, which is also feasible with the milling manufacturing process [99, 100].

3.5.3 Fillet radius between lenses

This subsection will study the influence of the fillet radius in the transition area between lens elements. As illustrated in Fig.3.20, the fillet radius R_T between lens elements cannot be avoided from manufacturing point of view. One method to enhance the fillet radius is to use the micro milling cutter, and the tolerance is strongly dependent on the manufacturing process. In the previous simulations, R_T has been set as 0.2 mm in the lens array modeling, based on the investigation of several corresponding manufacturing companies. [99, 100]

The simulation results of different fillet radii are demonstrated in Fig.3.21(a), where the green curve represents the previous distribution with 0.2 mm fillet radius. Although the four curves can roughly match with each other, there is still a slight disparity between the curves. To give a clear description of this disparity, the luminance distribution between 100 mm and 200 mm will be magnified in Fig.3.21(b). The luminance of the green curve is mostly under 1 cd/m^2, whereas the yellow curve is completely over 2 cd/m^2. It is obvious that with the increase of the fillet radius, the luminance value will also rise within

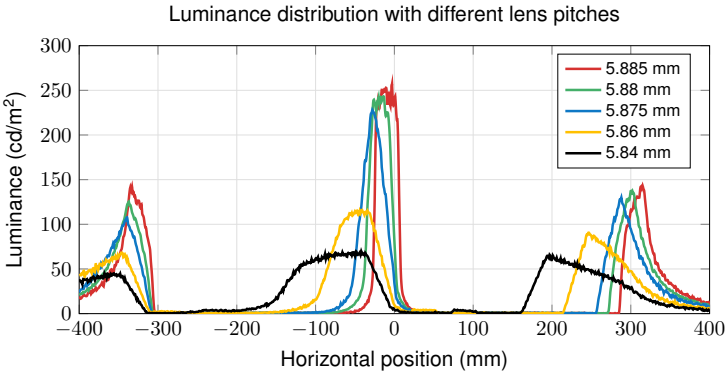

(a)

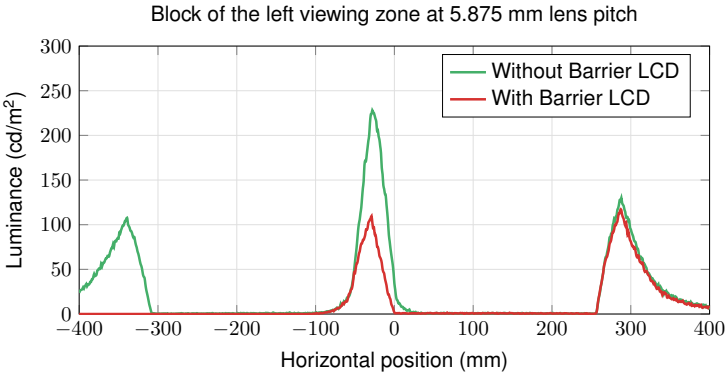

(b)

Figure 3.19: Simulation results of the lens pitch variation when viewing direction 5 is activated. (a) Luminance distribution with different lens pitches. It can be seen that a pitch variation of 20 µm will cause a significant distortion. (b) Test of the barrier LCD function under 5 µm pitch variation, where the red curve represents the luminance distribution with the barrier LCD. The left viewing zone is eliminated, and the red curve at the right viewing zone can correspond with the green curve. (c) Continued on the next page.

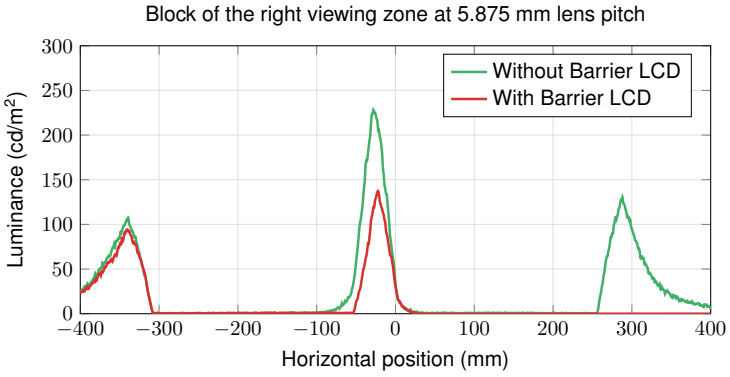

(c)

Figure 3.19: continued-(c) Demonstration of blocking the right viewing zone under 5 µm pitch variation.

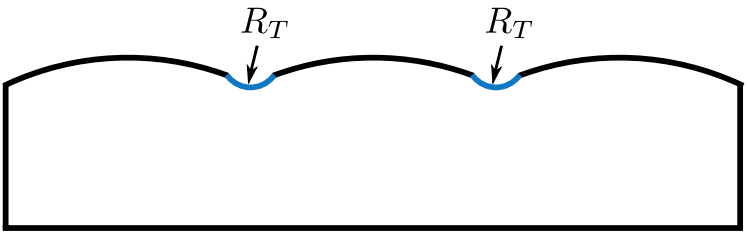

Figure 3.20: Illustration of the lens fillet radius R_T.

the magnified area, which could lead to a higher crosstalk. As demonstrated in Fig.3.10 and Tab.3.6, the crosstalk for direction 7 at 49 mm depends on the luminance value of direction 5. Since 49 mm is a place between two humps of direction 5, a larger luminance value (caused by the fillet radius) will lead to a higher crosstalk for direction 7.

To summarize, although the fillet radius will not significantly affect the system performance, it should still be carefully determined considering the 3D image quality and the manufacturing cost.

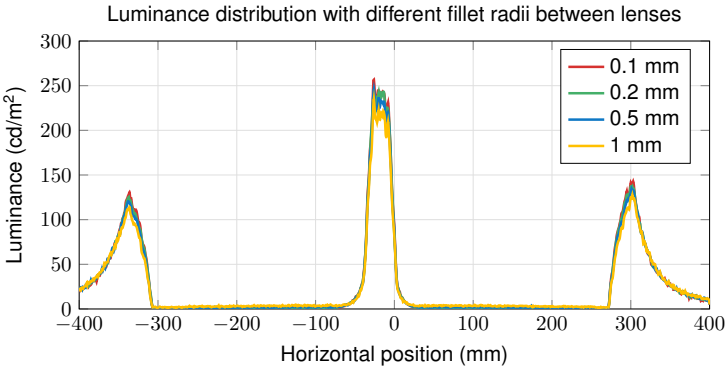

(a)

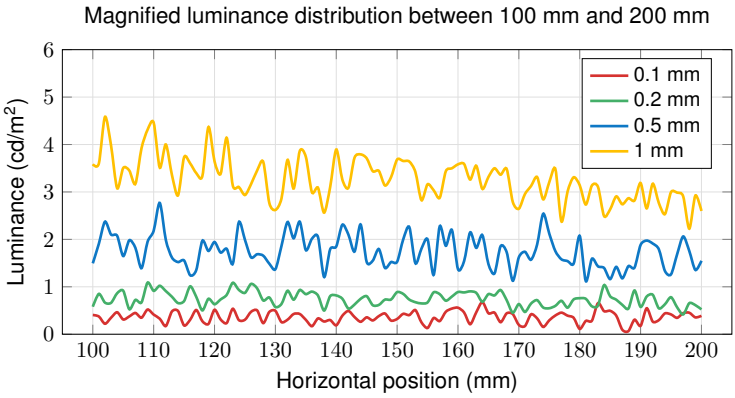

(b)

Figure 3.21: Simulation results of the fillet radius variation when viewing direction 5 is activated. (a) Luminance distribution with four different fillet radii. There is a slight disparity between the four curves. (b) Magnified luminance distribution between 100 mm and 200 mm to demonstrate the disparity between the four curves. It is clear that the increase of the fillet radius will cause the increase of the luminance values within the magnified area.

3.5.4 Lens array thickness

The lens array thickness defines the distance between the barrier LCD and the lens curving surface, and the thickness also influences the distance from the LED array to the lens surface. Therefore, the lens array thickness is an important parameter to guarantee the system performance, whose nominal value is 13.45 mm according to the system modeling. Simulation results with different thickness variations are demonstrated in Fig.3.22, where the green curve represents the original distribution with the nominal thickness value. In the central viewing zone, the five curves can still match with each other. But in the left and the right viewing zone, a larger thickness variation would shift the luminance profile away from the original distribution. This indicates that the distance between the central viewing zone and the left/right viewing zone will vary from the designed value. By controlling the thickness variation under 0.2 mm, the influence on the system performance is still acceptable, as can be seen from the blue and the yellow curve in Fig.3.22. For the current manufacturing technologies, the ± 0.2 mm thickness tolerance can be realized without large difficulty. Hence, the lens array thickness should not be a critical parameter in the manufacturing process.

3.6 Summary of the simulation results

This chapter has established a DB system based on the assumed vehicle CID application. The DB system has been modeled in the optical design software OpticStudio to test the functionality. Through the analysis of the simulation results, the designed function of the barrier LCD could be verified. The proposed DB system proves to be able to selectively block the light rays towards the unwanted viewing zone. Therefore, the potential view conflict caused by the side leak can be completely solved by the new DB concept. At last, the lens array tolerance has been discussed by analyzing four parameters of the lens array, where the lens pitch has been evaluated as the most sensitive parameter to influence the luminance distribution. It has been demonstrated that the tolerance achieved with the current milling manufacturing technologies can generate an acceptable system performance. To summarize, the simulation results have proved the feasibility of the suggested DB concept, which is able to create many new two-user applications.

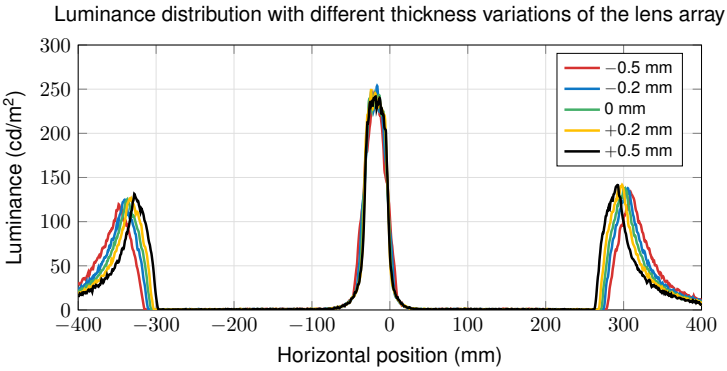

Figure 3.22: Simulation results of different lens array thicknesses when viewing direction 5 is activated. The luminance distributions can accord with each other in the central viewing zone, but shows noticeable difference in the left and the right viewing zone. ± 0.2 mm thickness variation can still provide an acceptable distribution profile, whereas ± 0.5 mm thickness variation has already produced an obvious shift of the distribution profile.

4 Implementation and Prototype

This chapter will describe the prototype construction of the proposed DB concept. Due to financial and time restrictions, the system model demonstrated in the last chapter has not been completely realized. Instead, an adapted and simplified prototype has been implemented in this work to verify the key function of the concept. As a result, the simulation model of the implemented prototype should also be adapted, and the obtained new simulation results will be used as reference to evaluate the experimental results.

4.1 Ideal display system with the proposed directional backlight

The new display structure based on the proposed DB can be illustrated in Fig.4.1. The DB concept has been extensively explained in the previous chapters, which consists of three main components: LED array, barrier LCD and lens array. The image LCD is placed on top of the DB, and the contents on the image LCD can be illuminated into the desired directions.

The parameters as well as the tolerance of DB have already been discussed in the previous chapters. It should be addressed that the refresh rate of the three electrical components (LED array, barrier LCD and image LCD) should be higher than 240Hz to provide a comfortable perception. The designed display system can create a new function, that four different images can be successively sent to four different directions without conflict. Based on this new feature, various novel multi-user applications can be created, which are not possible with the multiview 3D technologies. The new function as well as the applications have been explained in Sec.2.6, hence will not be repeated in this section.

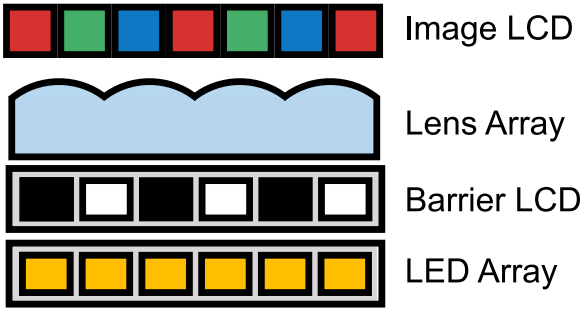

Figure 4.1: Ideal display system with the proposed DB concept.

4.2 Implemented system structure

As already mentioned, the ideal display system demonstrated in Fig.4.1 has not been achieved. Instead, a simplified prototype has been established in this work to check the feasibility of the proposed DB concept. The adjustment of the main components is listed in Tab.4.1.

Table 4.1: Adjustment of the main components in the final prototype

Component	Adjustment
Image LCD	Removed in the final prototype.
Lens array	Transition between lenses is changed to a plane surface.
Barrier LCD	Barrier LCD will be replaced by chrome mask.
LED array	LED array will be replaced by a normal LCD.

The adjustment of the components is mostly owing to the financial considerations. The LED pitch of the designed LED array is smaller than 1 mm. For the general display size 292 mm x 109 mm in automotive applications, more than 300 LEDs are necessary in the horizontal direction. The manufacturing of such a LED array requires very high development cost. Concerning the barrier LCD, the acquisition of a customized monochrome LCD is also not convenient, as the monochrome LCD is no longer state of the art and the series production of monochrome LCD has been stopped at most display suppliers.

Regarding the lens array, the manufacturing of the transition zones between lenses can largely influence the total cost. The fillet radius described in Sec.3.5 will lead to a better system performance than the plane transition, which will be demonstrated in the last section of this chapter. However, the lens array with fillet radius is much more expensive than the one with plane transition surface.

As for the decision to remove the image LCD, the component cost is not the main reason, since a standard LCD can be used in the system. The removal of image LCD is due to the limited system brightness. In the final prototype, the LED array will be replaced by a standard LCD to achieve the pixel-wise backlight illumination. The brightness of the standard LCD is less than 5% of the designed LED array. If the image LCD still remains in the system, the final output brightness would be very low, which would make it difficult for the measurement and data evaluation. Considering that the image LCD is not the essential part of the new concept, it has been decided to remove the image LCD in the final prototype.

Although the proposed DB concept has to be adapted due to cost reasons, the key function of the three components should still be maintained in order to prove the most basic and important contribution of the new DB concept: the rays towards the unwanted viewing zones can be eliminated. In terms of the LED array, the key function is to provide a pixel-wise illumination. This can also be achieved through a standard automotive LCD, as demonstrated in Fig.4.2, where the first and third pixel from the left side are activated in both components. By modulating the transmission of corresponding subpixels in LCD, it is able to generate the intended illumination pattern. Furthermore, the pixel size of the standard automotive LCD is much smaller than 1 mm, which can fulfill the concept requirement.

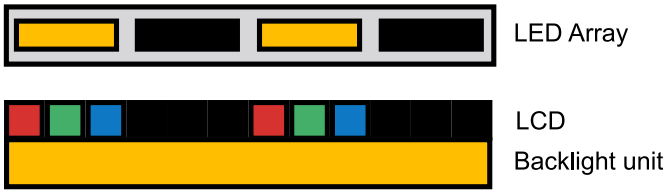

Figure 4.2: LED array will be replaced by a standard LCD to ensure the pixel-wise illumination. The first and third pixel from the left side are activated in both the LED array and the LCD.

For the barrier LCD, the key function is to block the rays towards the unwanted lenses, while the rays to the desired lenses can still propagate through the barrier LCD. Similar effects can also be achieved through a chrome mask. As illustrated in Fig.4.3, the rays encountering the mask will be absorbed, whereas the rays traveling through the gap will not be affected. With a suitable design of the chrome and gap width, it is possible to approximate the white-black pattern on the barrier LCD. However, the image pattern on the barrier LCD can be changed in different situations, but the chrome is fixed on the glass substrate, which can not be adjusted after manufacturing. To solve this problem, a special mechanical equipment has been designed to horizontally move the chrome mask and change the ray modulation. The mechanical equipment will be discussed in the next section.

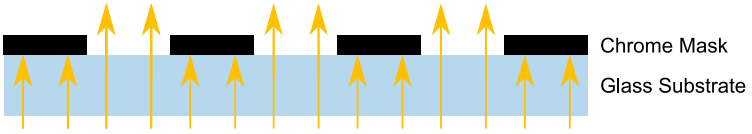

Figure 4.3: Modulation of the light rays through the chrome mask. The incident rays will be absorbed at the black rectangles, which are the chrome mask. For the gap between the chrome mask, the rays can further propagate without being influenced.

Regarding the lens array, the transition between lenses will be changed from fillet radius to a plane surface, as demonstrated in Fig.4.4. Micro milling cutters are required to produce the fillet radius, and the manufacturing over the whole lens array with the size 292 mm x 109 mm would be relatively slow and expensive. On the contrary, the plane surface can be realized with a forming-diamond tool, which is also illustrated in Fig.4.4. The manufacturing with the forming-diamond tool is cheaper and more efficient compared to the micro milling cutter. Therefore, a plane surface has been finally decided as the transition between lenses, and the influence on the system performance will be analyzed afterwards.

After the adjustment of the components have been discussed, the implemented system structure can be demonstrated in Fig.4.5. And the final prototype should be established based on this structure. It is clear that the final prototype will be a simplified implementation of the proposed concept, and it is not able to realize the new multi-user display applications, which have been previously shown in Sec.2.6. However, the most basic and important feature of the proposed DB

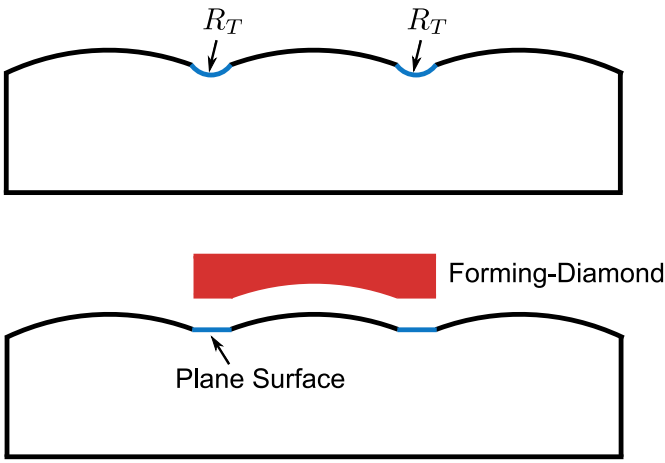

Figure 4.4: Change of the lens transition from fillet radius to a plane surface. The plane surface can be manufactured with the forming-diamond tool, which is more efficient than the fillet radius.

concept is expected to be verified with the final prototype, that the rays towards the unwanted viewing zones can be eliminated. If this feature can be proven in the experiments, the feasibility of the proposed concept will also be confirmed. Then it can be stated that the introduced applications could be realized with an upgrade of the components.

4.3 Component specification

This section will focus on the specification of the three main components. The LCD display used in the prototype is a standard automotive display, whose parameters are fixed and will be first introduced. As for the chrome mask and the lens array, some parameters have also been predefined by the manufacturer, which cannot be freely designed in the system modeling. As a result, the final system modeling needs to be adapted due to the predefined parameters. Then the complete specification of the chrome mask and the lens array can be determined based on the new system modeling.

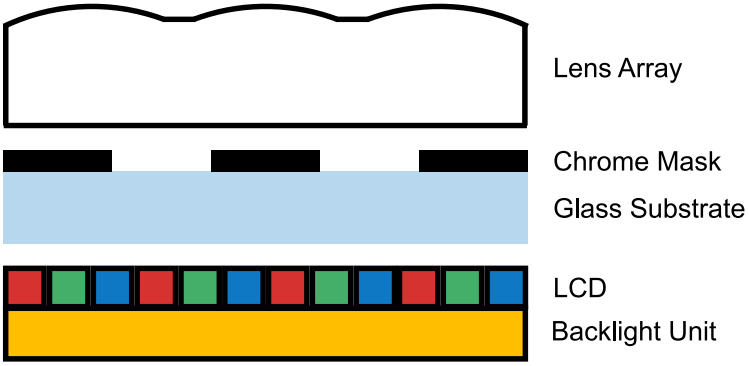

Figure 4.5: Final system structure with three main components: LCD with backlight unit, chrome mask and lens array.

4.3.1 LCD display specification

At first, the specification of some LCD display parameters is listed in Tab.4.2.

Table 4.2: Specification of the LCD display

Parameter	Specification
Screen Size (Diagonal)	12.3" (312.42 mm)
Outline Dimension	310.0 mm (H) × 128.0 mm (V) × 8.2 mm (T)
Active Area	292.0 mm (H) × 109.5 mm (V)
Number Of Pixels	1920 (H) × 3(R, G, B) × 720 (V)
Pixel Pitch	0.1521 mm (H) × 0.1521 mm (V)
Luminance	Minimum 600 cd/m^2 at 50 cm in the perpendicular direction.

The specification of the pixel pitch does not provide the information about the subpixel and the black matrix. To get more information, the LCD display has been analyzed under the microscope, with the result demonstrated in Fig.4.6. The pixel size could also be evaluated in the microscope image. It can be seen that the detected pixel pitch is around 152.16 µm, which accords with the

specification. Subpixel width is around 39.8 µm, and the width of the black matrix is around 10.9 µm. These two sizes will be subsequently used in the new simulation model.

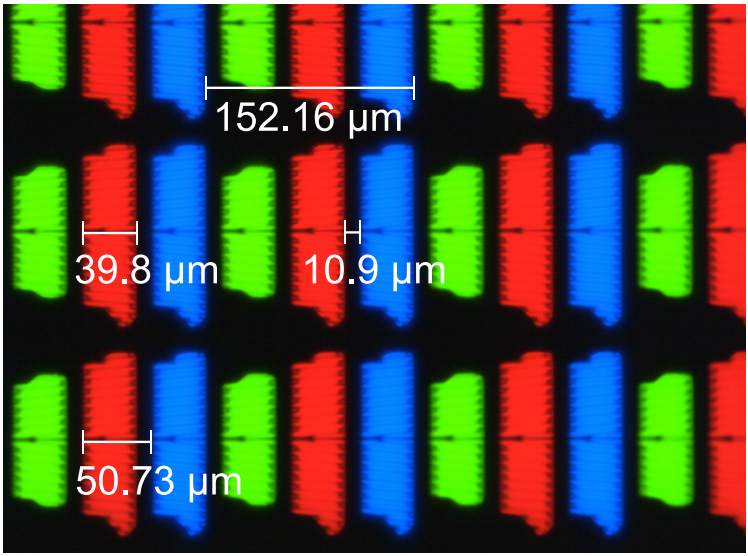

Figure 4.6: Microscope image of the LCD display. Pixel size can be roughly evaluated by drawing a line across the pixel and reading the line length in the software. The observed pixel pitch is 152.16 µm. Subpixel width is around 39.8 µm and the width of the black matrix is approximately 10.9 µm.

In addition, thickness and refractive index of the display glass and polarizer (on top of the color filter) are given in Fig.4.7. It should be noted that the polarizer consists of multiple thin layers, whose refractive index is all around 1.48. For simplification the polarizer is considered as one layer in the system modeling.

To further explore the radiation characteristic of the LCD display, a conoscopic measurement has been carried out. The result is shown in Fig.4.8(a), where the luminance distribution of the display is illustrated in spherical coordinates. Considering the automotive applications, the maximum polar angle has been set as 60°. The radiation is more concentrated in the vertical direction than in the horizontal direction, since the user movement is supposed to be limited in the vertical direction. The luminance distribution over the horizontal line HH'

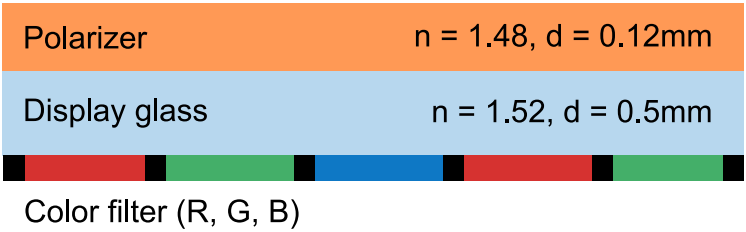

Figure 4.7: Thickness and refractive index of the display glass and polarizer, which are located on top of the color filter.

is further demonstrated in Fig.4.8(b). It can be seen that the maximum value appears in the perpendicular direction (0°), and the luminance will decrease with a larger polar angle towards the left and the right side.

In the next step, the display has been measured by a spectrometer to obtain the color information and the luminance output, when the white, red, green and blue image is successively demonstrated on the display. The measurement results are listed in Tab.4.3, which will be also used in the adapted simulation model.

Table 4.3: Luminance and color space of white, red, green and blue image

Parameter		White	Red	Green	Blue
Luminance (cd/m^2)		857.2	171.5	606.3	81
Color coordinates (CIE 1931)	x	0.3	0.661	0.284	0.147
	y	0.314	0.299	0.674	0.064

4.3.2 Predefined specification of the chrome mask and the lens array

Regarding the chrome mask, the parameters should be decided based on the new system model. As already explained, some parameters of the chrome mask are predefined by the supplier, which can be seen in Tab.4.4.

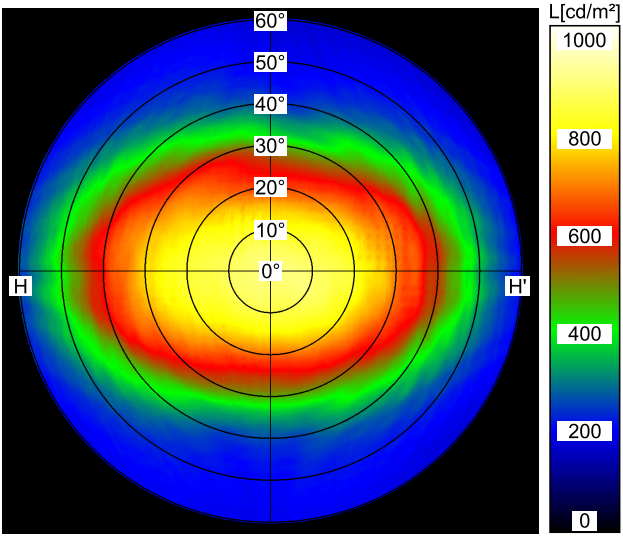

(a)

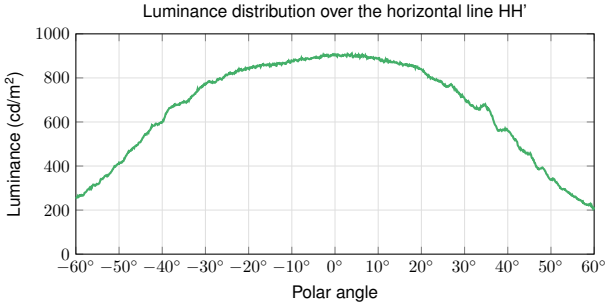

(b)

Figure 4.8: Conoscopic measurement of the LCD display, when a white image is shown. (a) Plot of the measured luminance distribution in spherical coordinates. Maximum polar angle has been set as 60° in the conoscopic measurement. (b) Plot of the luminance distribution over the horizontal line HH' in (a). Luminance will decrease with a larger polar angle towards two sides.

Table 4.4: Predefined parameters of the chrome mask

Parameter	Specification
Type of glass	Soda lime
Plate size	228.6 mm × 228.6 mm (± 0.5 mm)
Plate thickness	3.0 ± 0.1 mm
Cr Absorbance	3.0 ± 0.3
Cr film thickness	100 ± 10 nm

For the chrome mask, the most important function is to block the unwanted light rays. The measurement of chrome absorbance is illustrated in Fig.4.9. A white square has been shown on the display, and its luminance will be measured by a camera, which is located perpendicularly 60cm away from the display. In Fig.4.9, the yellow square stands for the measurement result without chrome mask, with an average value of 867.2 cd/m^2. The black square represents the result after placing chrome mask on top of the display, with an average value of 2.1 cd/m^2, which indicates a transmission rate of 0.24%. As a result, the absorbance of the chrome mask can be calculated as 2.62, and this value should be sufficient to prove the proposed concept. The concrete mask pattern will be determined through the new system modeling, which will be demonstrated in the subsequent section.

As for the lens array, it will be made of the material Poly Methyl Methacrylate (PMMA). Other lens parameters will also be determined in the new system modeling.

4.3.3 Adaption of system modeling to determine the lens array and the chrome mask

The system modeling described in Sec.3.1 should be adapted, because some parameters have already been predefined, which cannot be freely designed in the modeling. The comparison of the input parameters between the final and the previously assumed system modeling is shown in Tab.4.5. To keep the system performance, the design of the viewing zones will not be changed, hence, L, a and m remain the same. But other input parameters will be different. As for the

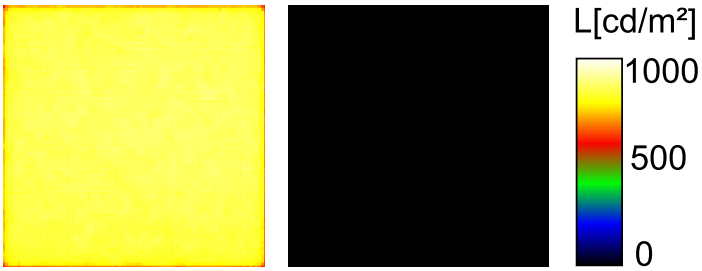

Figure 4.9: Measurement of the chrome mask absorbance. A white square is shown on the display, and a camera is placed perpendicularly 60cm away from the display to measure the luminance. The yellow square on the left side represents the original luminance. The black square on the right side represents the measurement result with chrome mask on top of this square. The average luminance of the yellow square is 867.2 cd/m^2, and the black square has an average value of 2.1 cd/m^2.

Table 4.5: Comparison of the input parameters

Parameter	L	a	m	t	n_1	n_L
In assumed system	600 mm	30 mm	10	0.6 mm	1.51	1.51
In final system	600 mm	30 mm	10	0.6084 mm	—	1.49

pixel-wise backlight, four LCD pixels will be combined as one unity, which means four LCD pixels will be simultaneously turned on and off, leading to a new pitch of 0.6084 mm. Besides, the lens array will be made of PMMA with a refractive index of 1.49. These two changes have been reflected in Tab.4.5.

In the final system, the chrome mask will be directly put on the display. As a result, the medium between the pixelwise backlight (LCD pixel) and the barrier layer (chrome layer) consists of three layers. This is different to the assumed system, where only one layer exists as the front medium. Therefore, in the final system modeling, the refractive index of the front medium can not be described with one refractive index. The concrete structure is further illustrated in Fig.4.10, where the thickness and the refractive index of the three intermediate layers are directly labeled in the figure.

After knowing the LCD pixel pitch, the intermediate materials as well as the lens materials, it is possible to determine other lens parameters. The deduction

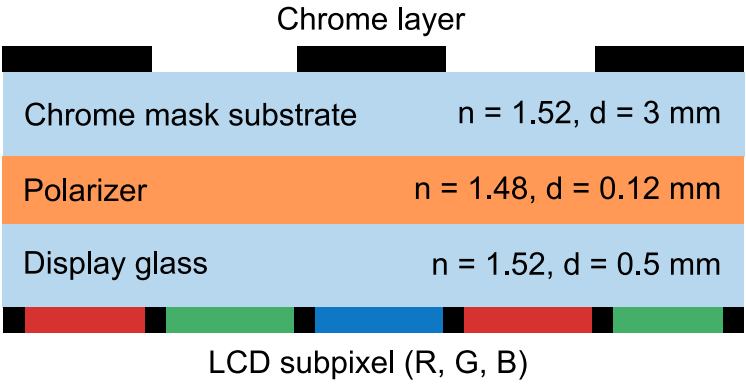

Figure 4.10: Illustration of the medium between the LCD pixel and the chrome mask in the final prototype. RGB subpixels are represented by the RGB rectangles at the bottom, while the three black rectangles at the top stand for the chrome layer. In total there are three layers between the LCD pixel and the chrome mask. The refractive index and the thickness of each layer are also given in the figure.

process will be omitted, and the result is listed in Tab.4.6. The Lens array with the required parameters has been manufactured and the final product is shown in Fig.4.11(a). As already mentioned, a planar transition surface will be applied between lenses. which is illustrated in Fig.4.11(b), with a transition width of 0.389 mm.

Table 4.6: Calculated lens parameters (unit in mm)

Parameter	***R***	***p***	***d***
Value	5.844	5.963	14.229

Then the last step is to determine the parameters of the chrome layer. Based on the explained system modeling, the allowable positions of the chrome layer can be calculated and demonstrated in Eq.4.1.

$$1.57\,\text{mm} < h < 5.36\,\text{mm}. \tag{4.1}$$

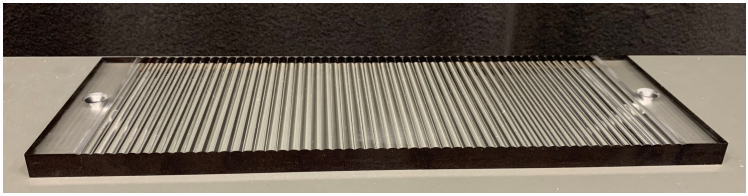

(a)

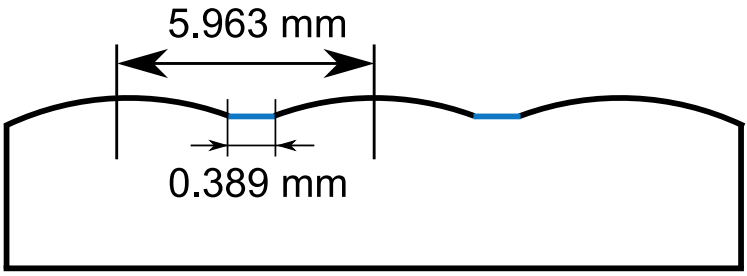

(b)

Figure 4.11: Final manufactured lens array. (a) Photo of the product. Two rectangular extrusions on the left and the right side will be used for the fixation of lens array in the experiment. The side faces have been processed with black varnish to reduce the reflection. (b) Planar transition surface between lenses. The width of the transition has been measured as 0.389 mm.

Eq.4.1 indicates the chrome mask can be placed at any positions between 1.57 mm and 5.36 mm to realize the designed function. Actually in the final system, the distance between the chrome layer and the LCD pixel has already been defined by the three intermediate layers, as demonstrated in Fig.4.10. The total thickness of the three layers is 3.62 mm, which can meet the requirement in Eq.4.1.

Subsequently the width and the pitch of the chrome pattern can be determined and illustrated in Fig.4.12(a). The chrome layer will be produced in the shape of one rectangle array with 3.028 mm width and 6.056 mm pitch.

Chrome mask with the required parameters has been manufactured and one product photo is demonstrated in Fig.4.12(b). In the final product, two extra

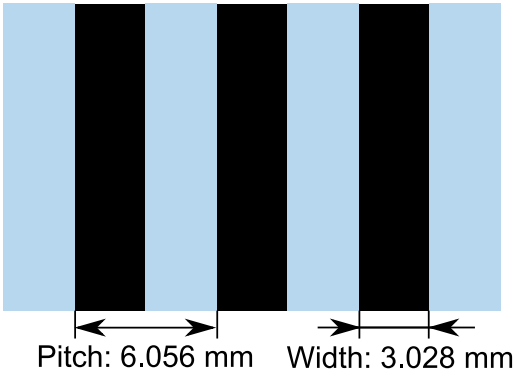

(a)

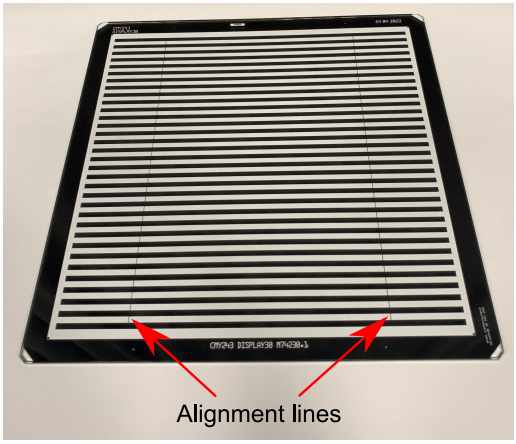

(b)

Figure 4.12: Pattern of the chrome layer. (a) Chrome will be produced as narrow rectangles on the glass substrate. The width of one rectangle is 3.028 mm, and the distance between two rectangles is 6.056 mm. (b) Demonstration of the manufactured chrome mask with the designed pattern. Two extra lines perpendicular to the rectangles have been added to the pattern, which will be used for the alignment between the lens array and the chrome mask.

lines perpendicular to the rectangles have been added into the chrome pattern, as highlighted in Fig.4.12(b). The line width is 0.3 mm, and the distance between the two lines is 128.1 mm, which is 0.1 mm larger than the width of the lens array. Based on the system concept, the chrome mask will be put under the lens array. In the experiment, the placement of the chrome mask should be finely adjusted, till the lens array is completely located within the two lines. As a result, the lens array can be aligned approximately parallel to the chrome mask, as demonstrated in Fig.4.13(a). Maximum angular misalignment will appear when the lens profile intersects with the boundary points of the two alignment lines, as illustrated in Fig.4.13(b). The angular misalignment θ in this case can be calculated as around 0.2°, with which the essential function of the proposed concept can still be demonstrated.

4.4 Prototype construction

The system, which contains the three introduced components, should be built up in the prototype. A precise alignment of all components is necessary to ensure the system performance. In the ideal system design, the components should be assembled with optical bonding to reach a stable and accurate alignment. However, optical bonding is not feasible in the final prototype, because the chrome mask has to be shifted during the experiment to reach different ray modulations. Therefore, the relative positions between the three components need to be controlled by special mechanical equipments. For the final system structure, there are mainly three types of alignments to be designed:

1. Alignment of the component vertical positions, so that three components can stay in contact with each other.
2. Alignment of the relative angle between the three components.
3. Horizontal position of the chrome mask should be adjustable.

The placement of the lens array will be first introduced because it is simply fixed onto the mounting table through two mechanical parts, as demonstrated in Fig.4.14. During the whole experiment, the lens array will stay static. In this section, the system structure will first be analyzed in the CAD software, and the real implemented prototype will be shown at the end of this section.

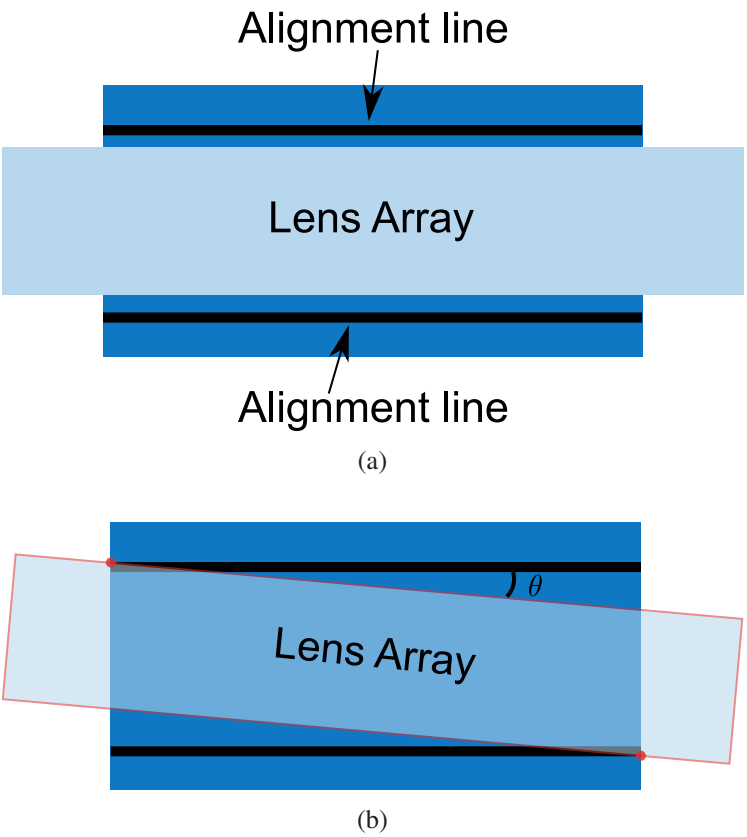

Figure 4.13: Adjustment of the relative angular position between the lens array and the chrome mask based on two alignment lines. For a clean observation, the rectangle array is not drawn in the figure. (a) Ideal alignment when the lens array is completely within the two lines. the angular misalignment can be neglected. (b) Demonstration of the maximum angular misalignment, when the lens array profile intersects with the boundary points of the two lines. The maximum angular misalignment θ is approximately 0.2°.

As for the LCD display, the position control is illustrated in Fig.4.15, where the display is fixed on the vertical and rotary stage through an adapter plate. As a result, the LCD can be shifted in the vertical direction, which enables

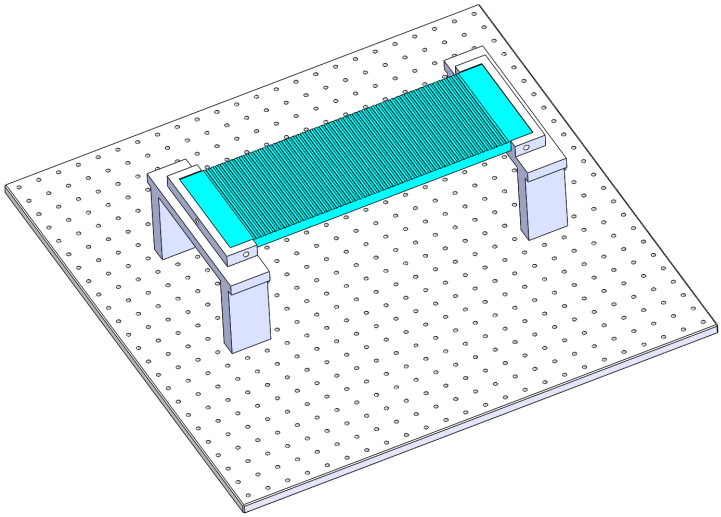

Figure 4.14: Fixation of the lens array on the mounting table. There are two extra extrusions on two sides of the lens array in the final prototype. The lens array is fixed by two mechanical parts onto the mounting table.

the contact of all components. In addition, the LCD can also be rotated by the rotary stage to change its angular position. Because a precise angular alignment between the lens array and the LCD display is required, a rotary stage with fine adjustment 0.01° has been chosen for the prototype.

The chrome mask will be directly put on the LCD display without constraints from other equipments, so the chrome mask can be moved freely. As discussed in the last section, the angular alignment of the chrome mask will be achieved through two special alignment lines, where the edge of the lens array should be located within the two lines. Simultaneously, the chrome mask needs to be moved in the horizontal direction to approach the modulation of the barrier LCD.

The horizontal shift of the chrome mask is realized through a translation stage, which is combined with a mechanical part, as can be seen in Fig.4.16(a) and (b). The alignment implementation is illustrated in Fig.4.16(c), where the black-

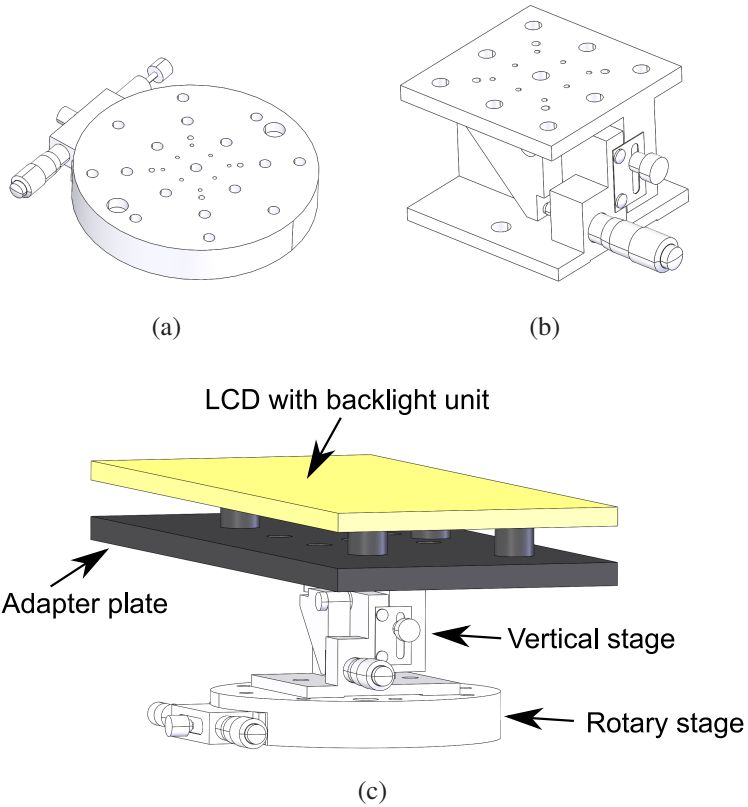

Figure 4.15: Fixation of the LCD display. (a) Rotary stage used in the prototype to realize angular adjustment. (b) Vertical stage used in the prototype to change the vertical position. (c) LCD display consists of the LCD and the backlight unit. The LCD display will be fixed on one adapter plate, which is screwed onto the vertical stage. The LCD display can then be driven up and down by the vertical stage, and it can also be rotated through the rotary stage.

white stripes represent the chrome mask, which is placed between the lens array and the display. In the experiment, the intended horizontal displacement should be set at the translation stage, then the mechanical part shown in Fig.4.16(b) will shift the chrome mask to transmit the displacement. It should be pointed out that after every horizontal alignment, the relative angle between the lens array and the chrome mask should be checked by inspecting the two alignment lines.

In Fig.4.16, in order to provide a clear view of the chrome mask alignment, the equipments to hold the lens array and the LCD display are not drawn. A perspective of the whole system is demonstrated in Fig.4.17(a). As comparison, the camera image of the final prototype is shown in Fig.4.17(b).

4.5 Simulation results of the implemented prototype

To simulate the prototype performance, a new system model needs to be created in OpticStudio according to the final component parameters. The chrome layer will be modeled as an absorbing layer with 0.24% transmission. As for the LCD display, the characteristics described in Sec.4.3 should be correctly configured to achieve an accurate simulation result. The configuration in the simulation software is similar to the assumed example in Sec.3.2, hence, a detailed description of the simulation model will be omitted.

Simulation results of viewing direction 5 will be first demonstrated. To begin with, a qualitative description of viewing direction 5 without chrome layer will be shown, where only the glass substrate of chrome mask will be considered in the simulation. The ray propagation after the lens array is demonstrated in Fig.4.18(a). Same to previous simulations, a detector plane is located 600 mm away from the DB to record the simulation results. Then the illuminated area on the detector is shown in Fig.4.18(b). In both figures, three major viewing zones (left, central, right) can be observed. However, two extra minor viewing zones have appeared, which didn't exist in the previous simulations. This is caused by the planar transition surface in the lens array. Referring to Fig.4.11(b), there is a planar surface with 0.389 mm width between two lenses. So instead of being scattered at the fillet radius, light rays incident on the plane surface will be

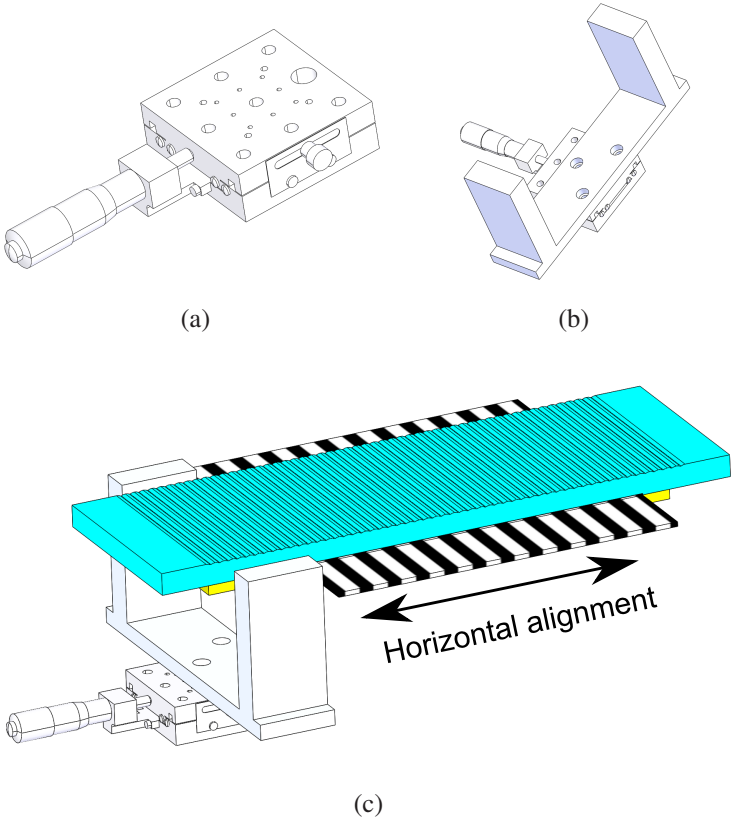

Figure 4.16: Horizontal shift of the chrome mask. (a) Translation stage used in the prototype to realize the horizontal adjustment. (b) Special mechanical part is screwed on the translation stage, which will be used to shift the chrome mask. (c) Chrome mask is represented by the black-white stripes in the figure. During the experiment, the horizontal displacement set to the translation stage will be transferred to the chrome mask.

refracted in a more concentrated manner. As a result, the minor viewing zones will be created in the middle between two major viewing zones.

Then the luminance of the DB should be quantitatively evaluated, where the assessment method is same to the method explained in Fig.3.7. The average

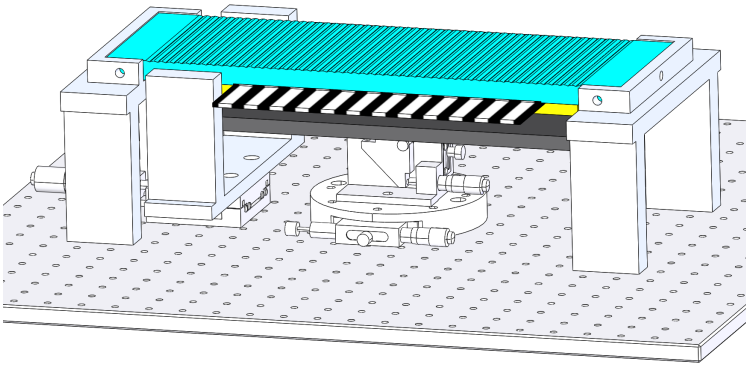

(a)

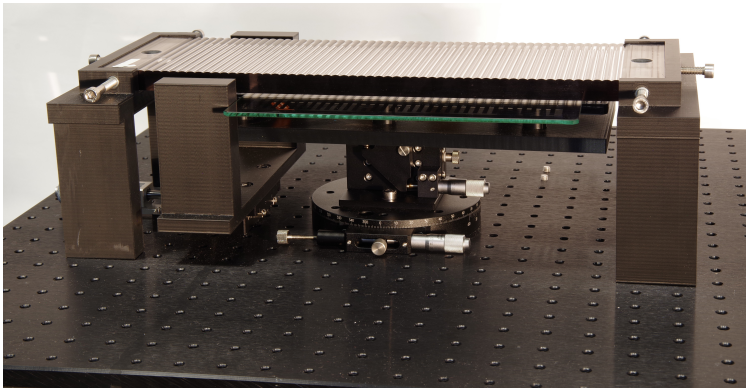

(b)

Figure 4.17: View of the whole system with all components. (a) System view generated in the modeling software. (b) Camera image of the final prototype.

luminance of the square, which is located on the center of the lens array top surface, is calculated in the simulation. The side length of the square should be adjusted to 23.852 mm, based on the final lens pitch. In addition, the pixel size on the detector is set as 4 mm to match the camera in the experiment, whose diameter of the entrance pupil is 4 mm.

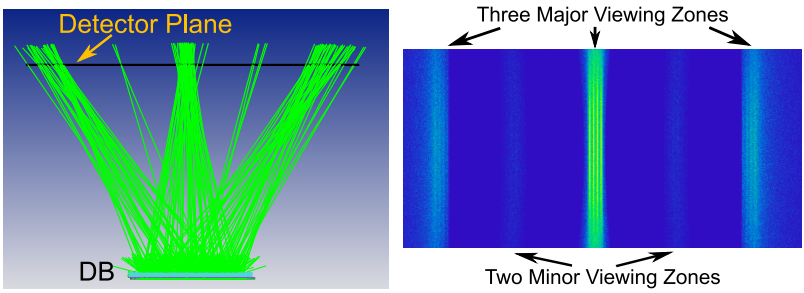

Figure 4.18: Qualitative description of the system output, when viewing direction 5 is activated in DB. (a) Ray propagation after the lens array. (b) Illuminated area on the detector plane, which is 600 mm away from the DB. As designed, three viewing zones (central, left and right) are created on the detector plane. Two extra minor viewing zones have appeared in the simulation, which are caused by the planar transition surface in the lens array.

After the designed luminance at every pixel along the horizontal centerline of the detector is calculated in the simulation, the luminance distribution of viewing direction 5 without chrome layer can be plotted in Fig.4.19(a). The three major viewing zones as well as the two extra minor viewing zones can be clearly observed in the distribution, where the minor viewing zone is in the middle between two major viewing zones.

In the next step, the chrome mask will be added in the simulation. Fig.4.19(b) shows the result when the chrome layer is set to block the left viewing zone of direction 5. According to Fig.4.19(b), the left viewing zone can be completely eliminated, while the right viewing zone remains roughly the same as the original distribution. Then the chrome layer is set to block the right viewing zone, with the result demonstrated Fig.4.19(c). It is clear that the right viewing zone can be effectively suppressed, and the left viewing zone is almost unaffected. In addition, it can be observed that the corresponding minor viewing zone has been eliminated simultaneously with the major viewing zone, because the light rays towards the corresponding transition area will also be blocked by the chrome layer.

In addition, simulation results of viewing direction 6 and 7 are shown in Fig.4.20. The original luminance distribution without the chrome layer is de-

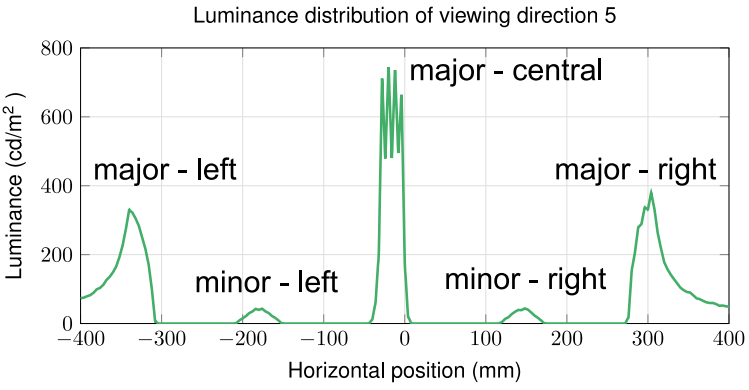

(a)

(b)

Figure 4.19: Luminance distribution of viewing direction 5 along the horizontal centerline of the detector plane. (a) Original luminance distribution without chrome layer, where three major viewing zones (central, left and right) and two minor viewing zones can be observed. (b) Comparison of the luminance distributions, after the chrome mask has been set to block the left viewing zone. (c) Continued on the next page.

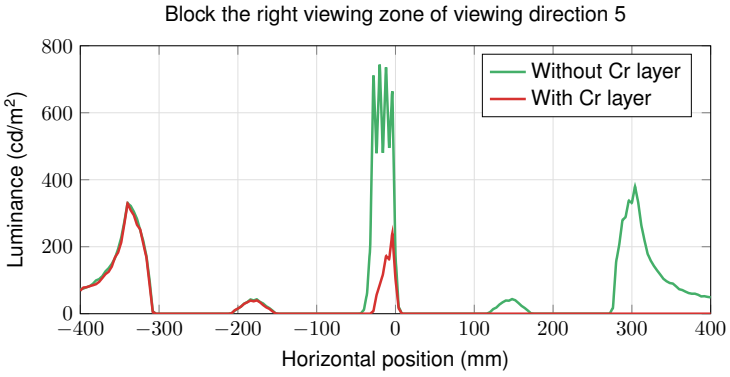

(c)

Figure 4.19: continued-(c) Comparison of the luminance distributions after the chrome mask has been set to block the right viewing zone.

monstrated in Fig.4.20(a), where the two extra minor viewing zones have also appeared. Then the chrome layer will be added in the simulation to block the left and the right viewing zones, with the results illustrated in Fig.4.20(b) and (c) respectively. It can be seen that the unwanted viewing zones have been successfully eliminated after using the chrome layer, while the desired viewing zones could still be generated in the same position.

As for the other seven viewing directions, similar effects can also be observed with a proper chrome layer configuration. The simulation results of other viewing directions will not be shown because of the high similarity to the results of viewing direction 5, 6 and 7.

Based on Fig.4.19 and Fig.4.20, it can be concluded that the final prototype is able to demonstrate the essential function of the proposed DB concept: light towards the unwanted viewing zone can be selectively blocked through a specially designed barrier layer. Subsequently, the prototype will be characterized in the experiment, and the measurement results should be compared with the simulation results shown in this section.

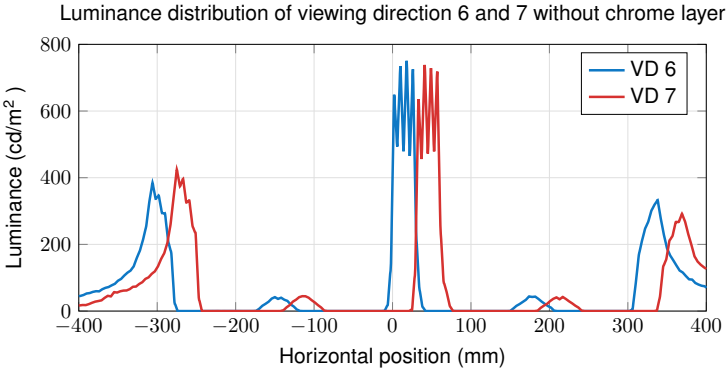

(a)

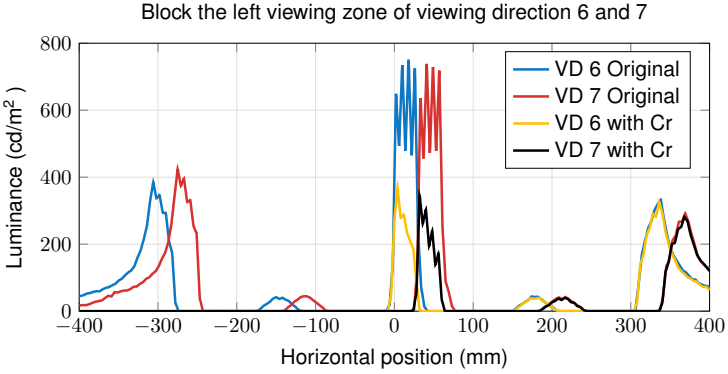

(b)

Figure 4.20: Simulation results of viewing direction 6 and 7. VD in the legend of the figure stands for "viewing direction". (a) Original luminance distribution without chrome layer. (b) Luminance distribution when the chrome layer is set to block the left viewing zones of viewing direction 6 and 7. (c) Continued on the next page.

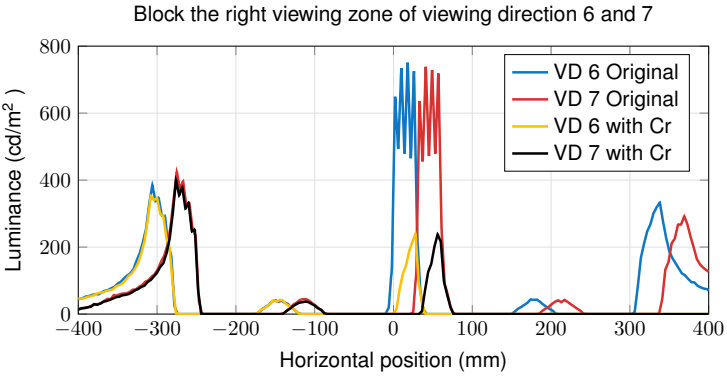

(c)

Figure 4.20: continued-(c) Luminance distribution when the chrome layer is set to block the right viewing zones of viewing direction 6 and 7.

5 Experiments and Result Analysis

This chapter will present the experimental process for measuring the constructed prototype. At first a qualitative description of the prototype performance will be given. Then the luminance distribution of different viewing directions will be measured to obtain a quantitative evaluation. At last, the measurement results will be compared with the simulation results demonstrated in Sec.4.5.

5.1 Qualitative observation

This section will give an intuitive description of the illumination output from the prototype. In the simulation, a detector plane with 800 mm width has been placed 600 mm away from the DB to record the luminance distribution. Because it is difficult to set up such a large detector in the experiment, a piece of paper has been put over the prototype to record the incident light, as demonstrated in Fig.5.1(a). The plane paper is placed around 600 mm away from the DB to simulate the detector plane. To reduce external illumination, the experiment will be conducted in the dark room. When the ambient light is turned off, only the light rays coming from the prototype will fall on the paper. Therefore, the intensity distribution at the designed 600 mm can be registered on the paper, as can be seen in Fig.5.1(b).

Viewing direction 5 has been turned on in Fig.5.1(b), and the three major viewing zones along the horizontal direction can already be observed in the figure. It should be pointed out that a pure glass plate with 3 mm thickness (same to the chrome mask) is now placed between the lens array and the LCD display. The chrome mask has not been used since it will block the viewing zones.

Furthermore, the luminance distribution on the paper can be measured by the camera. At first, measurement results of viewing direction 5 are demonstrated in

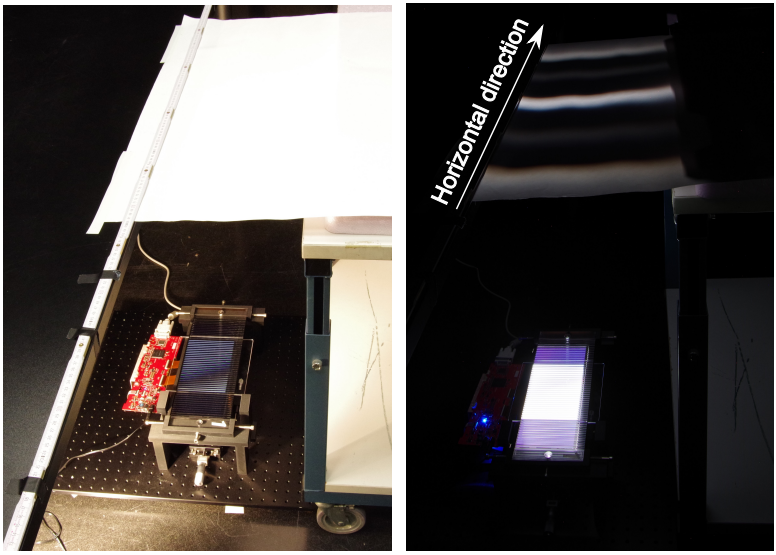

Figure 5.1: Measurement of the intensity distribution using a white paper. (a) One piece of white print-paper is placed with roughly 600 mm distance to the lens array. (b) When ambient light is turned off in the dark room, the intensity distribution of the DB at 600 mm distance can be recorded.

Fig.5.2. Based on the automotive CID application, the luminance value within the horizontal range (−400 mm, 400 mm) is plotted, where the horizontal position is referred to the horizontal distance regarding the display center. The luminance distribution has been shown in Fig.5.2(a) and (b) with different scales, to respectively highlight the center and the side viewing zones. The distribution profile is more concentrated in the central viewing zone, and becomes dispersed towards two sides, which matches the previous simulation results. In addition, the two extra minor viewing zones can also be seen in Fig.5.2(b).

In the next step, the chrome mask will be put between the lens array and the LCD display to replace the glass plate. At first the chrome mask is set to block the left viewing zone of direction 5, with the luminance distribution demonstrated in Fig.5.3(a). Compared to the original distribution in Fig.5.2(b),

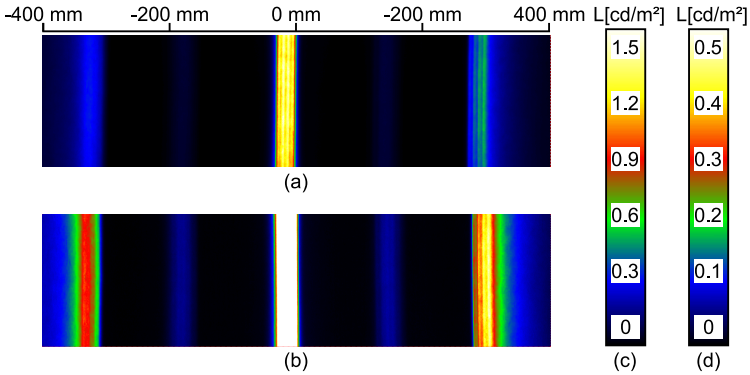

Figure 5.2: Measurement of the luminance distribution within (−400 mm, 400 mm) on the paper, when viewing direction 5 is activated on the DB. In this case, a glass plate is placed between the lens array and the LCD display to enable all viewing zones. (a) Measured luminance distribution on the paper, with the scale shown in (c). (b) Demonstration of the luminance distribution with a different scale to highlight the left and the right viewing zone, with the scale shown in (d).

the left viewing zone is now successfully eliminated, while the right viewing zone is almost not affected. Fig.5.3(b) shows the luminance distribution on the paper, when the chrome mask is shifted to block the right viewing zone. It can be observed that the luminance value on the right side has been significantly reduced.

Similar measurements have also been carried out for viewing direction 6 and 7. Fig.5.4 describes the luminance distribution on the paper, when viewing direction 6 is activated. The original luminance distribution with a normal glass plate is demonstrated in Fig.5.4(a), where three major viewing zones and two minor viewing zones are visible. Then the chrome mask will be used to block the left viewing zone, with the result shown in Fig.5.4(b). It is clear that the luminance on the left side has been largely reduced, while the luminance on the right side remains roughly the same. Then the block of the right viewing zone is demonstrated in Fig.5.4(c), where the right viewing zone has been significantly suppressed.

The measurement result of viewing direction 7 is shown in Fig.5.5, where the block of the corresponding viewing zone can also be clearly observed. The

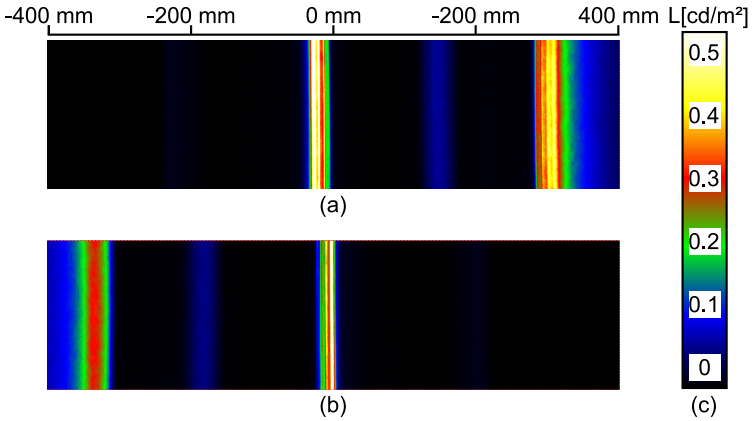

Figure 5.3: Measurement of the luminance distribution within (−400 mm, 400 mm) on the paper, when the glass plate is replaced by the chrome mask to block the corresponding viewing zone of viewing direction 5. (a) Luminance distribution when the chrome mask is set to block the left viewing zone, with the scale shown in (c). (b) Luminance distribution when the chrome mask is set to block the right viewing zone, with the scale shown in (c).

analysis of other seven viewing directions will be omitted because of the high similarity to viewing direction 5, 6 and 7. To sum up, a piece of paper has been placed approximately 600 mm away from the lens array, and the paper can be considered as a detector plane to record the illumination output from the prototype. Furthermore, the luminance distribution on the paper can be measured by the camera, where the output of viewing direction 5, 6 and 7 has been described in this section. As expected, the measurement results have proven the key function of the proposed DB concept, that the light rays towards the unwanted viewing zone can be selectively eliminated.

5.2 Quantitative measurement

In the last section, a qualitative observation of the system output has been conducted. To further evaluate the prototype characteristic, the luminance directly from the constructed DB will be measured with the same assessment

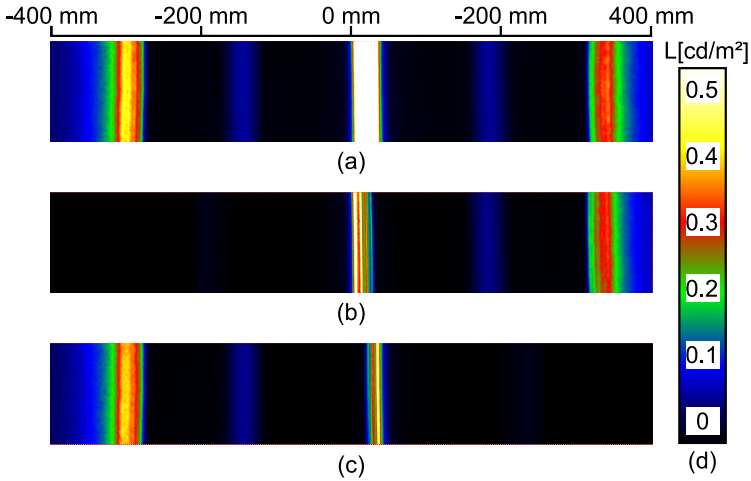

Figure 5.4: Measurement of the luminance distribution within (−400 mm, 400 mm) on the paper, when viewing direction 6 is activated on the DB. (a) Original luminance distribution when a pure glass plate is placed between the lens array and the LCD display. (b) Luminance distribution when the chrome mask is used to replace the glass plate, and the chrome mask is set to block the left viewing zone. (c) Luminance distribution when the chrome mask is set to block the right viewing zone. (d) Scale for the luminance distribution in (a), (b) and (c).

method used in the simulation. The experiment process will be explained in detail by demonstrating the measurement of viewing direction 5, then the measurement result of viewing direction 6 and 7 will be given at the end of this section.

5.2.1 Experiment set up

The experiment configuration is demonstrated in Fig.5.6. The prototype is fixed on the ground, which will not be moved during the experiment. The camera is mounted to a equipment on the table, and the table surface is parallel to the display top surface. The coordinate system is also illustrated in Fig.5.6, where the x axis represents the lateral movement in the horizontal direction. The z axis is perpendicular to the display top surface, and the display center is also

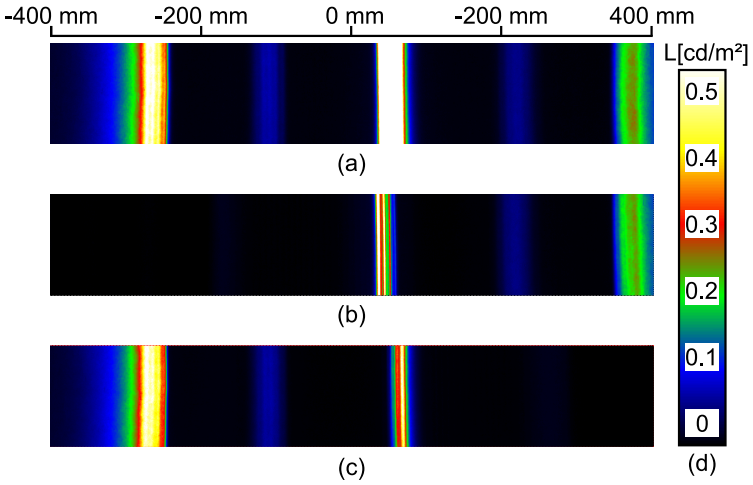

Figure 5.5: Measurement of the luminance distribution within (−400 mm, 400 mm) on the paper, when viewing direction 7 is activated in DB. (a) Original luminance distribution when a pure glass plated is placed between the lens array and the LCD display. (b) Luminance distribution when the chrome mask is used to replace the glass plate, and the chrome mask is set to block the left viewing zone. (c) Luminance distribution when the chrome mask is set to block the right viewing zone. (d) Scale for the luminance distribution in (a), (b) and (c).

located on the z axis. In the simulation, the detector plane is set to be 600 mm away from the lens array. In the experiment, the reference plane is considered to be the entrance pupil of the camera. Therefore, the distance between the entrance pupil and the lens array in the z direction should be controlled at 600 mm.

The test image for viewing direction 5 is demonstrated in Fig.5.7. The lines in the image stand for the pixels of viewing direction 5. Each line covers vertically 420 Pixels, while horizontally it contains 4 pixels, resulting in a line width of 0.6084 mm. The distance between two lines is 6.084 mm, since there are in total ten individual viewing directions.

The last step in the experiment preparation is to align the display panel with the lens array. As explained in Sec.4.4, the lens array is fixed on the mounting table, and the angular alignment of the display is achieved by the rotary stage.

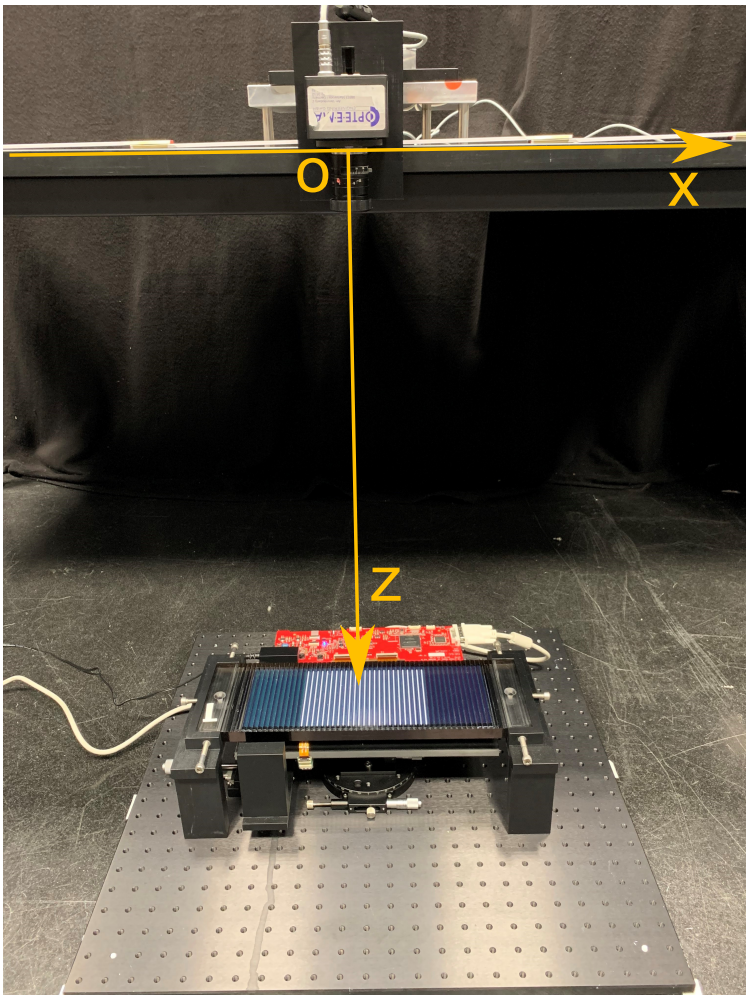

Figure 5.6: Experiment configuration. The prototype is fixed on the ground, and the camera is mounted to a equipment on the table. The x axis defines the lateral movement of the camera, and the z axis is perpendicular to the display top surface. The distance between the entrance pupil of the camera and the lens array should be kept at 600 mm.

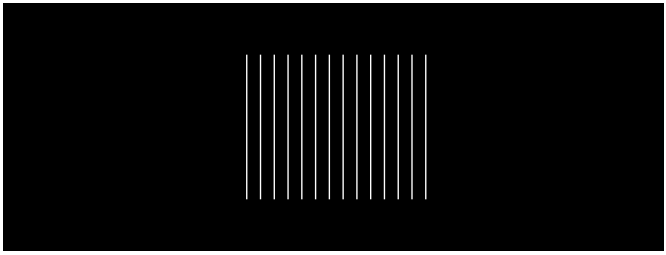

Figure 5.7: Test image for viewing direction 5, which will be shown on the LCD display with the resolution 1920 × 720. There are 14 lines in the image, representing the pixels corresponding to viewing direction 5. Each line contains 4 × 420 pixels.

When the test image for viewing direction 5 is shown on the display, a pure glass plate with 3 mm thickness is inserted between the lens array and the display to help create the original system output without barrier layer. The camera can be moved to one position in the central viewing zone to capture the luminance distribution of the DB, which can be used to evaluate the alignment. Fig.5.8 illustrates the recorded images at −4 mm under four different angular adjustments. It should be noticed that the position value given in this chapter denotes the coordinate on the x axis if there is no extra description. In every camera image, there are 14 separate rectangles in the middle. Those rectangles represent the surface of 14 lenses, which are illuminated by the 14 lines in the test image. The correct angular alignment is demonstrated in Fig.5.8(a), where the illuminated pattern in each rectangle is consistent in the vertical direction. If the angular misalignment increases, the pattern in each rectangle will start to tilt, as shown in Fig.5.8(b)-(d). It can be observed that the output luminance is quite sensitive to the angular adjustment, and 0.1° misalignment can already lead to an obvious change in the luminance image. Therefore, the display should be well aligned with the lens array during the experiment.

5.2.2 Measurement of the original luminance distribution

At first a pure glass plate is used between the lens array and the LCD display to obtain the original system output without barrier layer. To demonstrate the measurement process, the camera is moved to the position −27 mm, which

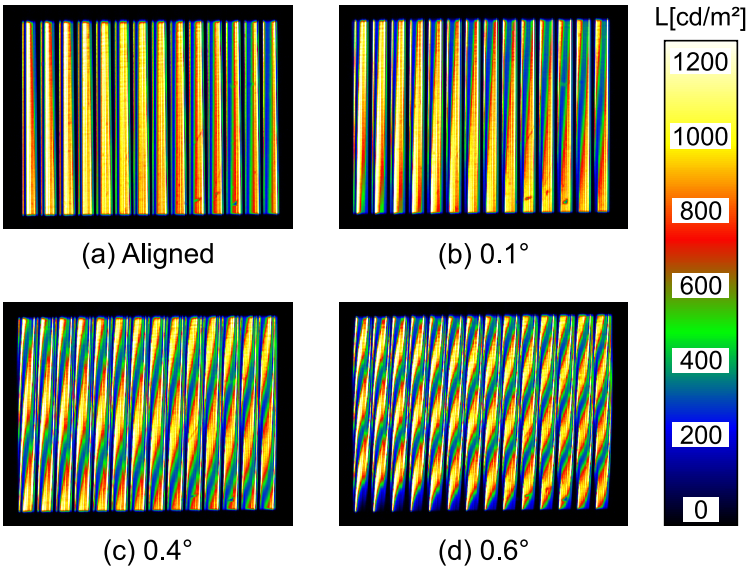

Figure 5.8: Angular alignment between the display and the lens array by analyzing the camera image. Test image for viewing direction 5 is shown on the display, and the camera is placed at -4 mm (x axis) to capture the luminance distribution of the DB, with the scale drawn on the right side. (a) Display is correctly aligned with the lens array, where the illuminated pattern is consistent in each rectangle. (b) 0.1° misalignment. (c) 0.4° misalignment. (d) 0.6° misalignment. The pattern in each rectangle starts to tilt with an increasing angular misalignment.

should be in the central viewing zone of viewing direction 5. When the test image for viewing direction 5 is shown on the LCD display, the luminance image of the DB can be recorded by the camera and it is illustrated in Fig.5.9. Similarly, 14 separate rectangles can be observed in the middle of the image, because 14 lens surfaces are illuminated by the 14 lines in the test image. The drop of the luminance value between two lenses is caused by the plane transition surface, where the incident light will be refracted to other directions.

In the simulation, the average luminance of one specific square, which is located on the center of the lens array top surface, is used to represent the DB luminance. The same method should also be used in the experiment. As pre-

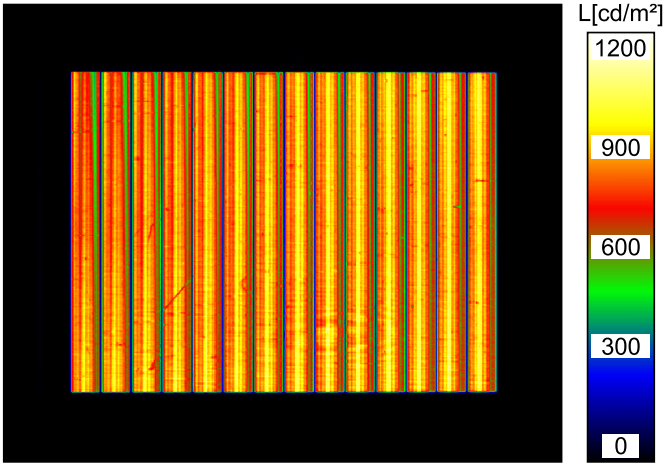

Figure 5.9: Camera-captured luminance image of the DB, when the camera is moved to the position −27 mm on the x axis. A glass plate is currently inserted between the lens array and the LCD display to produce the original system output without barrier layer. The test image for viewing direction 5 is activated on the LCD display. In total 14 lenses are light up by the 14 lines in the test image, producing the bright rectangles in the middle of the figure.

viously explained, the side length of the measuring square is 23.852 mm, which equals the width of four lenses. For the luminance distribution at −27 mm, the measuring square is illustrated in Fig.5.10(a), resulting in an average luminance of 776 cd/m^2.

Although the final luminance value should be read from the central square with 23.852 mm side length, the average luminance of different rectangular shapes can also be investigated to further evaluate the luminance distribution. A coordinate system is established in Fig.5.10(b), with the origin located at the center of the 14 bright rectangles. If a new rectangle is set to be centered at the origin, this rectangle can be described by the coordinate (x, y) of one rectangle vertex, as shown in Fig.5.10(b). It should be noticed that the unit for both x and y directions is equal to the lens pitch. As a result, the standard square shown in Fig.5.10(a) can be described with the vertex coordinate (2, 2).

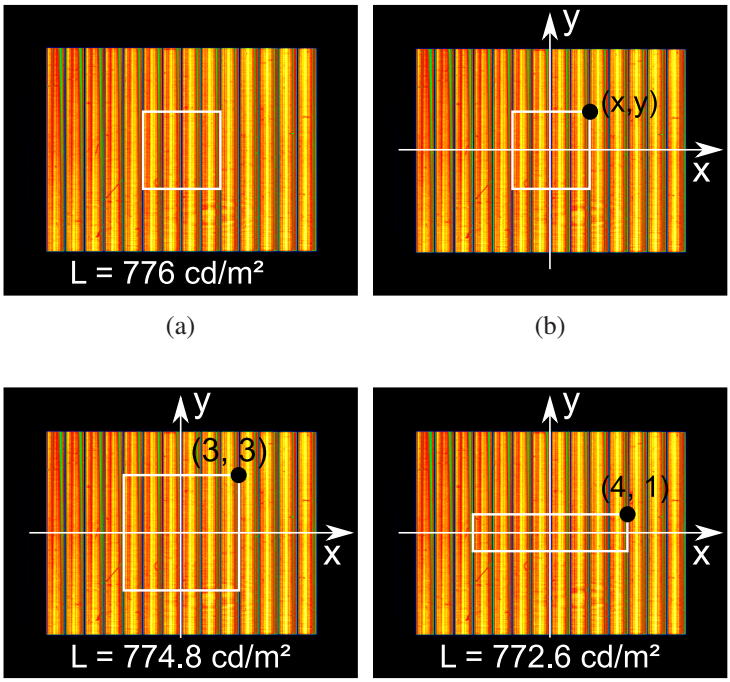

Figure 5.10: Average luminance of different rectangular shapes. (a) Average luminance is 776 cd/m^2 of the specified square with 23.852 mm side length. (b) Definition of a new rectangle with its center at the coordinate origin, which is also the center of the 14 illuminated lens surfaces. Then the new rectangle can be described by the coordinate (x, y) of the upper right vertex. Unit for both x and y direction is equal to the lens pitch. (c) Rectangle with the vertex coordinate (3, 3) yields the average luminance 774.8 cd/m^2 . (d) Rectangle with the vertex coordinate (4, 1) has the average luminance 772.6 cd/m^2.

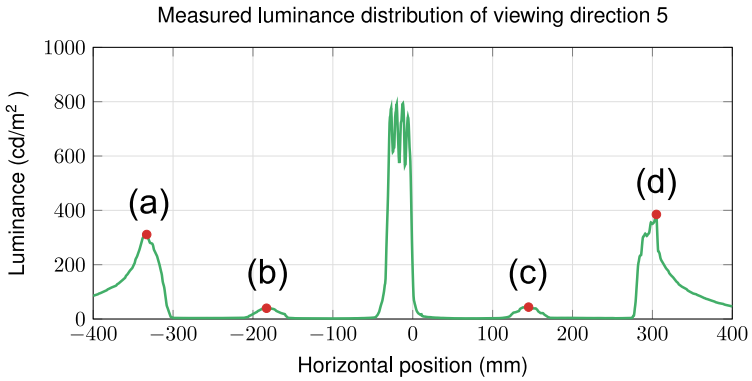

Figure 5.11: Measured average luminance of viewing direction 5 within (−400 mm, 400 mm) in the horizontal direction. Three major viewing zones and two minor viewing zones appear in the distribution. Four red points on the luminance profile denote the peak of the corresponding viewing zone at −333 mm, −183 mm, 145 mm and 305 mm.

Then one new rectangle is created with the vertex coordinate (3, 3), as demonstrated in Fig.5.10(c). The average luminance within this rectangle is 774.8 cd/m^2. Another rectangle with the vertex coordinate (4, 1) yields an average luminance of 772.6 cd/m^2, as can be seen in Fig.5.10(d). The luminance distribution within each lens is similar to each other, since the three different rectangles in Fig.5.10 provide very close average luminance.

The luminance image captured at −27 mm has been analyzed as an example. In the experiment, the camera should be moved within (−400 mm, 400 mm) to measure the luminance distribution in the horizontal direction. The measurement result of viewing direction 5 is shown in Fig.5.11, where the demonstrated luminance value represents the average luminance of the specified square in each luminance image. As expected, three major viewing zones and two minor viewing zones can be observed from the luminance distribution.

The four red points in Fig.5.11 denote the peak of the corresponding viewing zone. As for the central viewing zone, there are several peaks in the distribution profile, which will be analyzed in the last section of this chapter. Then, in order to provide a further observation of the DB output, the luminance images captured at other four peak positions are demonstrated in Fig.5.12. Fig.5.12(a) shows the luminance image at the peak of the left viewing zone, where the

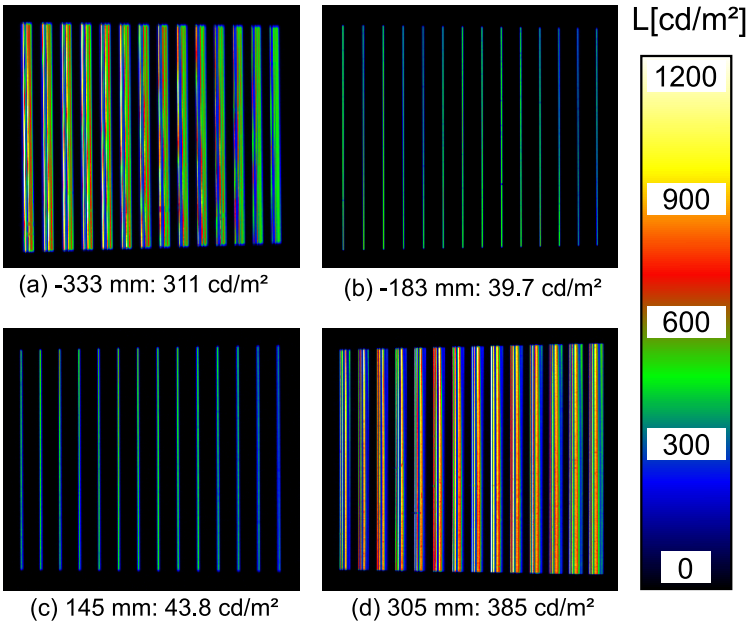

Figure 5.12: Luminance image captured at the peak of the four viewing zones. The subtitle for each figure describes the peak position and the obtained average luminance of the previously specified measuring square. (a) Luminance image taken at −333 mm with average luminance 311 cd/m^2. (b) Luminance image taken at −183 mm with average luminance 39.7 cd/m^2. (c) Luminance image taken at 145 mm with average luminance 43.8 cd/m^2. (d) Luminance image taken at 305 mm with average luminance 385 cd/m^2.

average luminance of the specified square is 311 cd/m^2. In Fig.5.12(a), 14 bright rectangles can be seen since 14 lens surfaces are illuminated by the lines in the test image. Besides, the rectangles on the left side appear to be larger than the rectangles on the right side. This is supposed to be caused by the asymmetric image capture. When the camera is moved to −333 mm to photograph the DB, the lens array is tilted to the camera, causing the lens on the left side to be closer to the camera than the lens on the right side. In addition, there is also a gap between two bright rectangles in Fig.5.12(a), which results from the plane transition surface between lenses.

Fig.5.12(d) demonstrates the luminance image at the peak of the right viewing zone, where the average luminance of the specified square is 385 cd/m^2. The bright rectangle is larger at the right side due to the asymmetric image capture, and a gap between two bright rectangles also appear due to the planar transition surfaces. Fig.5.12(b) and Fig.5.12(c) show the luminance image taken at the peak of the two minor viewing zones. As explained before, light rays incident on the transition surface have created the minor viewing zone. Therefore, the luminance pattern in Fig.5.12(b) and (c) consists of 14 lines, representing the illuminated transition area between lenses.

Till now the measurement of the original luminance distribution with a pure glass plate has been explained, where the measurement of viewing direction 5 is demonstrated as an example. The luminance distribution of viewing direction 6 and 7 can also be obtained using the same method, and the results will be analyzed in Sec.5.3.

5.2.3 Measurement of the luminance distribution with the chrome mask

In this step, the chrome mask will be inserted between the lens array and the the LCD display to block the unwanted viewing zones. In every measurement, the chrome mask should be first placed at one initial horizontal position, and all subsequent movement will refer to this initial position. Various methods can be implemented to set up the initial position of the chrome mask, and this experiment has primarily used a special line image on the display to define the initial position. This line image is demonstrated in Fig.5.13, where the center of this line is coincident with the center of the eighth line in the test image for viewing direction 5. Besides, the line image in Fig.5.13 contains 20 pixels in the horizontal direction, leading to a line width of 3.042 mm. And the width of one chrome rectangle is 3.028 mm, as previously mentioned in Sec.4.3. By placing one chrome rectangle within the line shown in Fig.5.13, the center of the corresponding chrome rectangle can be aligned approximately to the center of the eighth line in the test image for viewing direction 5. The current position of the chrome mask can be registered with the horizontal translation stage, which is considered as the reference point for the subsequent mask adjustment.

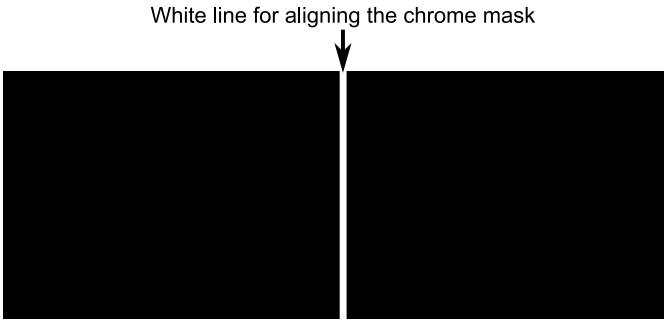

Figure 5.13: Special line image on the display to define the initial horizontal position of the chrome mask. The center of this line coincides with the center of the eighth line (counted from the left side) in the test image for viewing direction 5. This line covers 20 pixels in the horizontal direction, leading to a line width of 3.042 mm. In the experiment, one chrome rectangle on the chrome mask should be placed within this line, and the current position will be used as the initial position of the chrome mask.

According to the barrier modulation explained in Sec.2.5, the chrome mask should be moved 1.27 mm to the left side to block the left viewing zone, while the right viewing zone can be blocked by moving the chrome mask 1.27 mm to the right side. With the help of the horizontal translation stage, the chrome mask can be moved in the horizontal direction with 10 µm step. Then in the experiment, the chrome mask has been first shifted 1.27 mm to the left side, when viewing direction 5 is activated on the display. The distribution of the average luminance within the specified square can be recorded by the camera, as explained in the last section. The measurement result is compared with the original luminance distribution in Fig.5.14(a), where the red curve stands for the luminance distribution with the chrome mask. As expected, the left viewing zone has been successfully eliminated, where the luminance value has dropped from 300.9 cd/m^2 to 0.9 cd/m^2 at the original peak position -333 mm. On the contrary, the red curve in the right viewing zone is almost coincident with the green curve, indicating that the right viewing zone can be normally perceived with the current chrome mask position. As for the central viewing zone, its luminance value has been reduced, since the chrome mask will block part of the light rays heading towards the central lens. Generally, the measurement results shown in Fig.5.14(a) can effectively prove the designed DB function.

In the next step, to block the right viewing zone, the chrome mask will be shifted 1.27 mm to the right side of the initial position. The measurement results is shown in Fig.5.14(b), where the red curve denotes the measured luminance distribution with the chrome mask. Compared to the green curve, which represents the original luminance distribution, the right viewing zone can be completely eliminated after using the chrome mask. The luminance value has decreased from 385 cd/m^2 to 1.45 cd/m^2 at the original peak position 305 mm. In the left viewing zone, the red curve and the green curve have shown high coincidence. Therefore, the measurement result demonstrated in Fig.5.14(b) also confirms the key function of the proposed DB concept.

5.2.4 Measurement results of viewing direction 6 and 7

The measurement process of viewing direction 5 has been explained in the last section, and the key function of the proposed DB could be verified by the obtained luminance distribution. To further confirm the system functionality, measurement results of viewing direction 6 and 7 will be analyzed.

In the experiment, the same process conducted in the measurement of viewing direction 5 has been applied to measure the luminance distribution of other viewing directions. It is important to note that the test image should be adapted for different viewing directions. Apart from the test image, the system set up, the measurement procedure and the data evaluation are consistent with the method used for viewing direction 5. Therefore, the concrete measurement process will be omitted, and the measurement results of viewing direction 6 and 7 are demonstrated in Fig.5.15.

In Fig.5.15(a), the original luminance distribution is illustrated when a glass plate is placed between the lens array and the display. The blue curve and the red curve represent the distribution of viewing direction 6 and 7 respectively. As expected, three major viewing zones and two minor viewing zones can be observed in each luminance distribution. In the next step, the chrome mask will be inserted to replace the glass plate. The chrome mask is first placed to block the left viewing zone, with the measurement result demonstrated in Fig.5.15(b). The yellow and the black curve stand for the luminance distribution with the chrome mask. Compared to the original luminance distribution, the

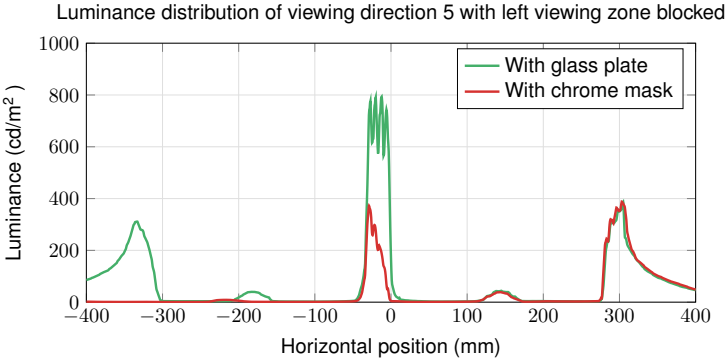

(a)

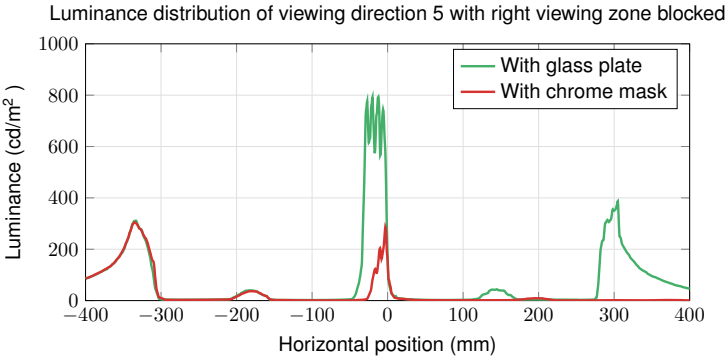

(b)

Figure 5.14: Measured average luminance distribution of the specified measuring square, when viewing direction 5 is activated and the chrome mask is used in the prototype. Green curve in each figure represents the original luminance distribution with a pure glass plate, whereas the red curve denotes the luminance distribution with the chrome mask. (a) Chrome mask is moved 1.27 mm to the left side of the initial position to block the left viewing zone. It can be seen that the left viewing zone is completely suppressed, while the two distribution profiles are almost coincident in the right viewing zone. (b) Chrome mask is moved 1.27 mm to the right side of the initial position to block the right viewing zone. Now the right viewing zone of the red curve has been eliminated, while in the left viewing zone the red curve can well match the green curve.

left viewing zone of the yellow and the black curve has been successfully eliminated, while the right viewing zone remains roughly unchanged.

Then the chrome mask will be shifted to block the right viewing zone, with the measurement results shown in Fig.5.15(c). The obtained luminance distributions are also represented by the yellow and the black curve. Compared with the original luminance distribution, it can be observed that the new obtained luminance value in the right viewing zone is around zero, while the luminance distribution in the left viewing zone is almost coincident with the original distribution. In addition, the luminance value in the central viewing zone has been reduced with the chrome mask, which can also be observed in Fig.5.15(b). As already explained, this effect appears because part of the light rays towards the central viewing zone will be blocked by the chrome layer.

To summarize, measurement results of viewing direction 5, 6 and 7 have been analyzed, where the chrome mask was set to block the left and the right viewing zone respectively. The results shown in Fig.5.14 and Fig.5.15 can prove the key function of the proposed DB concept, that the light rays towards the unwanted viewing zone can be selectively blocked. According to the measurement results, the use of the chrome mask has created almost the same influence on the luminance distribution of the three viewing directions. This consistency can prove the stability of the developed prototype. As for the other seven viewing directions, the measurement results will not be demonstrated due to the high similarity and consistency with the three analyzed viewing directions.

5.3 Result analysis

In this section, the measurement results will be first compared with the simulation results, and the disparities will be analyzed to gain a further understanding of the constructed prototype. Then the prototype performance will be evaluated by analyzing the measurement results.

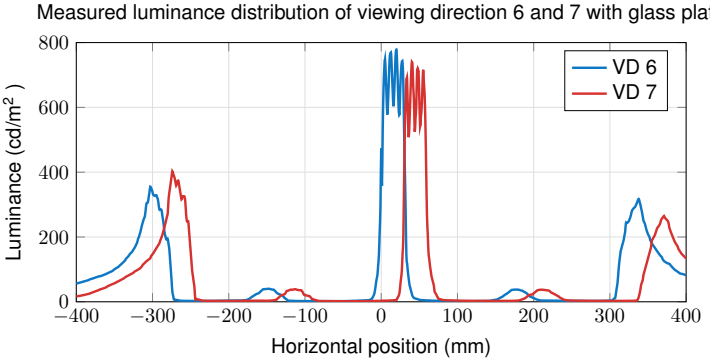

(a)

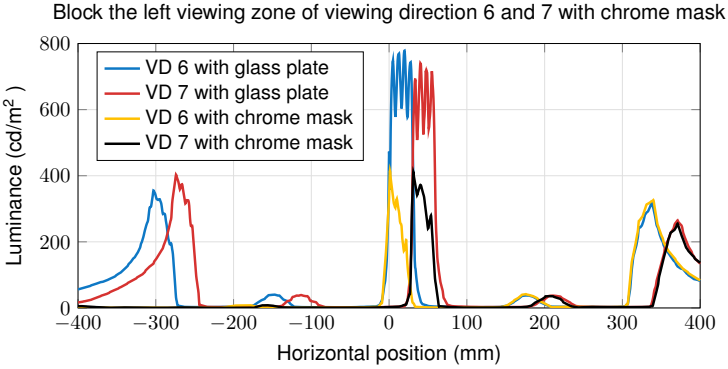

(b)

Figure 5.15: Measured luminance distribution of viewing direction 6 and 7. The abbreviation "VD" in the legend stands for "viewing direction". (a) Original luminance distribution when a glass plate is placed between the lens array and the display. (b) Chrome mask is used between the lens array and the display to block the left viewing zone. It can be seen that the luminance value in the left viewing zone has been significantly reduced. (c) Continued on the next page.

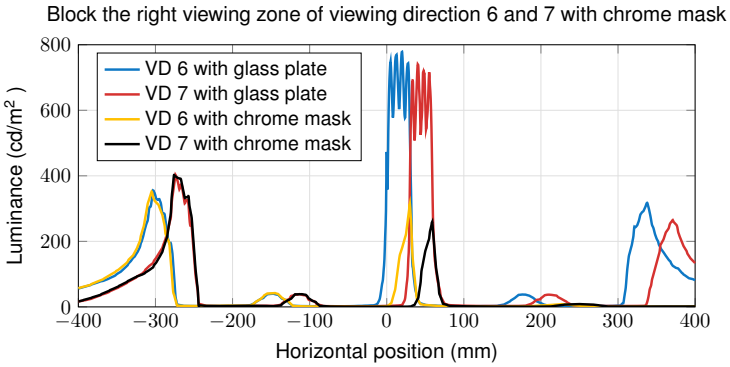

(c)

Figure 5.15: continued-(c) Chrome mask is used between the lens array and the display to block the right viewing zone. It is obvious that the right viewing zone has been eliminated.

5.3.1 Comparison of the measurement and simulation result

The simulated and measured original luminance distribution of viewing direction 5 are drawn together in Fig.5.16(a), where the blue curve stands for the simulation result and the red curve stands for the measurement result. At the most positions, the two curves can roughly match each other, which proves the correctness of the simulation model and the prototype setup. In Fig.5.16(a), one obvious disparity between the two curves can be observed in the central viewing zone.

To provide a clear view of this disparity, the luminance distribution within (−50 mm, 20 mm) is magnified in Fig.5.16(b). Both luminance distributions fluctuate within (−30 mm, 0 mm), where four local maximums and 3 local minimums can be seen. This fluctuation is consistent with the system design, because each line in the middle of the test image covers horizontally four display pixels. According to the spectral measurement demonstrated in Sec.4.3, the luminance generated from the green image is 606.34 cd/m^2, which occupies around 70% of the white image luminance. Therefore, the green subpixel will also provide the highest luminous intensity within one display pixel. As a result,

the four green subpixels in each line have produced the four local maximums in the central viewing zone.

Although the measured and the simulated luminance distribution demonstrate similar fluctuations in the central viewing zone, the simulated distribution is always under the measured distribution. The peak value of the simulation result is 743 cd/m^2 at -20 mm, while the peak value of the measurement result is 791 cd/m^2 at -20 mm. Furthermore, the minimum value of the simulated result is 479 cd/m^2 at -24 mm, which is also lower than the minimum value 574 cd/m^2 of the measured result. This disparity is assumed to be caused by different detector pixel settings in the simulation and experiment.

Since the diameter of the camera entrance pupil is around 4 mm, the detector pixel is set to be a 4 mm $\times$ 4 mm square in the simulation (simulation software can only provide rectangular pixel shape). To study the influence of the pixel size, pixels of three different squares shapes, whose side length are 1 mm, 2 mm and 4 mm respectively, have been set on the detector plane. Then the simulated luminance distribution of viewing direction 5 is shown in Fig5.17(a). It is obvious that the pixel size can significantly influence the obtained luminance distribution in the central viewing zone. Then the luminance distribution within (-50 mm, 20 mm) is magnified in Fig.5.17(b). Because a smaller pixel size can record finer luminance change in the horizontal direction, the distribution with smaller pixel size shows a stronger fluctuation. Despite the difference in luminance values, all three distributions own four local maximums and three local minimums in the central viewing zone. When the side length is set to 1 mm, the maximum detected value is over 1100 cd/m^2, which is larger than the maximum measured luminance. According to Fig.5.17, it is clear that a different configuration of the detector pixel can lead to a different luminance distribution. Furthermore, the camera entrance pupil has a circular shape, while the detector pixel has a square shape. This shape difference will also contribute to the deviation between the obtained luminance values. Therefore, the disparity observed in Fig.5.16(a) can be explained by different detector settings in the simulation and measurement. Apart from the disparity in the central viewing zone, the simulated and the measured luminance distributions show great coincidence, which can verify the correctness of the simulation model.

The next step is to compare the luminance distribution when the chrome mask is inserted into the system. Fig.5.18(a) compares the results when the

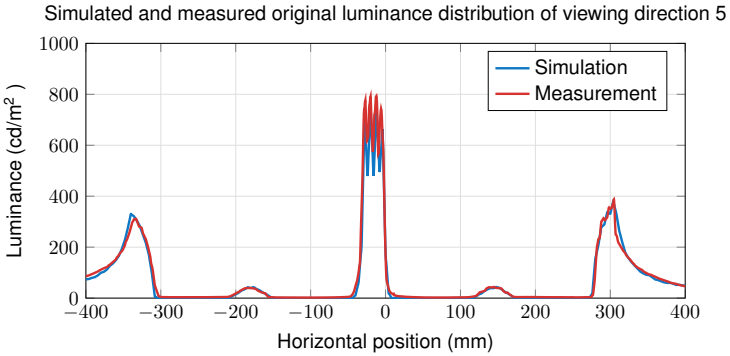

(a)

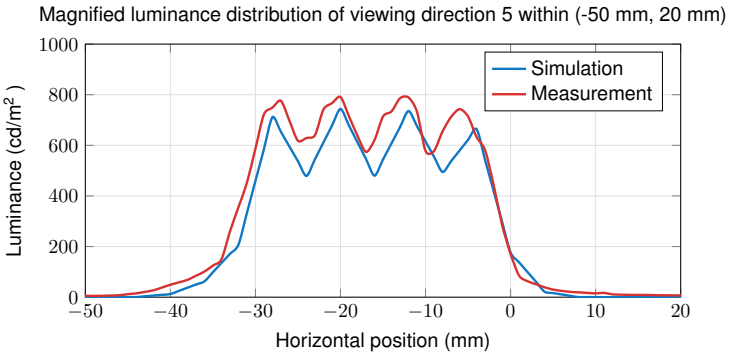

(b)

Figure 5.16: Comparison of the simulated and measured original luminance distribution of viewing direction 5. The blue curve in the figure stands for the simulation result, and the red curve stands for the measurement result. (a) Luminance distribution within (−400 mm, 400 mm), where the two curves can match each other at most positions. However, there is an obvious disparity in the central viewing zone. (b) Magnification of the luminance distribution within (−50 mm, 20 mm). Both curves demonstrate four local maximums and three minimums in the central viewing zone. The simulated luminance profile is below the measured luminance profile.

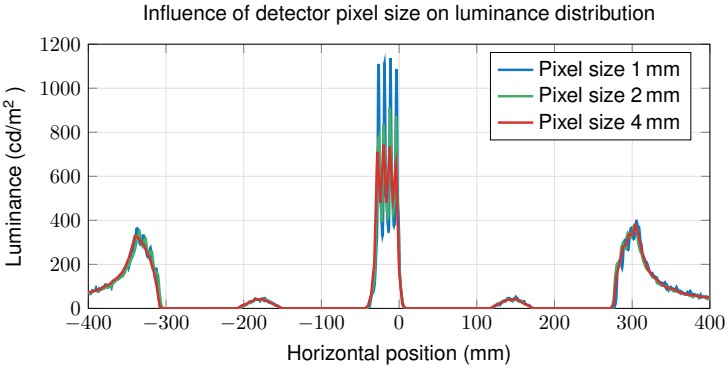

(a)

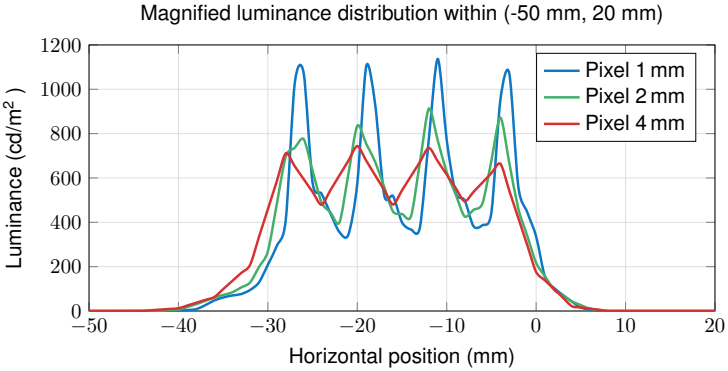

(b)

Figure 5.17: Influence of the detector pixel size on the luminance distribution of viewing direction 5. The detector pixel has a square shape. The "Pixel size" and "Pixel" in the legend of (a) and (b) indicate the side length of the square. The luminance distributions under three different side lengths (1 mm, 2 mm, 4 mm) are demonstrated. (a) Luminance distribution within (−400 mm, 400 mm). (b) Luminance distribution within (−50 mm, 20 mm).

chrome mask is placed to block the left viewing zone of viewing direction 5. The measurement and simulation results can roughly match each other, which further verifies the simulation model. However, two slight differences can still be observed in Fig.5.18(a). The first one appears within (330 mm, 400 mm) in the right viewing zone, where the simulated luminance value is smaller than the measurement result. The second difference can be found within the area (−230 mm, −200 mm), where the measured luminance distribution is above the simulated distribution. Similar differences also exist in Fig.5.18(b), when the chrome layer is set to block the right viewing zone. A discrepancy can be seen between the luminance distributions in the left viewing zone in Fig.5.18(b), and the measurement results shows a small bump within (180 mm, 220 mm).

To gain a further understanding of these two discrepancies observed between simulation and measurement, the luminance distribution of viewing direction 6 and 7 will be analyzed in Fig5.19. The comparison of the original luminance distributions without chrome mask is demonstrated in Fig.5.19(a), where there is a good agreement between the simulation and measurement. The disparity in the central viewing zone is due to the detector pixel setting, as previously explained. Then the chrome mask will be used to first block the left viewing zone, with the results illustrated in Fig.5.19(b). Similarly, there is also a discrepancy between the luminance distributions in the right viewing zone, and the measurement results have shown a small bump within (−200 mm, −150 mm) on the left side. Apart from these two differences, the measured luminance value of viewing direction 7 is obviously higher than the simulation result in the central viewing zone, as can be seen within (30 mm, 60 mm) in Fig.5.19(b). Subsequently the results of blocking the right viewing zone are demonstrated in Fig.5.19(c). As expected, the discrepancy in the left viewing zone and the distribution bump on the right side can both be observed. Besides, in the central viewing zone, the measured luminance value of viewing direction 6 is higher than the simulation result.

According to the comparison of luminance distributions shown in Fig.5.18 and Fig.5.19, some disparities can always be observed between the simulation and measurement results, which deserve a further investigation. The disparity in the central viewing zone without chrome mask can be explained with the different detector settings, which will not be repeated here. The next step is to study the disparity in the left or right viewing zone after the use of the chrome mask.

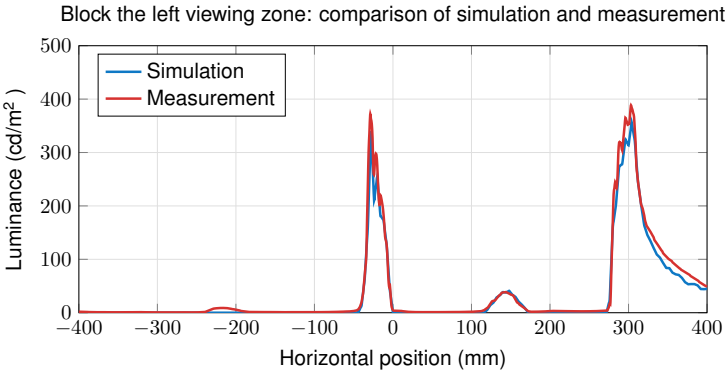

(a)

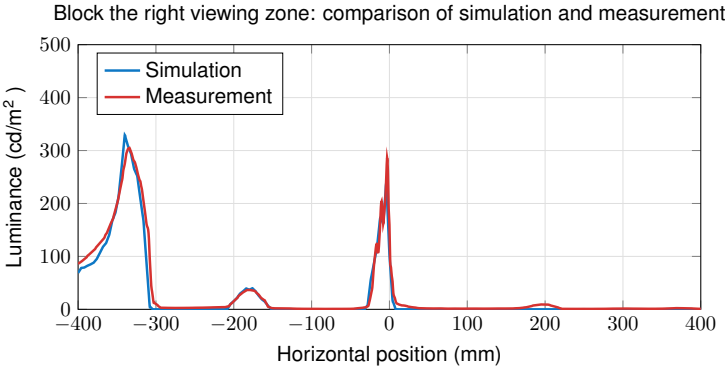

(b)

Figure 5.18: Comparison of the simulated and measured luminance distribution of viewing direction 5, when the chrome mask is used to block the corresponding viewing zone. (a) Block the left viewing zone. (b) Block the right viewing zone.

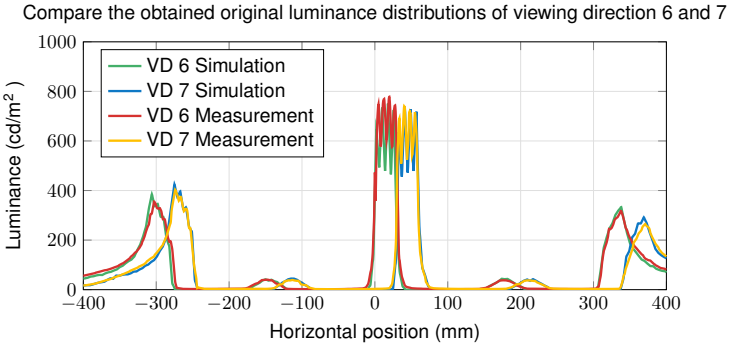

(a)

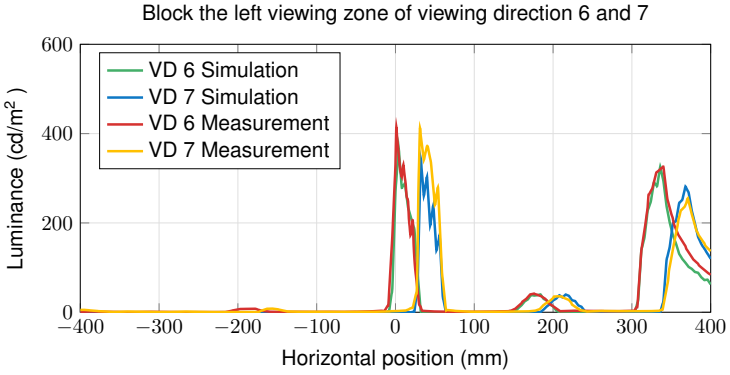

(b)

Figure 5.19: Compare the simulated and measured luminance distribution of viewing direction 6 and 7. "VD" in the legend of each figure is the abbreviation for "viewing direction". (a) Original luminance distribution when a glass plate is inserted between the lens array and the display. (b) Block the left viewing zone with the chrome mask. (c) Continued on the next page.

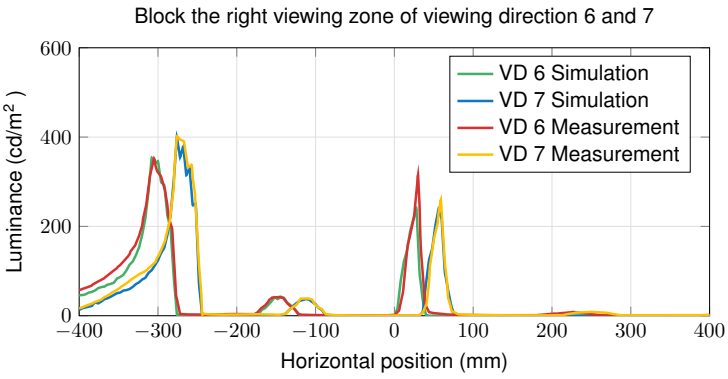

(c)

Figure 5.19: continued-(c) Block the right viewing zone with the chrome mask.

This could be related to the position error of the camera. In the experiment, when the camera is moved in the horizontal direction, the distance from the lens array to the camera entrance pupil should be controlled at 600 mm in the vertical z direction. Because the position adjustment has been manually conducted, the position error could appear during the measurement.

To study the influence of the camera position error, corresponding simulations have been carried out for viewing direction 7, since there is a larger discrepancy between the simulation and measurement in the central and side viewing zones. The detector plane has been placed with different distances to the lens array. The simulation result is demonstrated in Fig.5.20(a), where the luminance distributions with two extreme position errors, +20 mm and −20 mm, are represented by the blue and the red curve respectively. Compared to the green curve which represents the designed original position, there is an obvious disparity between the luminance distributions in all three viewing zones. To gain a deeper understanding of the discrepancy between the measurement and the simulation, the measured luminance distribution within (280 mm, 400 mm) is plotted in Fig.5.20(b) together with the simulation of different detector z-positions. The measurement result is represented by the black dashed line, which is consistently located between the green line (detector at 600 mm) and the blue line (detector at 620 mm). This indicates that the camera could have been positioned at z-distances greater than 600 mm in the experiment.

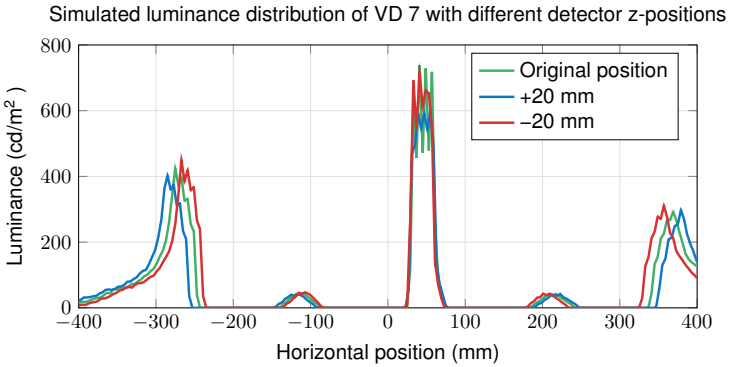

(a)

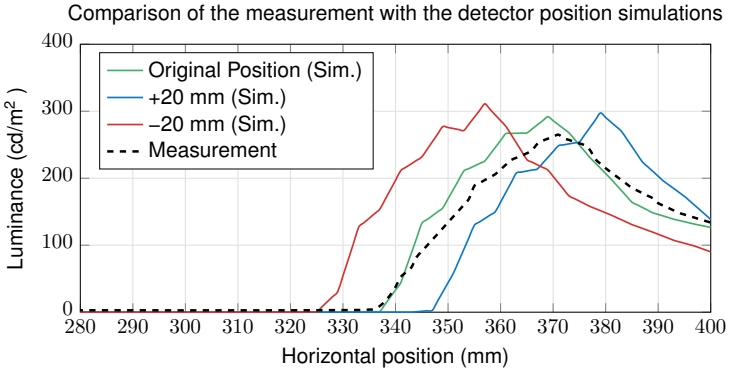

(b)

Figure 5.20: Influence of the detector z-position: (a) Simulated luminance distribution of viewing direction 7 with different detector z-positions. The original detector position is 600 mm away from the lens array. "+20 mm" in the legend indicates the detector is placed 620 mm away from the lens array, whereas "−20 mm" indicates a distance of 580 mm. (b) Comparison of the measurement with the simulation result from (a), where the black dashed line represents the measured luminance distribution. The abbreviation "Sim." in the legend stands for "Simulation".

Therefore, the discrepancy in the left and the right viewing zone, observed between the simulation and measurement results in Fig.5.18 and Fig.5.19, could be attributed to the deviation from the designed camera position. However, it should be pointed out that the 20 mm position error has been investigated to show the influence of the detector position, and the real position error should be much smaller than 20 mm in the experiment.

Another potential position error could also appear during the horizontal movement of the chrome mask, that the chrome mask has not been accurately moved to the desired position. To study the influence of this position error, simulation of viewing direction 7 has been performed when the chrome mask is moved to different horizontal positions to block the left viewing zone. Luminance distributions under ±0.1 mm position deviation are shown in Fig.5.21(a), which are represented by the blue and the red curve. Compared to the green curve which stands for the designed position, the luminance values in the central viewing zone have been primarily affected, whereas there is a good match between the luminance distributions at other positions. Furthermore, the simulated luminance distribution within (0 mm, 100 mm) is magnified in Fig.5.21(b), along with the measurement result represented by the black dashed line. It can be seen that both black line and red line (−0.1 mm position deviation) are located above the green line (designed position). This implies the chrome mask could have been placed below the designed horizontal position during the experiment. Hence, it is plausible to speculate that the disparity observed in the central viewing zone in Fig.5.18 and Fig.5.19 could be linked to the misplacement of the chrome mask.

The last disparity to be studied is the small bump in the measured luminance distribution, which has appeared in all measurement results with the chrome mask. In Fig.5.18(a), the bump appears roughly within the horizontal range (−230 mm, −200 mm), when the chrome mask is set to block the left viewing zone of viewing direction 5. However, when a pure glass plate is inserted between the lens array and the display, the measured value within (−230 mm, −200 mm) of the original luminance distribution is close to zero, as can be seen in Fig.5.12. Then it could be assumed that the use of the chrome mask has generated this bump area. In the previous simulations, the chrome layer is modeled as a simple absorbing layer, and the reflection at the interface between the chrome layer and the substrate glass is neglected, which could lead to this distribution mismatch.

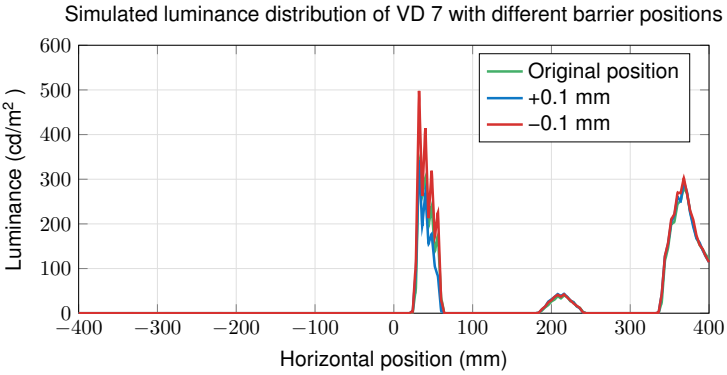

(a)

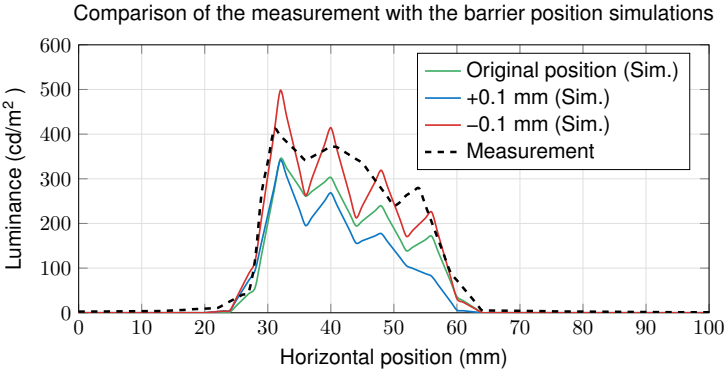

(b)

Figure 5.21: Influence of the chrome mask position: (a) Simulated luminance distribution of viewing direction 7 with different horizontal positions of the chrome mask, when the left viewing zone should be blocked. "+0.1 mm" means the chrome mask is placed 0.1 mm further than the designed horizontal position. (b) Comparison of the measurement with the simulation result from (a), where the black dashed line represents the measured luminance distribution. The abbreviation "Sim." in the legend stands for "Simulation".

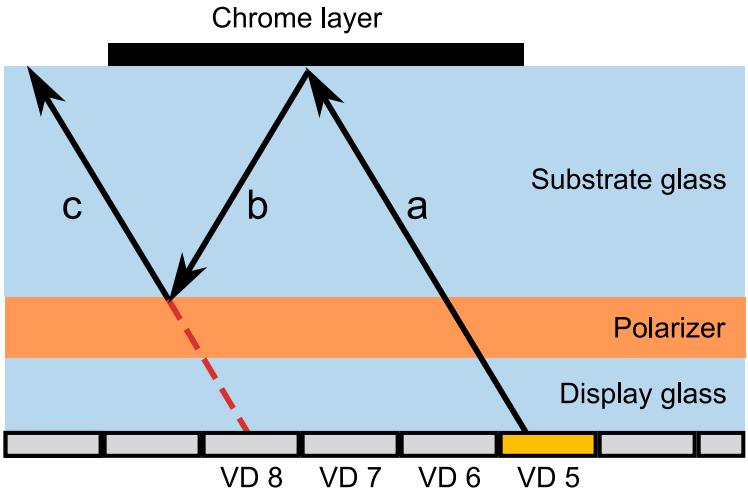

Figure 5.22: Influence of the reflection at the interface between the chrome and the substrate glass. Dimensions drawn in the figure are not scalable with real components. VD 5 in the figure indicates one pixel unit for viewing direction 5. Light ray “a” is emitted by VD 5, and is reflected at the interface between the chrome and the substrate glass, which results in the reflected ray “b”. Then the ray “b” will be reflected at the interface between the substrate glass and the display top polarizer, generating the reflected ray “c”. The luminance distribution induced by the ray “c” would appear to be created from viewing direction 8.

To explore the influence of the reflection, the propagation of one specific light ray is analyzed in Fig.5.22. It should be mentioned that the sizes drawn in the figure are not scalable with real components. VD 5 stands for one pixel unit for viewing direction 5, which is currently activated on the display. “a” represents one light ray coming from the VD 5, which propagates towards the chrome layer. After the reflection at the interface, the reflected ray “b” would turn back to the display. Then at the interface between the substrate glass and the polarizer, the reflection will create the ray “c”, which is able to leave the substrate glass without being blocked by the chrome. In this case, as indicated by the red dashed line, the ray “c” will illuminate the area, which originally should belong to viewing direction 8. This ray propagation can also well explain the previous observation, that the bump area does not belong to viewing direction 5.

According to the analysis of the ray propagation, the reflection at the interface between the chrome layer and the substrate glass should be considered in the simulation. In the simulation software OpticStudio, a specific material can be modeled by defining the refractive index and the extinction coefficient over the wavelength. This work has chosen to use the data listed in one publication to establish the Cr model [101]. With the newly adapted Cr model, the luminance distribution of viewing direction 5 can be re-simulated. The new simulation result is demonstrated in Fig.5.23(a) together with the measurement result, when the chrome mask is set to block the left viewing zone of viewing direction 5.

In Fig.5.23(a), the red curve stands for the simulated luminance distribution with the adapted Cr model. Within the horizontal position (−230 mm, −200 mm), a bump area also appears at the red curve. At other horizontal positions, the red curve is similar to the previous simulation result, and the deviations from the measured green curve in the right and central viewing zone have already been analyzed. To have a clear view of the bump area, the luminance distribution within (−250 mm, −150 mm) is magnified in Fig.5.23(b), where the red curve also represents the new simulation result and the green curve represents the measurement result. The bump of the red curve exists roughly between (−225 mm, −200 mm), with the maximum value 9.2 cd/m^2 appearing at −216 mm. The position of the maximum simulated luminance shows a good agreement with the measurement result, because the maximum measured luminance is also located at −216 mm with the value 8.88 cd/m^2. The bump of the green curve is dispersed within a larger area, which can be roughly considered between (−240 mm, −185 mm). The discrepancy of the bump width could have been caused by the variation between the simulation model and the constructed prototype. In the simulation, every component demonstrated in Fig.5.22 is configured as an ideal rectangular volume without geometric tolerances. Additionally, each lens in the lens array is modeled identically with the same radius and pitch. But it is expected that the prototype exhibits variations from the simulation model, which will lead to the distribution difference, as previously elaborated in Sec.3.5.

Despite the discrepancy of the bump width, the simulation result with the adjusted Cr model is consistent with the measurement result. Then this would support the assumption, that the reflection at the Cr surface leads to the unexpected bump at the measured luminance distribution.

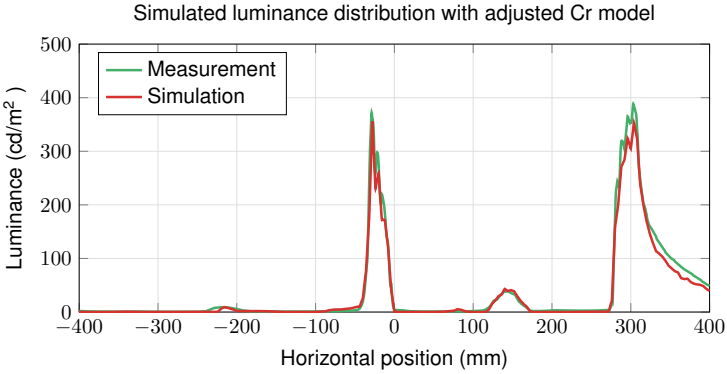

(a)

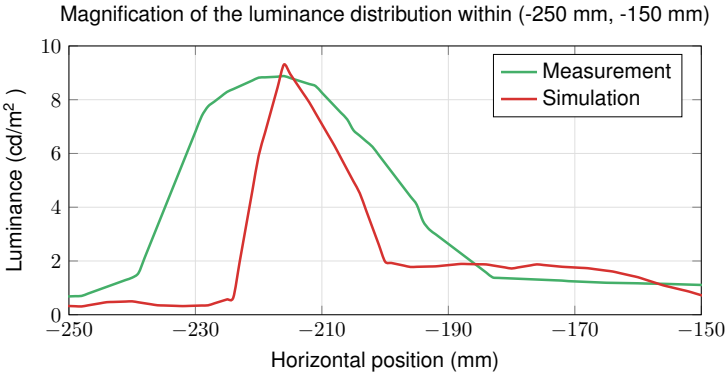

(b)

Figure 5.23: Simulated luminance distribution of viewing direction 5 with the adapted Cr model, when the chrome mask is set to block the left viewing zone. The red curve stands for the new simulation result and the green curve stands for the measurement result. (a) Luminance distribution within (−400 mm, −400 mm). A bump has appeared at the red curve within (−230 mm, −200 mm). (b) Magnification of the luminance distribution within (−250 mm, −150 mm). The peaks of the green and the red curve are both located at −216 mm, with the luminance value 8.88 cd/m^2 and 9.2 cd/m^2 respectively.

To sum up, this subsection has further analyzed several settings in the simulation, which could have led to the discrepancy between the measurement and simulation results. The detector pixel size can influence the steepness of the distribution fluctuation in the central viewing zone. The vertical position of the detector plane will noticeably impact the distribution profiles in the left and right viewing zone, whereas the misalignment of the chrome mask will mainly influence the central viewing zone. Subsequently, the reflection at the interface between the chrome layer and its substrate glass can lead to a bump area in the luminance distribution. These factors have been evaluated in the simulation, and the adapted simulation results can provide an explanation for the observed measurement outcomes. Based on the analysis, it can be concluded that the established simulation model offers a reliable representation of the DB prototype.

5.3.2 Evaluation of the prototype performance

This subsection will focus on evaluating the key function of the proposed concept, which is the block of the light rays towards unwanted viewing zones. The corresponding measurement results are demonstrated in Tab.5.1. The first row in the table defines the viewing zones to be evaluated. In the first row, the cell “V5 L” stands for the left viewing zone of viewing direction 5, and “V5 R” indicates the right viewing zone of viewing direction 5. Other cells can also be interpreted in the same way. The second row defines the position of the maximum measured luminance value in the corresponding viewing zone, when a glass plate is inserted between the lens array and the display. Regarding the left viewing zones, the distance between the peak of viewing direction 5 and viewing direction 6 is 30 mm, which is same to the designed value. The distances between other peaks can also match the designed 30 mm.

In the third row of Tab.5.1, the original luminance values at the corresponding peak positions are demonstrated. In the experiment, the chrome mask has been used to block the unwanted viewing zones, and the resulted luminance value at the original peak position is given in the fourth row. Then the last row “Transmission” describes the result of the fourth row divided by the third row. It is notable that all transmission values are under 0.5%, indicating a high effectiveness of the light block.

Table 5.1: Comparison of the measured luminance value at the peak positions

Viewing zone	**V5 L**	**V6 L**	**V7 L**	**V5 R**	**V6 R**	**V7 R**
Peak position (mm)	-333	-303	-274	305	338	371
Original luminance (cd/m^2)	311	355	403	385	317	265
Luminance with Cr (cd/m^2)	0.9	0.84	1.07	1.45	0.97	1.3
Transmission	0.29%	0.24%	0.27%	0.38%	0.31%	0.49%

To summarize, the implemented prototype has achieved the designed function of the proposed DB concept. Light rays towards the unwanted viewing zones can be effectively blocked after using the chrome mask. The luminance transmission at the original peak positions can be restricted under 0.5%. For the assumed automotive CID application, this prototype could significantly reduce the potential view conflict between the left and the right viewing zone.

6 Summary and Outlook

This chapter will provide a summary of this dissertation, and present the key contributions of the work. In addition, an outlook will be given for the future development.

6.1 Summary

This work has proposed a novel display backlight concept for multi-user display applications. The proposed DB concept was originally inspired by the 3D display technologies, but the DB concept can also be used to create other new display applications, where the direction of the light needs to be modulated.

This dissertation consists of six chapters. The first chapter introduces the motivation and provides an overview of the state-of-the-art technologies. The drawbacks of some popular 3D display technologies have been analyzed. Among them, the multiview technology has been widely used in the commercial products due to the compatibility with the conventional 2D displays and its simple implementation. However, the multiview technology suffers from the resolution reduction and the image flip, which will largely reduce the 3D image quality. Then the DB concept, which consists of one LED matrix backlight and one lens array, has been proposed to create a full resolution 3D image through time multiplexing. But the traditional DB concept suffers from the side leak effect, that the light rays coming from one LED will meet multiple lenses and then get refracted into different directions. The side leak could lead to the view conflict, that one image will be simultaneously perceived by multiple users. The resulted view conflict largely restricts the DB performance in multi-user applications. To provide a high quality multi-user application, this work will further develop the traditional DB concept and intend to eliminate the view conflict.

The second chapter describes the new proposed concept with an extra barrier LCD. At first the side leak effect has been studied in a quantitative model of the original DB system. It has been demonstrated that the view conflict can be solved if a monochrome LCD (barrier LCD) is placed into an appropriate position between the matrix backlight and the lens array. By showing the special white-black image pattern on the barrier LCD, the light rays towards the unwanted lens will be blocked, whereas the light rays towards the desired lens can further propagate. The selective block of the light rays can be combined with time multiplexing to create a better multi-user viewing experience. Then the position and the modulation of the barrier LCD has been studied to prove the feasibility of the concept. Based on the new concept, several prominent use cases have been demonstrated, which are not restricted within the 3D display application. Other applications, for example the split view function, are also believed to have a huge potential in the future multi-user display market.

The third chapter demonstrates the simulation of the proposed DB. The system parameters are determined based on the assumed automotive CID application. The DB system has been modeled in the optical design software Zemax OpticStudio to test the functionality. Through the analysis of the simulation results, the designed function of the barrier LCD could be verified. The proposed DB system is able to selectively block the light rays towards the unwanted viewing zone. As a result, the potential view conflict caused by side leak can be completely solved. Subsequently, lens array tolerance has been discussed by evaluating the variation of four lens array parameters. It has been shown that the tolerance with current manufacturing technologies can create an acceptable system performance.

The fourth chapter shows the prototype construction of the proposed DB. Due to financial restrictions, the proposed system has not been completely realized. Instead, an adapted and simplified prototype has been implemented to only verify the key function of the concept. The barrier LCD is replaced by a chrome mask, and the LED matrix backlight is replaced by a normal LCD display. In addition, the transition between the lenses is changed to plane surface, and the image LCD is removed due to low brightness. Then the construction of the final prototype has been explained, with the focus on the manual alignment between the components. Due to the change of the system design, the simulation model of the DB has also been adapted. At last, the new simulation results with the

adapted system model have been shortly analyzed, which should be further compared with the subsequent measurement results.

The fifth chapter explains the experimental process to evaluate the implemented prototype. At first a qualitative observation of the prototype has been given, when a piece of paper was used as the detector plane to capture the illumination output. In the subsequent quantitative measurement, the luminance directly from the DB has been recorded with the camera. In the experiment, a glass plate is first placed between the lens array and LCD display to create the original luminance distribution. To block the left or the right viewing zone, the chrome mask is inserted into the system to replace the glass plate. The obtained measurement result has been compared with the simulation result, and the disparity can be well explained by adjusting the simulation configurations. The good consistency between the measurement and simulation has in turn proved the correctness of the simulation model. According to the qualitative and quantitative measurement results, the light rays towards the unwanted viewing zone can be selectively eliminated. Hence, the key function of the suggested DB concept has been verified through the experiment.

6.2 Key Contributions

The motivation behind this work is to develop a new 3D display technology, which is capable of delivering high-quality image in multi-user applications. In Sec.1.2.5, the prior DB approach was introduced, which can provide a full-resolution view image with low crosstalk value. But this approach is affected by the side leak effect, which could cause view conflict between multiple users. Towards the end of Chapter 1, a question arises whether a new compact DB concept can be developed to overcome the side leak and thus enable high-quality multi-user applications.

Upon reviewing the entire book, we are confident that Chapter 2-5 have provided a comprehensive response to the raised question. A new concept is proposed by inserting an additional barrier LCD into the original DB system. We have successfully validated the concept by establishing and employing a simulation model, as can be seen in Sec.3.4. Then a prototype has been implemented to enable the experimental verification of the concept, with the results analyzed in Sec.5.3.

To sum up, the main contribution of this dissertation is the introduction of a novel DB concept to solve the side leak problem, with the effectiveness verified through both simulation and experiment. The proposed DB also attains a compact form by integrating only one additional LCD into the existing system. Additionally, aside from the 3D perception generation, many new applications can be created based on the concept, as illustrated in Sec.2.6. As a result, the new concept is able to bring numerous advantages in multi-user applications.

6.3 Outlook

Firstly, limitations of the implemented prototype will be pointed out. The simplified prototype can only prove the key function of the concept, that the unwanted viewing zone can be eliminated by an extra barrier layer. But the chrome mask has to be manually shifted in the experiment, which makes it impossible to realize the time-multiplexing method. Besides, no concrete image can be sent to the user, since the image LCD has not been implemented in the final prototype. Due to these limitations, the prototype is not able to create realistic display applications to the user.

For the future studies, the complete DB system should be established to test the full functionality of the proposed concept. This requires a high-luminance matrix backlight, a customized monochrome LCD and a normal color LCD. For the two-user application, the refresh rate of all components should be higher than 240 Hz to avoid the flickering. In addition, an eye-tracking device can also be used to detect the user's eye positions, thereby providing an increased freedom of movement. If the complete DB system can be implemented, it is able to test the applications described in Sec.2.6 among different users. Then the proposed concept can be further developed based on the feedback from the user test.

Display devices are playing an increasingly important role in the daily life, and users are simultaneously expecting more special functions from the display. The proposed DB concept can provide various new multi-user applications with a compact system design. Especially the customized 3D scene and the split-view function are considered to have high potential. Therefore, it is strongly believed that the proposed DB concept will become a competitive candidate for the next generation display systems.

Bibliography

[1] 3M, "Privacy and Screen Protectors." https://www.3m.com/3M/en_US/privacy-screen-protectors-us/, 2023.

[2] C. P. Chen, J. H. Lee, T.-H. Yoon, and J. C. Kim, "Monoview/dual-view switchable liquid crystal display," *Opt. Lett.*, vol. 34, pp. 2222–2224, Jul 2009.

[3] C.-T. Hsieh, C.-H. Chang, C.-Y. Lin, C.-Y. Huang, C.-J. Hsu, C.-J. Tien, and K.-Y. Lo, "Dual-view blue phase liquid crystal display," *Journal of Display Technology*, vol. 11, no. 7, pp. 575–579, 2015.

[4] Y. Chen, N. Liu, G. Zhai, K. Gu, J. Wang, Z. Gao, and Y. Zhu, "Quality assessment for dual-view display system," in *2016 Visual Communications and Image Processing (VCIP)*, pp. 1–4, 2016.

[5] H. Deng, S. Li, L. Wang, Y. Xing, and Q.-H. Wang, "Dual-view integral imaging system with wide viewing angle and high spatial resolution," *IEEE Photonics Journal*, vol. 12, no. 3, pp. 1–11, 2020.

[6] CNET, "Mercedes SplitView tech is two screens in one ." https://www.cnet.com/roadshow/news/mercedes-splitview-tech-is-two-screens-in-one/, 2008.

[7] Mercedes-Benz, "Mercedes-Benz offers SplitView Technology ." https://media.mbusa.com/releases/mercedes-benz-offers-splitview-technology, 2012.

[8] M. Kawakita, H. Sasaki, N. Okaichi, H. Watanabe, M. Kano, J. Arai, and T. Mishina, "3D TV based on integral photography," in *Three-Dimensional Imaging, Visualization, and Display 2018* (B. Javidi, J.-Y. Son, and O. Matoba, eds.), vol. 10666, p. 1066604, International Society for Optics and Photonics, SPIE, 2018.

[9] J. Kim, C.-K. Lee, Y. Jeong, C. Jang, J.-Y. Hong, W. Lee, Y.-C. Shin, J.-H. Yoon, and B. Lee, "Crosstalk-reduced dual-mode mobile 3d display," *Journal of Display Technology*, vol. 11, no. 1, pp. 97–103, 2015.

[10] Statista, "Share of households with a computer at home worldwide from 2005 to 2019." https://www.statista.com/statistics/748551/worldwide-households-with-computer/, 2022.

[11] Statista, "Number of TV households worldwide from 2010 to 2026." https://www.statista.com/statistics/268695/number-of-tv-households-worldwide/, 2022.

[12] Statista, "Global smartphone penetration rate as share of population from 2016 to 2022." https://www.statista.com/statistics/203734/global-smartphone-penetration-per-capita-since-2005/, 2022.

[13] T.-Y. Lee, L.-Y. Chen, Y.-Y. Lo, S. S. Swayamprabha, A. Kumar, Y.-M. Huang, S.-C. Chen, H.-W. Zan, F.-C. Chen, R.-H. Horng, and H.-C. Kuo, "Technology and applications of micro-leds: Their characteristics, fabrication, advancement, and challenges," *ACS Photonics*, vol. 9, no. 9, pp. 2905–2930, 2022.

[14] T. Wu, C.-W. Sher, Y. Lin, C.-F. Lee, S. Liang, Y. Lu, S.-W. Huang Chen, W. Guo, H.-C. Kuo, and Z. Chen, "Mini-led and micro-led: Promising candidates for the next generation display technology," *Applied Sciences*, vol. 8, no. 9, 2018.

[15] J. K. Borchardt, "Developments in organic displays," *Materials Today*, vol. 7, no. 9, pp. 42–46, 2004.

[16] BOE Technology Group, "BOE launches the first 55-inch printed 4K OLED display." https://www.boe.com/en/company/dynamic-028a64bf06e14c4c9b1af2b67a2395a1, 2023.

[17] Sony Group, "Sony Launches World's First OLED TV." https://www.sony.com/en/SonyInfo/News/Press/200710/07-1001E/, 2023.

[18] LG Electronics, "The history of the OLED TV." https://www.lg.com/uk/lg-experience/inspiration/the-history-of-the-oled-tv, 2023.

[19] Apple Inc, "About the Liquid Retina XDR display on iPad Pro." https://support.apple.com/en-al/HT212527, 2022.

[20] LG Electronics, "LG QNED MiniLED TV." https://www.lg.com/levant_en/qned-tvs/2022/why-lg-qned, 2022.

[21] G. Tan, Y. Huang, M.-C. Li, S.-L. Lee, and S.-T. Wu, "High dynamic range liquid crystal displays with a mini-led backlight," *Opt. Express*, vol. 26, pp. 16572–16584, Jun 2018.

[22] H. Chen, G. Tan, and S.-T. Wu, "Ambient contrast ratio of lcds and oled displays," *Opt. Express*, vol. 25, pp. 33643–33656, Dec 2017.

[23] G. Hong, X. Gan, C. Leonhardt, Z. Zhang, J. Seibert, J. M. Busch, and S. Bräse, "A brief history of oleds-emitter development and industry milestones," *Advanced Materials*, vol. 33, no. 9, p. 2005630, 2021.

[24] X. Li, G. Zhai, J. Wang, and K. Gu, "Portable information security display system via spatial psychovisual modulation," in *2017 IEEE Visual Communications and Image Processing (VCIP)*, pp. 1–4, 2017.

[25] M. S. Kim, Y. J. Lim, S. Yoon, S.-W. Kang, S. H. Lee, M. Kim, and S.-T. Wu, "A controllable viewing angle lcd with an optically isotropic liquid crystal," *Journal of Physics D: Applied Physics*, vol. 43, p. 145502, mar 2010.

[26] E. Jeong, Y. J. Lim, J. M. Rhee, S. H. Lee, G.-D. Lee, K. H. Park, and H. C. Choi, "Viewing angle switching of vertical alignment liquid crystal displays by controlling birefringence of homogenously aligned liquid crystal layer," *Applied Physics Letters*, vol. 90, 02 2007. 051116.

[27] L. Rao, Z. Ge, and S.-T. Wu, "Viewing angle controllable displays with a blue-phase liquid crystal cell," *Opt. Express*, vol. 18, pp. 3143–3148, Feb 2010.

[28] Continental AG, "Continental Display with Private Mode Entertains Passengers and Reduces Driver Distraction." `https://www.continental.com/en/press/press-releases/switchable-privacy-display/`, 2022.

[29] Genesis, "Genesis GV80 Technology." `https://www.genesis.com/us/en/2022/genesis-gv80/technology.html`, 2022.

[30] Mercedes, "Mercedes Maybach S-Class." `https://www.mercedes-benz.co.in/passengercars/models/saloon/mercedes-maybach-s-class/overview.html`, 2022.

[31] J. Geng, "Three-dimensional display technologies," *Adv. Opt. Photon.*, vol. 5, pp. 456–535, Dec 2013.

[32] J. Hong, n. none, H.-J. Choi, J. Hahn, J.-H. Park, H. Kim, S.-W. Min, N. Chen, and B. Lee, "Three-dimensional display technologies of recent interest: principles, status, and issues [invited]," *Applied optics*, vol. 50, pp. H87–115, 12 2011.

[33] E. Lueder, *3D Displays*. Wiley Display Technologyl, 1 ed., 2012.

[34] W. A. IJsselsteijn, H. de Ridder, and J. Vliegen, "Effects of stereoscopic filming parameters and display duration on the subjective assessment of eye strain," in *Stereoscopic Displays and Virtual Reality Systems VII* (J. O. Merritt, S. A. Benton, A. J. Woods, M. T. Bolas, and M. T. Bolas, eds.), vol. 3957, pp. 12 – 22, International Society for Optics and Photonics, SPIE, 2000.

[35] M. Urvoy, M. Barkowsky, and P. Le Callet, "How visual fatigue and discomfort impact 3d-tv quality of experience: a comprehensive review of technological, psychophysical, and psychological factors," *annals of telecommunications - annales des télécommunications*, vol. 68, pp. 641–655, 12 2013.

[36] H. Urey, K. V. Chellappan, E. Erden, and P. Surman, "State of the art in stereoscopic and autostereoscopic displays," *Proceedings of the IEEE*, vol. 99, no. 4, pp. 540–555, 2011.

[37] S. Pastoor and M. Wöpking, "3-d displays: A review of current technologies," *Displays*, vol. 17, no. 2, pp. 100–110, 1997.

[38] J. Geng, "Volumetric 3D display using a DLP projection engine," in *Emerging Digital Micromirror Device Based Systems and Applications IV* (M. R. Douglass and P. I. Oden, eds.), vol. 8254, p. 82540I, International Society for Optics and Photonics, SPIE, 2012.

[39] G. Favalora, "Volumetric 3d displays and application infrastructure," *Computer*, vol. 38, no. 8, pp. 37–44, 2005.

[40] S. Reichelt, R. Haussler, N. Leister, G. Futterer, H. Stolle, and A. Schwerdtner, "Holographic 3-d displays - electro-holography within the grasp of commercialization," in *Advances in Lasers and Electro Optics* (N. Costa and A. Cartaxo, eds.), ch. 29, Rijeka: IntechOpen, 2010.

[41] W. Wan, W. Qiao, W. Huang, M. Zhu, Y. Ye, X. Chen, and L. Chen, "Multiview holographic 3d dynamic display by combining a nano-grating patterned phase plate and lcd," *Opt. Express*, vol. 25, pp. 1114–1122, Jan 2017.

[42] R. Stahl and M. Jayapala, "Holographic displays and smart lenses," *Optik & Photonik*, vol. 6, no. 2, pp. 39–42, 2011.

[43] S. Tay, P.-A. Blanche, and R. e. a. Voorakaranam, "An updatable holographic three-dimensional display," *Nature*, vol. 451, pp. 348–51, 02 2008.

[44] N. Dodgson, "Autostereoscopic 3d displays," *Computer*, vol. 38, no. 8, pp. 31–36, 2005.

[45] Y. Su, Z. Cai, Q. Liu, W. Zou, P. Guo, and J. Wu, "Design and fabrication of directional diffractive device on glass substrate for multiview holographic 3D display," in *2017 International Conference on Optical Instruments and Technology: Optical Systems and Modern Optoelectronic Instruments* (Y. Wang, B. Jia, K. Tatsuno, and L. Dong, eds.), vol. 10616, p. 1061616, International Society for Optics and Photonics, SPIE, 2018.

[46] W. Wan, W. Qiao, W. Huang, M. Zhu, Z. Fang, D. Pu, Y. Ye, Y. Liu, and L. Chen, "Efficient fabrication method of nano-grating for 3d holographic display with full parallax views," *Opt. Express*, vol. 24, pp. 6203–6212, Mar 2016.

[47] D. Fattal, Z. Peng, T. Tran, S. Vo, M. Fiorentino, J. Brug, and R. Beausoleil, "A multi-directional backlight for a wide-angle, glasses-free 3d display," *Nature*, vol. 495, pp. 348–51, 03 2013.

[48] G. J. Woodgate, D. Ezra, J. Harrold, N. S. Holliman, G. R. Jones, and R. R. Moseley, "Observer-tracking autostereoscopic 3D display systems," in *Stereoscopic Displays and Virtual Reality Systems IV* (S. S. Fisher, J. O. Merritt, and M. T. Bolas, eds.), vol. 3012, pp. 187 – 198, International Society for Optics and Photonics, SPIE, 1997.

[49] W. Matusik and H. Pfister, "3d tv: A scalable system for real-time acquisition, transmission, and autostereoscopic display of dynamic scenes," *ACM Trans. Graph.*, vol. 23, pp. 814–824, aug 2004.

[50] Sharp Corporation, "Stunning 3D Realism on Screen." `http://www.sharp-phone.com/fr-en/products/sh80f/`, 2022.

[51] Nintendo, "Nintendo 3DS Familie." `https://www.nintendo.de/Hardware/Nintendo-3DS-Familie/Nintendo-3DS-Familie-94560.html`, 2022.

[52] Alioscopy, "Alioscopy Glasses-Free 3D Displays." `https://www.alioscopy.com/en/3Ddisplays.php`, 2022.

[53] Dimenco, "Dimenco Simulated Reality." `https://www.dimenco.eu/`, 2022.

[54] Sony Group, "Spatial Reality Display." `https://electronics.sony.com/more/spatial-reality-display/p/elfsr1`, 2022.

[55] K.-H. Yoon and S.-K. Kim, "Expansion method of the three-dimensional viewing freedom of autostereoscopic 3D display with dynamic merged viewing zone (MVZ) under eye tracking," in *Three-Dimensional Imaging, Visualization, and Display 2017* (B. Javidi, J.-Y. Son, and O. Matoba, eds.), vol. 10219, p. 1021914, International Society for Optics and Photonics, SPIE, 2017.

[56] C. van Berkel and J. A. Clarke, "Characterization and optimization of 3D-LCD module design," in *Stereoscopic Displays and Virtual Reality Systems IV* (S. S. Fisher, J. O. Merritt, and M. T. Bolas, eds.), vol. 3012, pp. 179 – 186, International Society for Optics and Photonics, SPIE, 1997.

[57] C. van Berkel, D. W. Parker, and A. R. Franklin, "Multiview 3D LCD," in *Stereoscopic Displays and Virtual Reality Systems III*, vol. 2653, pp. 32 – 39, SPIE, 1996.

[58] C. van Berkel, "Image preparation for 3D LCD," in *Stereoscopic Displays and Virtual Reality Systems VI* (M. T. Bolas, S. S. Fisher, J. O. Merritt, M. T. Bolas, and S. S. Fisher, eds.), vol. 3639, pp. 84 – 91, International Society for Optics and Photonics, SPIE, 1999.

[59] H. Hwang, H. S. Chang, D. Nam, and I. S. Kweon, "3d display calibration by visual pattern analysis," *IEEE Transactions on Image Processing*, vol. 26, no. 5, pp. 2090–2102, 2017.

[60] A. J. Woods, "Crosstalk in stereoscopic displays: a review," *Journal of Electronic Imaging*, vol. 21, no. 4, p. 040902, 2012.

[61] W. Ijsselsteijn, P. Seuntiëns, and L. Meesters, *Human Factors of 3D Displays*, pp. 217 – 233. Wiley, 01 2006.

[62] F. Kooi and A. Toet, "Visual comfort of binocular and 3-d displays," *Displays*, vol. 25, pp. 99–108, 08 2004.

[63] D. Nam, J. Park, D. Park, and C. Y. Kim, "Autostereoscopic 3d - how can we move to the next step?," in *2011 10th Euro-American Workshop on Information Optics*, pp. 1–4, 2011.

[64] D. Li, D. Zang, X. Qiao, L. Wang, and M. Zhang, "3d synthesis and crosstalk reduction for lenticular autostereoscopic displays," *J. Display Technol.*, vol. 11, pp. 939–946, Nov 2015.

[65] S.-K. Kim, S.-K. Yoon, and K.-H. Yoon, "Crosstalk minimization in autostereoscopic multiveiw 3D display by eye tracking and fusion (overlapping) of viewing zones," in *Three-Dimensional Imaging, Visualization,*

and Display 2012 (B. Javidi and J.-Y. Son, eds.), vol. 8384, pp. 232 – 239, International Society for Optics and Photonics, SPIE, 2012.

[66] K.-H. Yoon, M.-K. Kang, H. Lee, and S.-K. Kim, "Autostereoscopic 3d display system with dynamic fusion of the viewing zone under eye tracking: principles, setup, and evaluation [invited]," *Appl. Opt.*, vol. 57, pp. A101–A117, Jan 2018.

[67] P. Hanhart, C. di Nolfo, and T. Ebrahimi, "Active crosstalk reduction system for multiview autostereoscopic displays," in *2015 IEEE International Conference on Multimedia and Expo (ICME)*, pp. 1–6, 2015.

[68] N. A. Dodgson, "On the number of viewing zones required for head-tracked autostereoscopic display," in *Stereoscopic Displays and Virtual Reality Systems XIII* (A. J. Woods, N. A. Dodgson, J. O. Merritt, M. T. Bolas, and I. E. McDowall, eds.), vol. 6055, pp. 241 – 252, International Society for Optics and Photonics, SPIE, 2006.

[69] Y. Liu, H. Ren, S. Xu, Y. Li, and S.-T. Wu, "Fast-response liquid-crystal lens for 3D displays," in *Advances in Display Technologies IV*, vol. 9005, pp. 1 – 10, SPIE, 2014.

[70] L.-L. Tian, F. Chu, W.-X. Zhao, L. Li, and Q.-H. Wang, "Fast responsive 2d/3d switchable display using a liquid crystal microlens array," *Opt. Lett.*, vol. 46, pp. 5870–5873, Dec 2021.

[71] O. H. Willemsen, S. T. de Zwart, W. L. IJzerman, M. G. H. Hiddink, and T. Dekker, "2D/3D switchable displays," in *Photonics in Multimedia* (A. Tervonen, M. Kujawinska, W. IJzerman, and H. D. Smet, eds.), vol. 6196, p. 61960H, International Society for Optics and Photonics, SPIE, 2006.

[72] C. Kim, J. Kim, D. Shin, J. Lee, G. Koo, and Y. H. Won, "Electrowetting lenticular lens for a multi-view autostereoscopic 3d display," *IEEE Photonics Technology Letters*, vol. 28, no. 22, pp. 2479–2482, 2016.

[73] Y. H. Won, J. Kim, C. Kim, D. Shin, J. Lee, G. Koo, and J. H. Sim, "Enhanced 3D performance by biconvex electrowetting lenticular lens structure," in *Three-Dimensional Imaging, Visualization, and Display 2018* (B. Javidi, J.-Y. Son, and O. Matoba, eds.), vol. 10666, p. 1066603, International Society for Optics and Photonics, SPIE, 2018.

[74] K. Hirano, J. Miyazaki, and T. Yendo, "Viewing zone control of super-multiview display with directional backlight," in *Three-Dimensional Imaging, Visualization, and Display 2015* (B. Javidi and J.-Y. Son, eds.),

vol. 9495, pp. 249 – 258, International Society for Optics and Photonics, SPIE, 2015.

[75] A. Boev, M. Georgiev, A. Gotchev, and K. Egiazarian, "Optimized single-viewer mode of multiview autostereoscopic display," in *2008 16th European Signal Processing Conference*, pp. 1–5, 2008.

[76] J. Liu, T. Malzbender, S. Qin, B. Zhang, C.-A. Wu, and J. Davis, "Dynamic mapping for multiview autostereoscopic displays," in *Stereoscopic Displays and Applications XXVI* (N. S. Holliman, A. J. Woods, G. E. Favalora, and T. Kawai, eds.), vol. 9391, pp. 400 – 407, International Society for Optics and Photonics, SPIE, 2015.

[77] K.-W. Chien and H.-P. D. Shieh, "Time-multiplexed three-dimensional displays based on directional backlights with fast-switching liquid-crystal displays," *Appl. Opt.*, vol. 45, pp. 3106–3110, May 2006.

[78] C.-H. Chen, Y.-C. Yeh, and H.-P. D. Shieh, "3-d mobile display based on moiré-free dual directional backlight and driving scheme for image crosstalk reduction," *Journal of Display Technology*, vol. 4, no. 1, pp. 92–96, 2008.

[79] H. Choi, S.-W. Min, S. Jung, J.-H. Park, and B. Lee, "Multiple-viewing-zone integral imaging using a dynamic barrier array for three-dimensional displays," *Opt. Express*, vol. 11, pp. 927–932, Apr 2003.

[80] J.-C. Liou and F.-H. Chen, "Design and fabrication of optical system for time-multiplex autostereoscopic display," *Opt. Express*, vol. 19, pp. 11007–11017, Jun 2011.

[81] Xpandvision, "Active 3D glasses." `https://xpandvision.com/product-category/3d-glasses/active`, 2022.

[82] Sony Group, "Active 3D glasses." `https://www.sony.com/electronics/support/television-projector-accessories-3d-glasses`, 2022.

[83] H. J. Lee, H. Nam, J. D. Lee, H. W. Jang, M. S. Song, B. S. Kim, J. S. Gu, C. Y. Park, and K. H. Choi, "A high resolution autostereoscopic display employing a time division parallax barrier," *SID Symposium Digest of Technical Papers*, vol. 37, no. 1, pp. 81–84, 2006.

[84] H.-J. Choi and M. Park, "A time-sequential autostereoscopic 3D display using a vertical line dithering for utilizing the side lobes," in *Holography, Diffractive Optics, and Applications VI* (Y. Sheng, C. Yu, and C. Zhou,

eds.), vol. 9271, p. 92710T, International Society for Optics and Photonics, SPIE, 2014.

[85] J.-C. Liou and F.-H. Chen, "A novel time-multiplexed autostereoscopic multiview full resolution 3D display," in *Stereoscopic Displays and Applications XXIII* (A. J. Woods, N. S. Holliman, and G. E. Favalora, eds.), vol. 8288, p. 82880U, International Society for Optics and Photonics, SPIE, 2012.

[86] H. Kwon and H.-J. Choi, "A time-sequential multiview autostereoscopic display without resolution loss using a multi-directional backlight unit and an LCD panel," in *Stereoscopic Displays and Applications XXIII* (A. J. Woods, N. S. Holliman, and G. E. Favalora, eds.), vol. 8288, p. 82881Y, International Society for Optics and Photonics, SPIE, 2012.

[87] C.-H. Yang, C.-Y. Hsu, Y.-P. Huang, and H.-P. D. Shieh, "High resolution time-multiplexed backlight with tracking system for multi-user applicable wide-viewing auto-stereoscopic lcd," *SID Symposium Digest of Technical Papers*, vol. 43, no. 1, pp. 301–304, 2012.

[88] D. Miyazaki, Y. Hashimoto, T. Toyota, K. Okoda, T. Okuyama, T. Ohtsuki, A. Nishimura, and H. Yoshida, "Multi-user autostereoscopic display based on direction-controlled illumination using a slanted cylindrical lens array," in *Stereoscopic Displays and Applications XXV* (A. J. Woods, N. S. Holliman, and G. E. Favalora, eds.), vol. 9011, pp. 401 – 409, International Society for Optics and Photonics, SPIE, 2014.

[89] Z. Zhuang, L. Zhang, P. Surman, S. Guo, B. Cao, Y. Zheng, and X. W. Sun, "Directional view method for a time-sequential autostereoscopic display with full resolution," *Appl. Opt.*, vol. 55, pp. 7847–7854, Oct 2016.

[90] P. Surman, R. S. Brar, I. Sexton, and K. Hopf, "Muted and helium3d autostereoscopic displays," *2010 IEEE International Conference on Multimedia and Expo*, pp. 1594–1599, 2010.

[91] J.-H. Lee, Y. Choi, I. Yanusik, A. Morozov, H. Hwang, D. Nam, and D. S. Park, "Glasses-free 2D/3D switchable display using an integrated single light-guide plate (LGP) with a trapezoidal light-extraction (TLE) film," in *Novel Optical Systems Design and Optimization XX* (A. J. Davis, C. F. Hahlweg, and J. R. Mulley, eds.), vol. 10376, p. 103760L, International Society for Optics and Photonics, SPIE, 2017.

[92] J. C. Schultz and M. J. Sykora, "Directional backlight with reduced crosstalk." Patent Application, November 2011. US Patent Application No. US2011285927A.

[93] M. Masaru, "Light source device and display." Patent Application, January 2012. US Patent Application No. US2012195072A1.

[94] G. Schroeder and H. Treiber, *Technische Optik*. Vogel, 2014.

[95] A.-H. Wang, Q.-H. Wang, X.-F. Li, and D.-H. Li, "Combined lenticular lens for autostereoscopic three dimensional display," *Optik*, vol. 123, no. 9, pp. 827–830, 2012.

[96] Nichia, "Nichia LED Products." `https://www.nichia.co.jp/en/product/led.html`, 2022.

[97] Zemax, "Zemax OpticStudio Applications." `https://www.zemax.com/`, 2022.

[98] Q.-H. Wang, X.-F. Li, L. Zhou, A.-H. Wang, and D.-H. Li, "Cross-talk reduction by correcting the subpixel position in a multiview autostereoscopic three-dimensional display based on a lenticular sheet," *Appl. Opt.*, vol. 50, pp. B1–B5, Mar 2011.

[99] SUSS MicroOptics, "MicroOptics Products ." `https://www.suss-microoptics.com/products`, 2022.

[100] UPT, "UPT Optiksystem ." `https://upt-optik.de/`, 2022.

[101] L. W. Bos and D. W. Lynch, "Optical properties of antiferromagnetic chromium and dilute cr-mn and cr-re alloys," *Phys. Rev. B*, vol. 2, pp. 4567–4577, Dec 1970.

Personal Publications

Journal Paper

[1] Jundong Zhou, Valeriano Ferreras Paz, and Wilhelm Stork. Compensation of lens manufacturing errors and inhomogeneities by filtering view images in three-dimensional lenticular displays. *Appl. Opt.*, 60(34):10660–10670, Dec 2021.

Patent

Based on the invention reports created within the scope of this project, the following patent drafts have been formulated by the commissioned patent attorney and submitted to the patent office.

[1] Jundong Zhou and Valeriano Ferreras Paz. Bildanzeigevorrichtung und verfahren zum betreiben einer bildanzeigevorrichtung. Patent Draft under Review at the German Patent Office with the Application Number 102022202502.4), 2023.

[2] Jundong Zhou and Valeriano Ferreras Paz. Verfahren und betriebsvorrichtung zum betreiben einer anzeigevorrichtung beispielsweise für ein fahrzeug, verfahren und erzeugungsvorrichtung zum erzeugen einer filterfunktion und anzeigesystem für ein fahrzeug. Patent Draft under Review at the German Patent Office with the Application Number 102023202638.4), 2023.

[3] Jundong Zhou and Valeriano Ferreras Paz. Verfahren und vorrichtung zum betreiben einer anzeigevorrichtung für ein fahrzeug und anzeigesystem für ein fahrzeug. Patent Draft under Review at the German Patent Office with the Application Number 102023202628.7), 2023.

[4] Jundong Zhou and Valeriano Ferreras Paz. Vorrichtung und verfahren zum anzeigen von aus unterschiedlichen blickwinkeln sichtbaren bildern.

Patent Draft under Review at the German Patent Office with the Application Number 102023204811.6), 2023.

List of Figures

List of Tables

Acknowledgments

Completing a Ph.D. project is a challenging task filled with both highs and lows. Just three months after starting this project, the COVID-19 pandemic has occurred and significantly reshaped our way of life. Throughout the entire project, there were numerous occasions when I felt unsure how to proceed. However, thanks to the precious assistance of many people, I consistently found the passion to continue my research. I deeply appreciate every support I have received, and I would like to express my gratitude to some people who have accompanied me on this remarkable journey.

First, I want to thank Prof. Dr. Wilhelm Stork for accepting me as a Ph.D. student and for making this dissertation possible. In every difficult phase, he could always give valuable suggestions and encourage me to move forward.

Next, I would like to express my gratitude to Dr. Valeriano Ferreras Paz (Vale) for his outstanding guidance and supervision. He has been with me throughout this entire journey, starting from the initial creation of the dissertation topic to the regular daily discussions, and all the way to the review and correction of each presentation, patent, paper, and the final dissertation. Under his support, I not only gained knowledge in optics and display technologies but also felt a strong connection with the working environment, language, and culture. It has been an absolute pleasure and honor to collaborate with him.

My research was supported by the Robert Bosch GmbH. I would like to thank Dr. Marcus Herrmann for providing me the opportunity to join the Product Area Display at Bosch, which allowed me to explore the world of display technologies. Additionally, I would like to express my gratitude to several colleagues at Bosch. Yasuhiro Wakita (Yasu) has been tremendously supportive, always ready to answer any basic display questions. Sven Fabian has provided valuable helps with the image preparation and the introduction into 3D displays. Stephan Kohlenbecker has been a constant source of support in the display lab. Dr. Benjamin Tränkle has offered constructive technical insights and inspirations related to 3D technologies. Dr. Tobias Werner has provided significant assistance in the optical simulation.

Then I want to thank the innovation team at Bosch, including Valeriano Ferreras Paz, Serdar Kantarci and Nadescha Heine. They have been making great effort to further develop and promote my Ph.D. project. I am looking forward to seeing the growth of the idea.

I also want to thank Erich Steinbeißer from the Institute für Technische Optik at the University of Stuttgart. He provided me numerous suggestions on the lens design of a 3D display.

Furthermore, I want to extend my gratitude to my family. Although I haven't been able to see my parents in the past three years due to the pandemic, every phone call with them brings me peace and power. I am also especially thankful to my wife, Xiwei Wang, for creating a lovely home environment. Regardless of the challenges I faced, I always knew there is someone standing by my side. I also give my best wishes for her own Ph.D. project.

Finally, I want to thank all those who have ever contributed to this wonderful journey.